NOVEL ACOUSTIC ARRAYS AND ARRAY PATTERN SYNTHESIS METHODS

by

LIXUE WU
B.Sc., East China Normal University, 1982
M.A.Sc., University of Victoria, 1989

A DISSERTATION SUBMITTED IN PARTIAL FULFILLMENT
OF THE REQUIREMENTS FOR THE DEGREE OF
DOCTOR OF PHILOSOPHY
in the Department of
Electrical and Computer Engineering

We accept this dissertation as conforming
to the required standard

Dr. A. Zielinski, Supervisor (Dept. of Elect. & Comp. Eng.)

Dr. P. Agathoklis, Departmental Member, (Dept. of Elect. & Comp. Eng.)

Dr. R. L. Kirlin, Departmental Member, (Dept. of Elect. & Comp. Eng.)

Dr. R. M. Clements, Outside Member, (Dept. of Physics & Astronomy)

Dr. J. S. Bird, External Examiner, (Simon Fraser University)

Supervisor: Dr. A. Zielinski

ABSTRACT

Directional acoustic beams are used in diverse sonar systems. For efficient transmission of a sonar signal, the sound energy is projected in a narrow beam. For reduced interference in reception, the sound signal is received from a narrow spatial sector. Typically, such beams have associated sidelobes which adversely affect sonar performance.

The goal of this thesis is to propose several novel acoustic arrays which are capable of generating desired search-light-type and fan-type beams with greatly reduced sidelobes. These novel acoustic arrays have fewer elements than conventional arrays of similar performance. The design of such novel arrays is inherently more difficult, however, since it involves nonlinear optimization. Such an optimization is normally computationally intensive and may not be globally convergent.

This difficulty has been overcome by newly developed concepts and associated array pattern synthesis methods. A new concept called the equivalent linear array is introduced; a design method based on this concept benefits from existing design techniques developed for linear arrays. The equivalent linear array concept is further developed to lead to a new and effective method for array radiation pattern synthesis. A second new concept called the scale-invariance radiation pattern is introduced, and the subsequent relation between two novel arrays is discovered. Using this concept an angle mapping approach is developed which transforms a radiation pattern generated by a circular ring array to that of an elliptic ring array. This approach takes advantage of methodologies developed for the design of circular ring arrays. A third concept, constraint directions, is introduced; a subsequent new iterative method for array pattern synthesis is developed to meet the need in compact receiving/transmitting array design. With the help of these new concepts, the proposed synthesis methods avoid the use of nonlinear optimization

techniques and merely require simple matrix operations. The methods can be applied to the problems of synthesizing radiation patterns of arrays with arbitrary sidelobe envelopes, with nonisotropic elements, and with nonuniform spacing between elements. The usefulness of the developed methodologies is demonstrated in various design examples. The methods developed provide powerful tools not only to design novel acoustic arrays but also to design antenna arrays.

Examiners:

Dr. A. Zielinski, Supervisor (Dept. of Elect. & Comp. Eng.)

Dr. P. Agathoklis, Departmental Member, (Dept. of Elect. & Comp. Eng.)

Dr. R. L. Kirlin, Departmental Member, (Dept. of Elect. & Comp. Eng.)

Dr. R. M. Clements, Outside Member, (Dept. of Physics & Astronomy)

Dr. J. S. Bird, External Examiner, (Simon Fraser University)

Table of Contents

List of Tables

List of Figures

Abbreviations

2-D	Two-dimensional
3-D	Three-dimensional
ELA	Equivalent linear array

Acknowledgments

I would like to thank my supervisor, Dr. A. Zielinski of the Department of Electrical and Computer Engineering, for his encouragement, guidance, and advice during the course of this research and for his help in the preparation of this thesis.

Financial assistance received from Dr. A. Zielinski (through the Natural Sciences and Engineering Research Council of Canada), the University of Victoria, and the BC Advanced Systems Institute is gratefully acknowledged.

I am grateful to my parents for making it possible for me to become what I am. A special and warm expression of gratitude is reserved for my son, Ken Wu, for his understanding and many sacrifices.

To my parents

Chapter 1

Introduction

1.1 Motivation

1.1.1 Sonar Systems

Sensing the ocean beyond visual range requires sonar systems [1]. Objects such as submersibles, ships and underwater beacons radiate acoustic energy and passive sonars can be used to determine their presence and their acoustical characteristics. On the other hand, in active sonar a directional beam of sound in the form of a short burst of energy is transmitted. If an object is in the beam, some of the sound is backscattered. The backscattered sound echo is detected by a receiver. The received signal is usually displayed as a function of travel time and direction. The common depth sounder is an example of this kind of sonar. Sidescan sonar uses a fan-type beam which is narrow in one dimension ($\sim 1°$) and relatively wide ($\sim 30°$) in the other. A short pulse is transmitted along the beam and the reflected echo from the bottom is sequentially recorded. The record represents an echo from a narrow strip of the bottom. The sonar is continuously moving forward, and the accumulation of successive returns produces an overall image of the bottom (Fig. 1.1).

The radiation pattern of a transmitting/receiving transducer plays an important role in system performance, and therefore it should be designed to suit various needs. Of particular interest is the presence of sidelobes in the radiation pattern

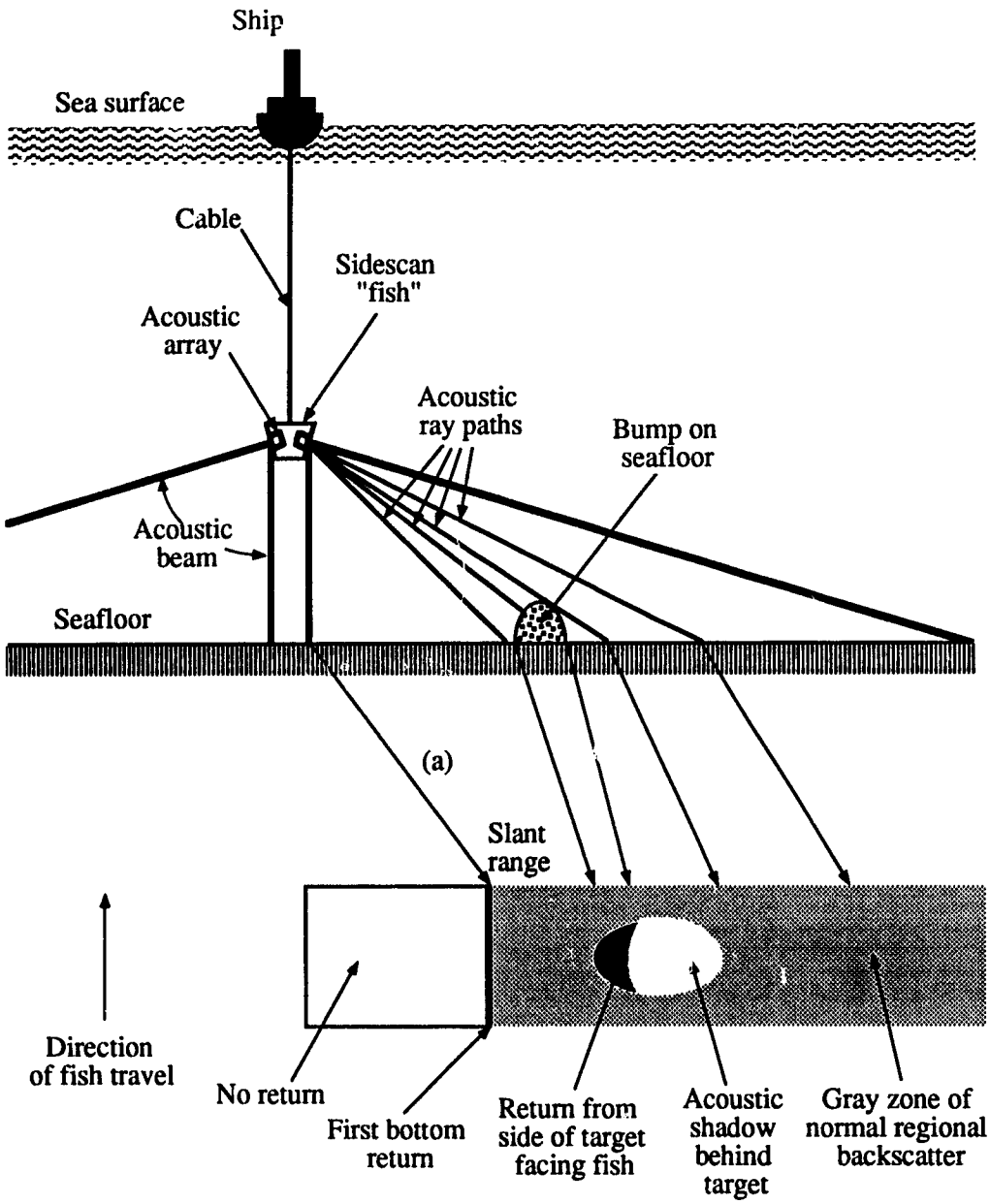

Figure 1.1: Geometry of sidescan sonar and topography of bottom. (a) Vertical profile of ship and "fish" moving into the page and sonar beam aimed athwartship. (b) Plan view of raw (uncorrected) sidescan image.

as illustrated in Fig. 1.2. These sidelobes adversely affect sonar performance since signals are admitted from sidelobe directions in addition to signals being detected in the main lobe direction.

1.1.2 Acoustic Transducers and their Radiation Patterns

Today's most common acoustic transducers are slabs of piezoelectric materials that expand, contract, or change shape when electrical voltages are applied. Since 1950, ceramic materials have been used because of their high output, mechanical strength, and ability to be shaped. A ceramic transducer commonly has a thin conducting electrode covering each face. A voltage applied across the electrodes causes the thickness of the slab to increase; reversal of the voltage causes the thickness to decrease. When the element is in water, these expansions and contractions cause sound radiation [2].

Often a principal goal in transducer or transducer array design is to achieve a specified radiation pattern $p(\theta, \phi)$, representing power density in watts per square meter, through suitable geometry and/or arrangement of sources. The specified pattern frequently embodies the intent to enhance radiation in certain directions and to suppress it elsewhere. Sonar systems use such directional transducers. In transmission, the sound energy is projected along a narrow beam to maximize output in a certain direction. In reception, the sound signal is received from a narrow spatial sector to reduce interference from other sectors. The other important use of directionality is to resolve the backscattered signals from closely spaced objects.

The directional responses of the transducer are the same when used as a source and as a receiver. A useful measure of this directional response is the power directivity function, which is the radiated power density $p(\theta, \phi)$ in the direction (θ, ϕ) divided by the radiated power density averaged over all directions; that is,

$$D(\theta, \phi) = \frac{p(\theta, \phi)}{(1/4\pi r^2) \int_0^{\pi} \int_0^{2\pi} p(\theta', \phi') r^2 \sin\theta' d\theta' d\phi'} \tag{1.1}$$

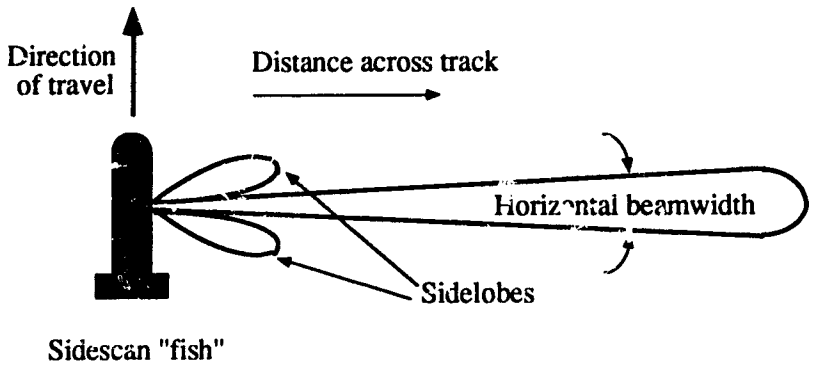

(a)

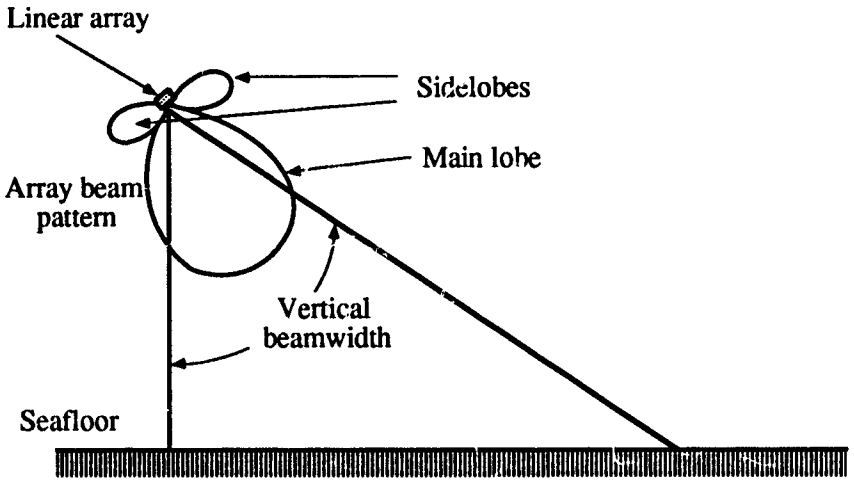

(b)

Figure 1.2: Typical radiation pattern of a sidescan sonar. (a) Plan view. (b) Vertical profile.

where r is the distance from the transducer and is assumed large enough to ensure the far field of the transducer.

1.1.3 Sidelobes in Radiation Patterns

Directional acoustic beams, such as search-light-type or fan-type beams, are widely used in sonar systems. A search-light-type beam can be generated by a circular piston transducer. The three-dimensional radiation pattern of such a transducer is shown in Fig. 1.3. A rectangular transducer can be used to produce a fan-type beam. The three-dimensional radiation pattern of such a transducer is shown in Fig. 1.4(a). However, the major problem encountered in these transducers is the existence of sidelobes in the radiation patterns. The first sidelobe level of a circular piston is about 17.6 dB down from the main lobe maximum, whereas the rectangular transducer offers only 13.5 dB suppression of its first sidelobe [3].

In fan-type beam applications it is possible to use a linear array of rectangular transducers to control the radiation pattern in the narrow beam direction by the application of proper weights to each element. In the broad beam direction, however, the radiation pattern is determined by the width of rectangular elements and still exhibits large first sidelobes (13.5 dB down) as shown in Fig. 1.4(b).

A rectangular planar array can be used to reduce sidelobes for both search light-type and fan type beams by suitably weighting its elements; however, the number of elements required to accomplish this task is about $M \times N$, where M, N are the array dimensions expressed in multiples of half wavelength [3]. This results in complexity, not only to the power distribution in transmission but also to the summing network in reception.

The goal of this thesis is to propose several novel acoustic arrays which are capable of generating the desired beams with greatly reduced sidelobe levels. These novel acoustic arrays require fewer elements than planar arrays to achieve the same performance. The design of such arrays is inherently more difficult, however, since it involves nonlinear optimization, a computationally intensive technique that may

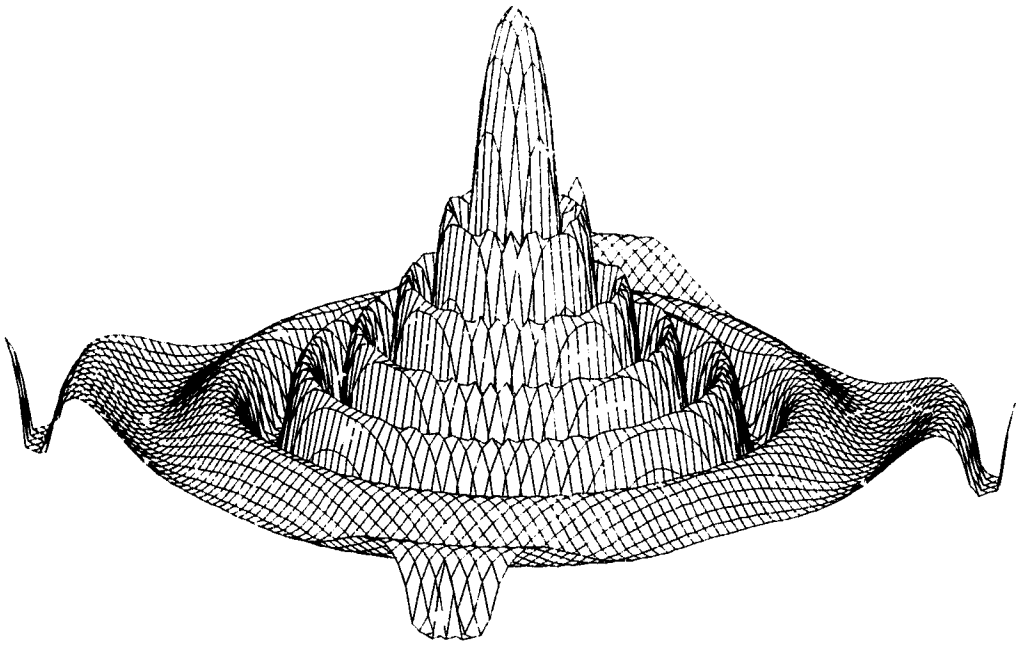

Figure 1.3 Three-dimensional radiation pattern of a circular piston transducer.

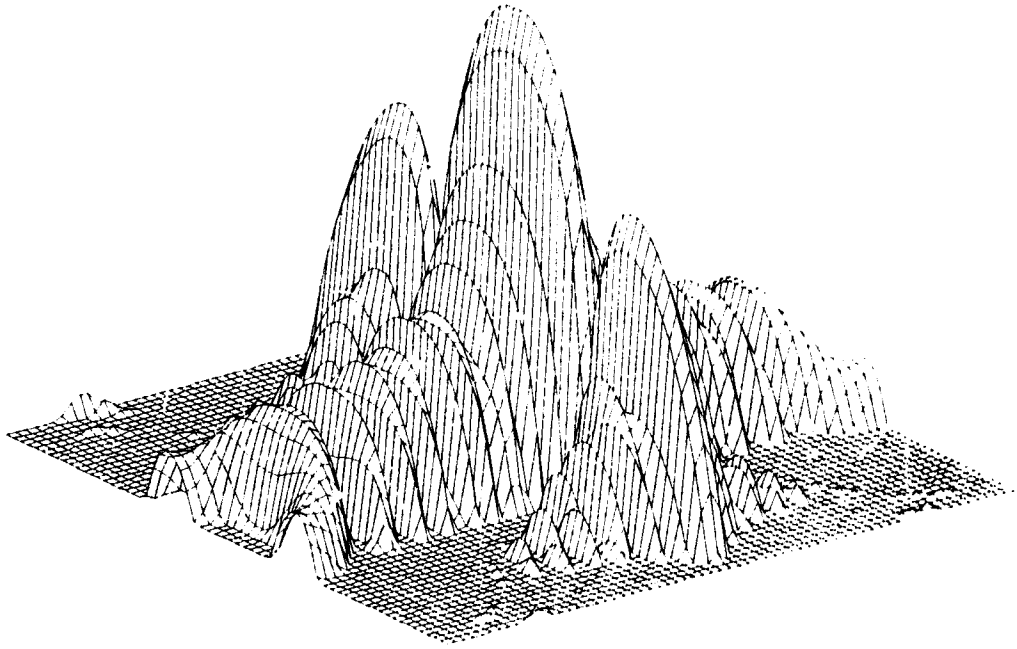

(a)

Figure 1.4: Three-dimensional radiation patterns of a linear array of rectangular transducers. (a) Uniform weighting of elements. (b) Dolph-Chebyshev weighting with postulated 30 dB sidelobe suppression.

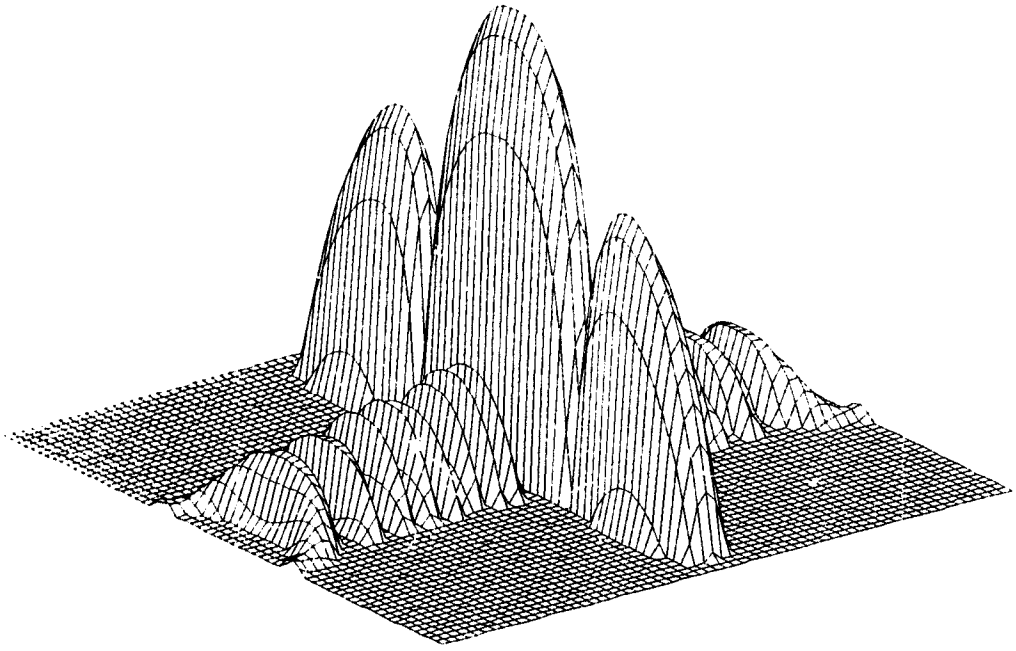

(b)

Figure 1.4: (Continued)

not be globally convergent [4]. The thesis presents new concepts and associated array pattern synthesis methods to overcome these difficulties. The new synthesis methods provide powerful tools not only for the design of novel acoustic arrays but also for antenna arrays.

1.2 Literature Review

In the mid-1940s, with the advent of high performance ceramic piezoelectric materials such as barium titanate, it became possible to make transducer elements into shapes such as rods, hollow cylinders, hollow spheres, sections of spheres, and paraboloids [5]. Each shape is characterized by a distinctive directional pattern when used as a source or receiver. Recently developed piezoelectric polymeric materials [6], such as KYNAR, available in the form of film and wire, now enable construction of inexpensive and innovative acoustic arrays. The use of arrays instead of single radiators makes it possible to tailor radiation patterns to almost any desired shape as well as to increase the gain and the power-handling capability.

A direct way of designing a transducer with a desired radiation pattern is to control the sensitivity distribution on the face of the transducer. This treatment is called shading, and the sensitivity distribution is called an aperture. In a classical paper, Taylor [7] derived a smooth aperture which yields the minimum beamwidth for a specified sidelobe level. If the transducer can be made to vibrate in such a way that its aperture function follows a Gaussian function, then the radiation pattern is also Gaussian and has no sidelobes [8]. Because of these attractive characteristics, researchers have attempted to produce an efficient truncated Gaussian transducer; their efforts are reported in the literature. Von Haselberg and Krautkramer [9] used an array of octagonal transducers to approximate a Gaussian function. Martin and Breazeale [10] and Du and Breazeale [11] showed that Gaussian beams can be obtained by having full plating on one face of

the circular piston element and a small electrode on the other face. Zerwekh and Claus [12] and Claus and Zerwekh [13] developed a Gaussian transducer that has a number of concentric ring electrodes, each driven by a different voltage (piecewise Gaussian) provided by a voltage divided network. All the above design methods followed the approach of exciting a uniformly polarized piezoelectric element with nonuniform (Gaussian) driving voltage and field.

From the practical point of view, however, construction of transducers with a continuously varying sensitivity distribution is a complex task. One way to reduce this complexity is to approximate the required sensitivity distribution on the transducer's face with a small number of constant sensitivity segments. The early work of using discrete constant sensitivity segments to approximate a continuous sensitivity was reported by the National Defense Research Committee [14, 15]; however, their work was limited to experimentation with only 2- and 3-level distributions. Later, Martin and Hickman [16] considered the problem of optimizing a bi-level sensitivity ratio between the central and outer segments and segment size ratio. Drost [17] approached the problem of optimizing a bi-level sensitivity distribution by coherently adding the predicted radiation patterns of the two levels. The sizes of the segments were chosen so that the first positive sidelobe of the wider segment canceled the first negative sidelobe of the narrower one. He then varied the sensitivity ratio to minimize all the sidelobes. Recently Zielinski and Wu [18] have used linear optimization techniques to create arrays of circular ring radiators with radial radiation patterns that approximate the radiation patterns of $\lambda/2$ spaced linear arrays. Most recently McGehee and Jaffe [19] have proposed an optimum mean square quantizer approach to choose the "best" segment sizes and sensitivity levels for a segmented transducer by minimizing the mean square error between a desired sensitivity distribution and its discrete level approximation. The piecewise approximation may achieve an acceptable radiation pattern in a segmented transducer but generally requires a large number of segments.

Furthermore, the relation between segment size and desired radiation pattern is unknown.

Varying the weighting coefficients of array elements provides the array designer with the ability to control radiation patterns. The designer has the ability to form a pattern with a main lobe and sidelobes, to control angular placement of the main beam, to select beam sharpness by choosing the length of the array, and to produce a shaped pattern without nulls. All of these form a basis for pattern synthesis; a large number of papers have been devoted to this area. Schelkunoff [20] developed the general concept of the array polynomial and the relation between pattern shape and polynomial zeros. Dolph [21] determined the array weights for a uniformly spaced linear array of isotropic elements that yield the minimum beamwidth for a specified sidelobe level. Villeneuve [22] described how Taylor's method [7] developed for continuous shading can be applied to discrete arrays. Hyneman [23] and Hyneman and Johnson refined shaped beam synthesis using pattern zero shifting to minimize ripple. Elliot and Stern [25] and Orchard, Elliot, and Stern [26] presented additional pattern synthesis techniques for arrays. Another technique for pattern synthesis is due to Woodward [27, 28]. This technique is based on the weighted superposition of a number of $(\sin u)/u$ patterns deflected by different amounts to one or the other side of the $u = 0$ axis, with peak amplitudes suitably chosen. The principal merit of this approach is its simplicity; however, undesirable ripple between sample points makes the results inferior to those produced by Elliot's methods. White [29] developed a method which deals with pattern extremes rather than pattern zeros, and this method may be simple to apply in some case. Other techniques are described by Schell and Ishimaru [30]. All of these techniques, however, are applicable only to arrays consisting of uniformly spaced elements with nondirectional radiation patterns (isotropic elements).

In a recent paper [31] Olen and Compton, Jr. presented a numerical synthesis

technique based on adaptive array theory that can be used for arrays consisting of a set of elements each with an arbitrary radiation pattern. This method is a numerical technique, and however, it does not yield analytic solutions for the required weights.

1.3 Organization of the Thesis

This thesis puts together the research results pertaining to two major themes: *Novel Acoustic Arrays* and *New Array Pattern Synthesis Methods.* The following is the outline of each chapter.

CHAPTER 1

This chapter introduces the basic concepts of sonar systems, focusing in particular on directional acoustic beams and the existence of sidelobes. The developed techniques for generating such beams and the associated pattern synthesis methods are briefly reviewed. The motivation of the research is addressed. The organization of the thesis is also discussed.

CHAPTER 2

In this chapter a novel array of circular ring radiators is proposed which generates a symmetric search-light-type narrow beam with greatly reduced sidelobes. Such a narrow beam can find several applications related to acoustic remote sensing, telemetry and specialized sonars. A design method is detailed which benefits from existing design techniques developed for linear arrays. The developed methodology requires only simple matrix operations and does not involve nonlinear optimization. The results demonstrate that radiation patterns with arbitrary sidelobe suppression can be achieved.

CHAPTER 3

This chapter introduces a convenient procedure to design a novel array of circular ring radiators. Several practical aspects associated with implementation of such an array are investigated. Specifically, the important aspect of sensitivity of the radiation pattern to finite tolerances associated with array implementation

is addressed. The results are presented in a tabular form convenient for a designer.

Chapter 3 also describes compact receiving/transmitting configurations for a piston transmitting element and a receiving array consisting of the same transmitting piston surrounded by several concentric circular rings of piezoelectric film or several concentric hollow cylinders operating in longitudinal mode. It is shown that such a configuration allows for good sidelobe suppression in the combined transmitting/receiving radiation pattern even for arrays with a small number of elements. A design example shows that a narrow beam of 8° beamwidth with more than 48 dB sidelobe suppression in transmitting/receiving pattern can be achieved with an array consisting of only 6 elements.

CHAPTER 4

In this chapter a novel array of elliptic ring radiators is proposed which generates a fan-type beam with controllable sidelobe level. Such an array can find several applications in specialized sonars such as sidescan sonars, sonars for fish finding and stock assessment, and obstacle avoidance systems. Two possible approaches to the design are presented. One approach utilizes a mapping which transforms a radiation pattern generated by a circular ring array to that of an elliptic ring array. This approach takes advantage of methodologies developed for the design of circular ring arrays. The other approach uses the concept of an equivalent linear array (ELA). This approach benefits from the existing design techniques developed for linear arrays. It requires only simple matrix operations and does not involve optimization. The design examples presented demonstrate that a fan-type beam with sidelobes suppressed to more than 40 dB in all possible directions is achievable.

CHAPTER 5

This chapter presents a new and effective method for array radiation pattern synthesis. The method allows the designer to formulate the synthesis of a desired pattern as an optimization problem. The proposed solution involves matrix operations based on the linear equivalent array approach, which lead to an easy

and effective computation. The advantage of this approach is that it requires only ordinary matrix operations instead of nonlinear optimization. Illustrations are presented to highlight the various aspects of the method. The proposed algorithm can be used to design arrays of uniformly spaced elements with nonisotropic and unequal radiation patterns.

CHAPTER 6

In this chapter an iterative method is developed for array pattern synthesis. In this method the synthesis problem is formulated as a well-determined or overdetermined optimization problem. The problem is then simplified by the concept of constraint directions. The iterative algorithm for obtaining an optimum solution is presented which does not involve any nonlinear optimization but only requires simple matrix operations. The proposed method can be applied to the problems of synthesizing radiation patterns of linear arrays with arbitrary sidelobe envelopes, with nonisotropic elements, and with nonuniform spacing between elements. The results are presented and compared with other methods. It is shown that the proposed iterative method yields superior results.

CHAPTER 7

A summary of the important contributions of the thesis and future research considerations are given in this chapter.

Chapter 2

Novel Arrays of Circular Ring Radiators

In this chapter we propose a novel acoustic array of circular ring radiators which can generate a search-light-type beam with greatly reduced sidelobes. We introduce a new concept called the *equivalent linear array* and apply it to the design of novel arrays.

2.1 Introduction

The circular piston is a widely used planar radiator [1]. One of the attractive features of such a radiator is its symmetric, search-light-type radiation pattern with the first sidelobe level of 17.6 dB below the main lobe maximum [32]. However, in some applications still lower sidelobe levels are desirable. In this chapter we propose an array, consisting of circular ring radiators, that is capable of generating a superior radiation pattern. A design procedure is described which benefits from the existing design techniques developed for linear arrays. The results indicate that radiation patterns with arbitrary sidelobe suppression can be achieved. The proposed configuration can readily be implemented as a receiving array using piezoelectric film and as a transmitting/receiving array using concentric hollow cylinders operating in longitudinal mode.

2.2 An Array of Circular Ring Radiators

The directivity function (radiation pattern) of a planar, circular disc radiator with radius r, of uniform sensitivity, placed in an infinite rigid baffle, is known to be [33]:

$$D_c(\theta) = r\frac{\mathrm{J}_1[(2\pi r/\lambda)\sin\theta]}{(\sin\theta)/\lambda} \tag{2.1}$$

where θ is the elevation angle, λ is the wavelength of the radiated signal and $\mathrm{J}_1(\cdot)$ is the first-order Bessel function of the first kind. Because of circular symmetry the directivity function does not depend on azimuth angle.

The directivity function of a circular ring radiator can be readily obtained by subtracting directivity functions of two disc radiators [34]. In this chapter and Chapter 3, we will simply call the circular ring radiator a ring radiator.

We consider an array formed by several concentric, contiguous (no gaps between rings) ring radiators. The ring radiators contribute to the overall directivity function with weighting coefficients c_i. Fig. 2.1 illustrates an array of three rings. Note that we also call the central, circular portion of the array a ring.

The directivity function of an array with N ring radiators as described above can be written as

$$\begin{aligned} D(\theta) &= 2\pi r_1^2 c_1 \frac{\mathrm{J}_1[(2\pi r_1/\lambda)\sin\theta]}{(2\pi r_1/\lambda)\sin\theta} \\ &\quad + \sum_{i=2}^{N} c_i \left\{ 2\pi r_i^2 \frac{\mathrm{J}_1[(2\pi r_i/\lambda)\sin\theta]}{(2\pi r_i/\lambda)\sin\theta} \right. \\ &\quad \left. - 2\pi r_{i-1}^2 \frac{\mathrm{J}_1[(2\pi r_{i-1}/\lambda)\sin\theta]}{(2\pi r_{i-1}/\lambda)\sin\theta} \right\} \end{aligned} \tag{2.2}$$

where r_i are outer radii of i-th ring, as indicated in Fig. 2.1.

By varying the weighting coefficients c_i and radii r_i, one can modify the overall

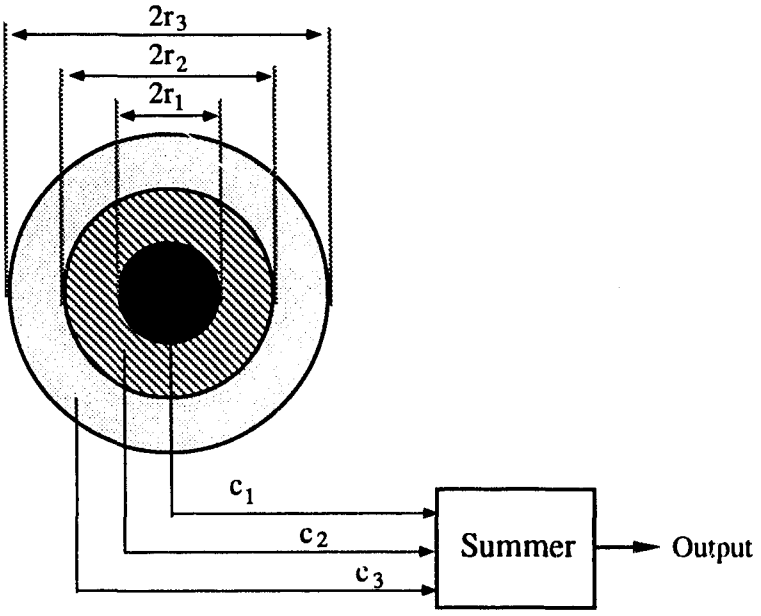

Figure 2.1: Geometry of an array of circular ring radiators (3 rings shown).

function D to approximate a certain desired function D_d. The error of approximation ϵ can be defined as

$$\begin{aligned} \epsilon^2 &= \|D - D_d\|^2 \\ &= < D - D_d, D - D_d > . \end{aligned} \tag{2.3}$$

Here we treat functions as vectors in Hilbert space and use the norm denoted by $\|\cdot\|$ to express the error function. The $< \cdot >$ denotes the inner product.

The objective of the design is to determine the array parameters as given in Eq. (2.2) that minimize the error ϵ. Nonlinear optimization algorithms can be used to find the optimum array parameters. These methods, however, have some inherent limitations. Specifically, the number of elements in the array must be determined before each search. In addition, the resultant directivity function is a priori unknown and depends on the selection of the desired directivity function.

The method proposed here allows for better control of the resultant directivity function by taking advantage of some closed-form solutions. Initially, we confine the design method to optimize the selection of weights c_i only, but later on we will extend it to include the variability of radii and the number of elements in the array. With this restriction the minimum of the error function given by Eq. (2.3) can be obtained by setting the N-dimensional gradient vector ∇ to zero, that is,

$$\nabla = \left[\frac{\partial \epsilon^2}{\partial c_1}, \ldots, \frac{\partial \epsilon^2}{\partial c_N}\right]^T = 0. \tag{2.4}$$

In the following developments it is convenient to map angle θ into a u-domain defined as

$$u = \frac{\pi d}{\lambda} \sin\theta \tag{2.5}$$

where d is a constant, which will be discussed later on.

Eq. (2.4), with the help of Eqs. (2.2), (2.3) and (2.5) can be written as

$$\sum_{j=1}^{N} c_j < D_i(u), D_j(u) > \;=\; < D_i(u), D_d(u) > \qquad i = 1, \ldots, N \tag{2.6}$$

where $D_i(u)$ is the directivity function of the i-th ring radiator.

The optimum coefficients c_i which minimize the error function can therefore be obtained as the solution to a set of N simultaneous linear equations.

We propose here a different approach which utilizes the existing design methods for linear arrays and allows for better control of the resultant directivity function. Furthermore, the method allows for variability of the ring width as an additional possible step to reduce the approximation error without resorting to nonlinear equations. The method, however, requires that we restrict the desired directivity function to the following form

$$D_d(u) = \sum_{i=1}^{M} w_i \phi_i(u); \qquad -\frac{\pi d}{\lambda} \leq u \leq \frac{\pi d}{\lambda} \tag{2.7}$$

where

$$\phi_i(u) = \cos((2i-1)u). \tag{2.8}$$

It can be shown that the functions $\cos((2i-1)u)$; $i = 1, \ldots, \infty$, form an orthogonal set spanning the Hilbert space $\mathcal{H}$. The desired directivity function $D_d(u)$ is a vector in the subspace $\mathcal{M}$ of the Hilbert space $\mathcal{H}$. Subspace $\mathcal{M}$ is spanned by a finite number of basis functions $\phi_i(u)$, $i = 1, \ldots, M$. Due to the nature of the directivity function of a ring radiator (that is, we can only expand a Bessel function by an infinite number of basis function $\phi_i(u)$), $D_i(u)$ is in $\mathcal{H}$-space but not in $\mathcal{M}$-subspace and therefore cannot be expressed exactly as a linear combination of M basis functions. It can, however, be best approximated (in minimum error ϵ sense) by its projection into $\mathcal{M}$-subspace.

We first consider the directivity function of the largest ring radiator $D_i(u) = D_N(u)$. Since $D_N(u)$ is in the $\mathcal{H}$-space, it can be expressed as

$$D_N(u) = \sum_{j=1}^{\infty} w_{j,N} \phi_j(u). \tag{2.9}$$

The projection of $D_N(u)$ into subspace $\mathcal{M}$ (for orthogonal basis) can be found by simply truncating the above expansion to M terms. Thus the projection of $D_N(u)$ into subspace $\mathcal{M}$ is

$$\hat{D}_N(u) = \sum_{j=1}^{M} w_{j,N}\phi_j(u). \tag{2.10}$$

Repeating the above procedure for all $D_i(u), i = N-1,\ldots,1$, we can obtain a series of projections $\hat{D}_i(u)$ of $D_i(u)$ in the subspaces $\mathcal{M}_i$ spanned by basis $\phi_j(u)$; $j = 1,\ldots,M-N+i$. Therefore, we have N projections in the subspace $\mathcal{M}$; among them there are M projections which are linearly independent. By linearly combining those linearly independent M projections, we can form the desired directivity function in the subspace $\mathcal{M}$ without introducing any additional error. It follows that the minimum number of ring radiators necessary to produce M linear independent projections is $N = M$. Using this approach, we can monitor the error introduced by truncation which depends on the width of each ring radiator. By varying this width we can reduce the truncation error to an acceptable value.

2.3 Design of an Array of Circular Ring Radiators

Based on the previous considerations we propose here a design technique for an array of ring radiators which closely approximates the prescribed radiation pattern. The technique takes advantage of the theory developed for linear arrays. Since linear array design is a mature and well-developed field, the technique offers obvious advantages.

2.3.1 Equivalent Linear Array of a Circular Ring Radiator

A linear array with $2N$ (even) point elements spaced uniformly by d has the directivity function given by [32]

$$D_l(u) = \sum_{j=1}^{N} w_j \cos((2j-1)u) \tag{2.11}$$

where $\{w_j\}$ are the weighting coefficients and u is defined in Eq. (2.5). Here, parameter d has a particular meaning as the spacing between array elements. Eq. (2.11) has the form which coincides with that postulated by Eqs. (2.7) and (2.8).

The directivity function of a ring radiator with outer and inner radii r_i and r_{i-1}, respectively, can be written as

$$D_r(u) = \pi r_i d \frac{\mathrm{J}_1[(2r_i/d)u]}{u} - \pi r_{i-1} d \frac{\mathrm{J}_1[(2r_{i-1}/d)u]}{u} \tag{2.12}$$

Assuming a linear array of infinite length, it is possible, by the proper selection of weighting coefficients w_j, to obtain the directivity function of the linear array equal to that of a ring radiator, that is

$$D_r(u) = \sum_{j=1}^{\infty} w_j \cos((2j-1)u); \qquad -\frac{\pi d}{\lambda} \leq u \leq \frac{\pi d}{\lambda}. \tag{2.13}$$

We call such an array the equivalent linear array to a ring radiator. Similarly, an equivalent linear array can be derived for a disc radiator with directivity function D_c given by Eq. (2.1).

As noted earlier the functions $\cos((2j-1)u)$ are orthogonal in the u-domain, namely their inner products, defined as

$$< \cos((2i-1)u), \cos((2j-1)u) > \; = \; \frac{4}{n\pi} \int_0^{\frac{n\pi}{2}} \cos((2i-1)u)$$

$$\cos((2j-1)u)du$$

$$= \begin{cases} 1 & \text{for } i = j \\ 0 & \text{otherwise} \end{cases} \tag{2.14}$$

where n is any positive integer.

The inner product definition given by Eq. (2.14) constrains the u-domain to range $[0, n\pi/2]$. This implies that the constant d defined in Eq. (2.5) must be equal to $n\lambda/2$. In order to avoid the grating lobes in the linear array with directivity function given by Eq. (2.11), the constant d has to be equal to $\lambda/2$. For this reason we subsequently set $n = 1$.

Applying the inner product defined by Eq. (2.14) to Eq. (2.13) we obtain

$$\sum_{j=0}^{\infty} w_j < \cos((2j-1)u), \cos((2i-1)u) > \;=\; < D_r(u), \cos((2i-1)u) > \tag{2.15}$$

which leads to the explicit expression for w_j:

$$w_j = \frac{4}{\pi} \int_0^{\frac{\pi}{2}} D_r(u) \cos((2j-1)u)du, \qquad j = 1, \ldots, \infty. \tag{2.16}$$

2.3.2 Design of an Array of Ring Radiators by the Equivalent Linear Array Method

The equivalent linear array method for the design of array of ring radiators is a technique in which all ring radiators are represented by a series of equivalent linear arrays. The directional response of the array of ring radiators is then the sum of the directivity functions of all equivalent linear arrays. The equivalent linear array of a ring radiator has in principle an infinite number of elements and associated weighting coefficients. In general, the amplitude of these coefficients decreases for elements far away from the centre of the array. It is therefore possible to truncate the equivalent linear array to a finite number of elements by disregarding

elements with small weighting coefficients. An equivalent linear array can also be found for a disc array. Because of the nature of Bessel function the weighting coefficients of a linear array equivalent to a disc radiator are small for elements far away from the array center. For a ring radiator a subtraction, however, is involved in the expression of the directivity function. Because of this subtraction the dominant weighting coefficients of the equivalent linear array become much smaller than that of the disc radiator. This causes the difficulty in truncation since the ratio between weighting coefficients is an important measure during the truncating. Furthermore, the computational round off error is doubled due to the subtraction. It is for this reason that we initially carry out the design using an array of disc radiators. We then transform such a disc array into the array of contiguous ring radiators having the same radiation pattern. Similar observations hold for arrays that is the weighting coefficients of a linear array equivalent to a disc array decrease much more rapidly than those of a ring array. This in turn introduces less error when the linear equivalent array is truncated. Truncation of the equivalent linear array is performed using the projecting process as described in Section 2.2. The truncated equivalent linear array of a ring radiator is the projection of its directivity function $D_i(u)$ into the subspace $\mathcal{M}_i$.

As an illustration of the above process, Fig. 2.2 shows radiation patterns of a disc radiator with $r = 5\lambda$ and its equivalent linear array truncated to 20 elements spaced by $d = \lambda/2$ (corresponding to 10 terms in the directivity function). We can observe only a small error (at higher order sidelobes) introduced by this truncation. It has been found that a similar truncation performed on an equivalent linear array to a ring radiator leads to much larger error.

To introduce the transformation, we consider an array of stacked discs as shown in Fig. 2.3(a). For the sake of exposition all concentric discs (and rings) are shown in a disassembled form. A disc radiator can be thought of as an assembly of concentric, contiguous ring radiators. This leads to an equivalent stacked ring array shown in disassembled form in Fig. 2.3(b). Finally, we construct

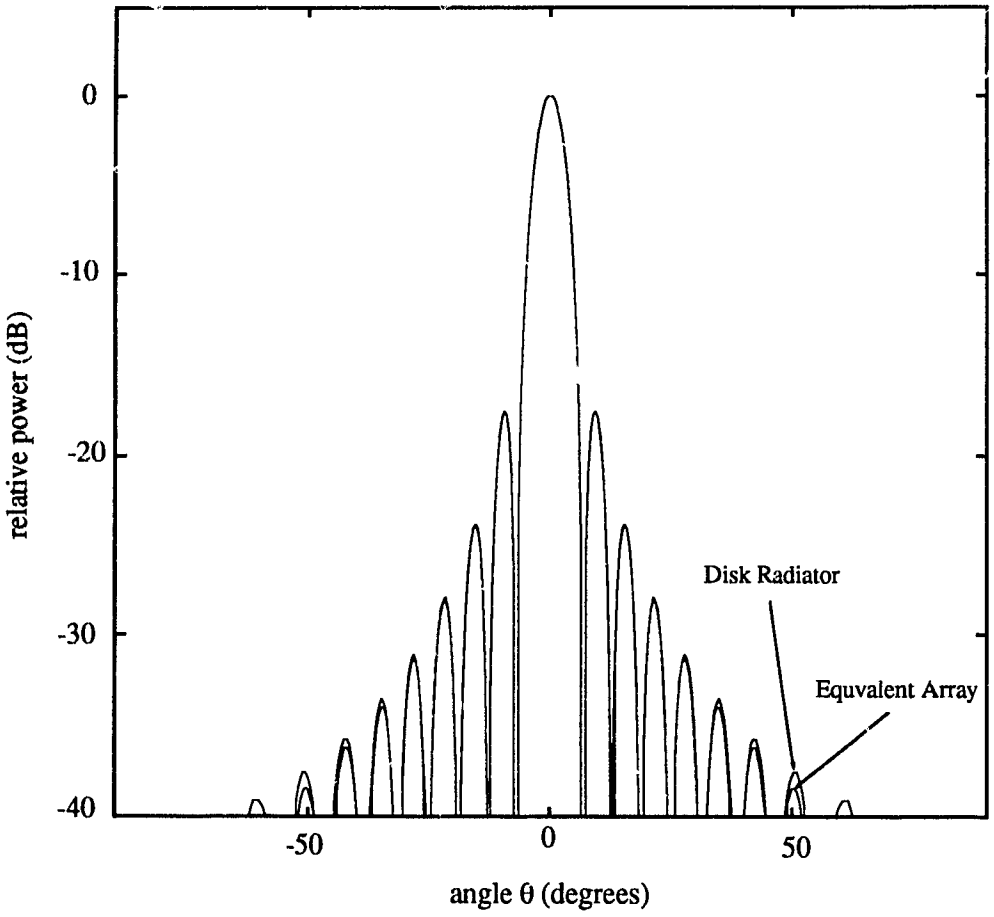

Figure 2.2: Beam patterns of a disc radiator with $r = 5\lambda$ and its equivalent linea array truncated to 20 elements (10 terms).

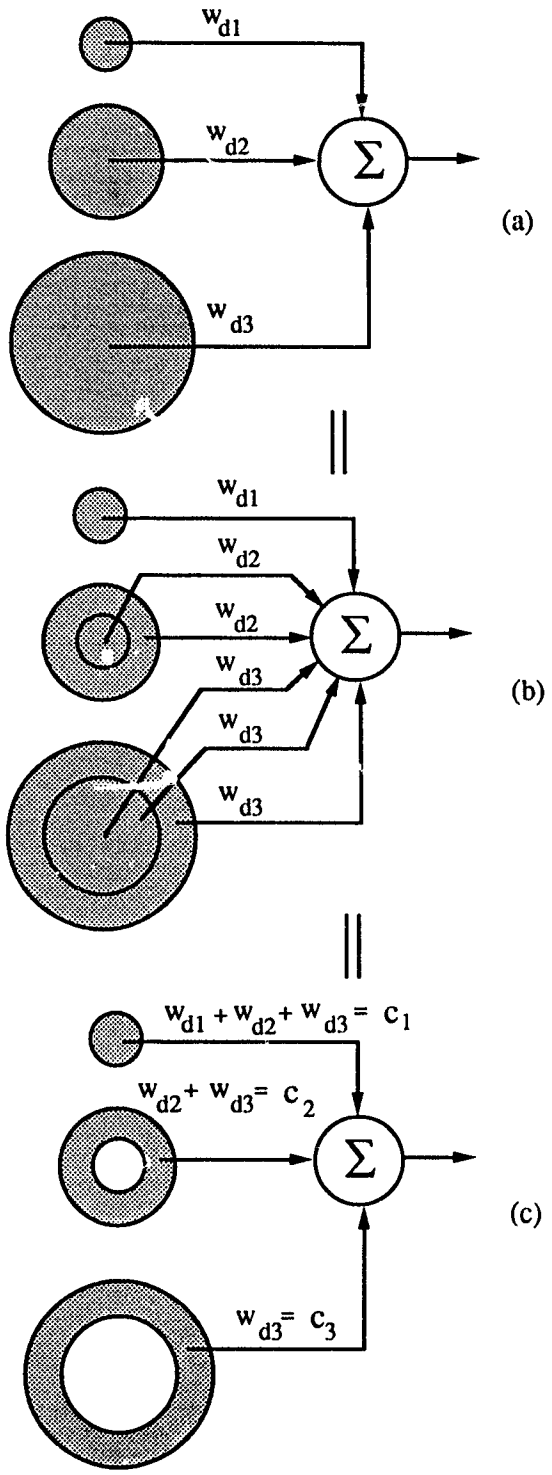

Figure 2.3: Identity of the array of disc radiators and the array of contiguous ring radiators. (a) Concentric disc array. (b) Equivalent stacked ring array. (c) Single layer ring array.

an equivalent, single layer concentric ring array with suitable weighting coefficients as shown in Fig. 2.3(c). In general, for a given vector of weighting coefficient $\mathbf{w}_d$ associated with a stacked disc array shown in Fig. 2.3(a), the vector of weighting coefficients $\mathbf{c}_r$ for an equivalent single layer ring array shown in Fig. 2.3(c) is given by

$$\mathbf{c}_r = \mathbf{A}\mathbf{w}_d \tag{2.17}$$

where the elements of matrix $\mathbf{A}$ are

$$a_{i,j} = \begin{cases} 1 & \text{for } i \leq j \\ 0 & \text{otherwise.} \end{cases} \tag{2.18}$$

The following are the design steps for obtaining the weighting coefficients for the array of contiguous ring radiators:

1. Design a linear array of point radiators which produces a desirable form of the directivity function (for example, associated with a Dolph-Chebyshev array). The N-dimensional column vector of weighting coefficients $\mathbf{w}_l$, spacing d, and size N of the array are therefore given [3]. We call such an array a *prototype*.

2. Consider a disc radiator and determine its radius in the follow steps:

   a) Select an arbitrary initial value of radius r for the disc.

   b) Find the equivalent linear array with spacing d of this disc. Such an array has in principle an infinite number of elements (and associated weighting coefficients). However, it can be truncated to a finite size N_r without an appreciable error in its radiation pattern. This can be done by neglecting coefficients with amplitudes less than a certain small percentage of the largest one. We denote this truncating threshold by δ. For a given size N_r of a truncated linear array the normalized

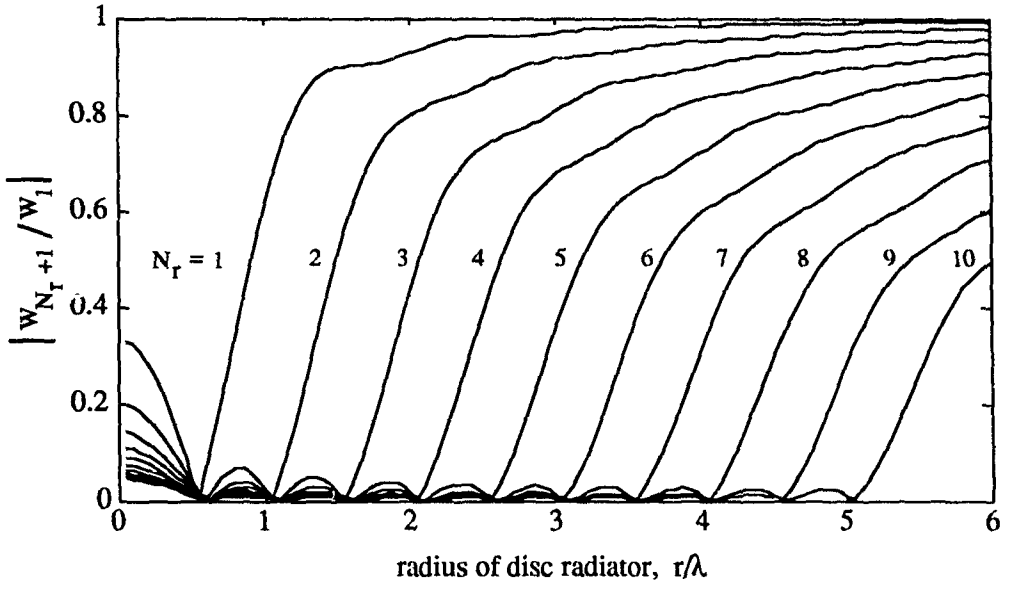

(a)

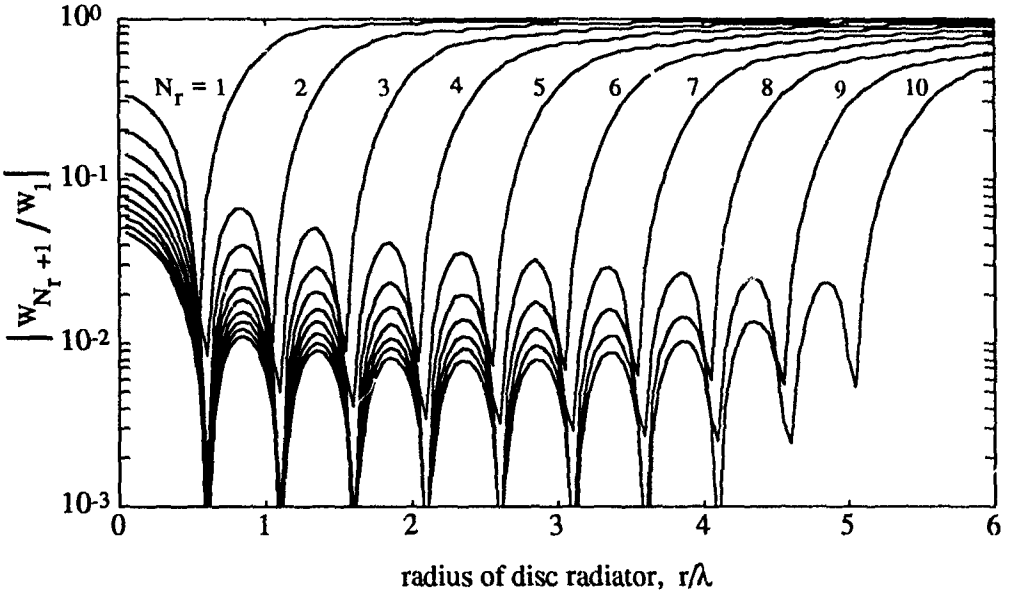

(b)

Figure 2.4: Weighting coefficient of a truncated equivalent linear array vs. radius of disc radiator for different values of N_r. (a) Linear scale. (b) Semi-logarithmic scale.

weighting coefficient $|w_{N_r+1}/w_1|$ is small and oscillates until the radius of a disc radiator reaches a certain critical value. Further increase in the radius leads to a rapid increase in coefficient values, as illustrated in Fig. 2.4 (a) (linear scale) and Fig. 2.4b (semi-logarithmic scale) for different values of N_r. The above information can be used to select the proper value of the truncating threshold δ. Fig. 2.5(a)-(c) shows N_r as a function of radius r for different choices of truncation threshold δ. We see that for a given size N_r of truncated linear array there is a certain tolerance in corresponding radius r of a disc radiator which satisfies a specified truncation threshold δ. The described method of choosing the disc radius allows us to monitor indirectly (through the amplitudes of discarded coefficients) the error introduced by truncation.

c) Vary radius r until $N_r = N$ for a certain $r = r_N$. Form the N-dimensional column vector of weighting coefficients $\mathbf{w}_N$:

$$\mathbf{w}_N = \begin{bmatrix} w_{1,N} \\ w_{2,N} \\ \vdots \\ w_{N,N} \end{bmatrix}. \tag{2.19}$$

3. Reduce the radius $r = r_N$ of the disc radiator until its equivalent linear array has the size of $N-1$ for a certain $r = r_{N-1} < r_N$. The augmented vector of weighting coefficients $\mathbf{w_{N-1}}$ is then formed as

$$\mathbf{w}_{N-1} = \begin{bmatrix} w_{1,N-1} \\ w_{2,N-1} \\ \vdots \\ w_{N-1,N-1} \\ 0 \end{bmatrix}. \tag{2.20}$$

4. Repeat step 3 to obtain an equivalent linear array of size $N-2, N-3, \ldots, 1$,

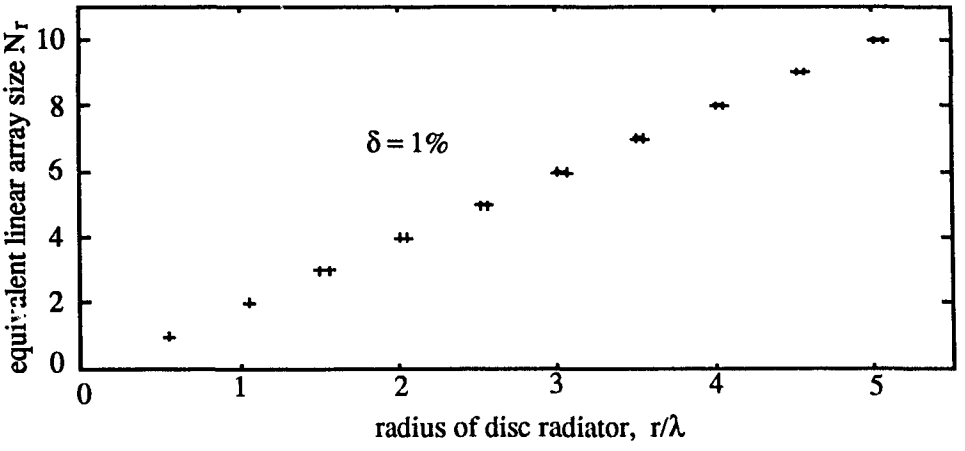

(a)

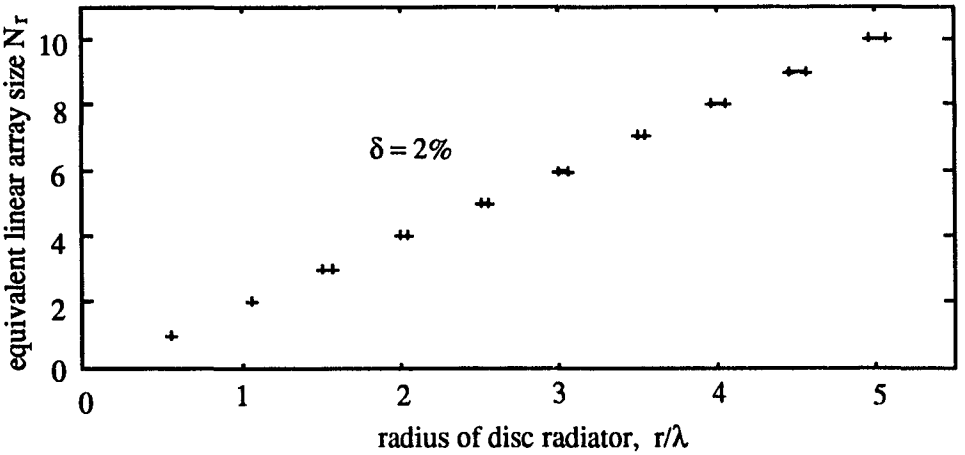

(b)

Figure 2.5: Size of equivalent linear array vs. radius of disc radiator for different truncation threshold δ. (a) $\delta = 1\%$. (b) $\delta = 2\%$. (c) $\delta = 3\%$.

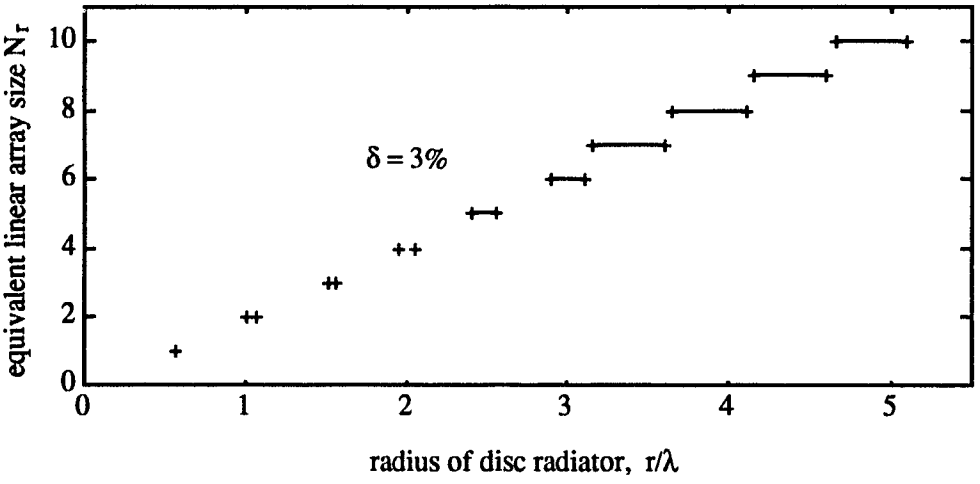

(c)

Figure 2.5: (Continued)

and form the subsequent augmented vectors of weighting coefficients:

$$\mathbf{w}_{N-2} = \begin{bmatrix} w_{1,N-2} \\ w_{2,N-2} \\ \vdots \\ w_{N-2,N-2} \\ 0 \\ 0 \end{bmatrix} \tag{2.21}$$

$$\mathbf{w}_{N-3} = \begin{bmatrix} w_{1,N-3} \\ w_{2,N-3} \\ \vdots \\ w_{N-3,N-3} \\ 0 \\ 0 \\ 0 \end{bmatrix} \tag{2.22}$$

etc.

5. Form the matrix of the weighting coefficients $\mathbf{W}$ as

$$\mathbf{W} = [\mathbf{w}_1, \mathbf{w}_2 \cdots \mathbf{w}_N]. \tag{2.23}$$

6. Solve the matrix equation

$$\mathbf{W}\mathbf{w}_d = \mathbf{w}_l \tag{2.24}$$

to obtain the vector of weighting coefficients $\mathbf{w}_d$ of disc radiators. Since the vectors $\mathbf{w}_1$, $\mathbf{w}_2, \ldots$, are projections of the directivity functions in the subspaces they are linearly independent. Thus the matrix $\mathbf{W}$ has full rank and the matrix equation (2.23) has an unique solution.

7. The vector of weighting coefficients of ring radiators $\mathbf{c}_r$ is then found according to Eq. (2.17) by the matrix equation:

$$\mathbf{c}_r = \mathbf{A}\mathbf{w}_d \tag{2.25}$$

where the elements of matrix **A** are given by Eq. (2.18).

This procedure does not result in a final radiation pattern exactly equal to the original radiation pattern of the prototype postulated in step 1 because of truncation errors. It does, however, approximate the required pattern very accurately.

To illustrate these points, we designed an array by applying the above design technique to a Dolph-Chebyshev linear array as a prototype [35]. We assumed that the prototype had 20 elements spaced by $d = \lambda/2$. Various degrees of sidelobe suppression were postulated in the prototype. The design of the ring array with closely matched radiation patterns was then performed. A truncation tolerance $\delta = 1\%$ was chosen, which resulted in a ring array of diameter 10λ consisting of 10 rings. The resulting radiation patterns are shown in Fig. 2.6(a)-(d) for 30 dB, 40 dB, 50 dB and 60 dB postulated side-lobe suppression, respectively. The dotted lines indicate the radiation patters of the Dolph-Chebyshev prototypes. We see that the resulting radiation patterns are almost identical to those of the postulated Dolph-Chebyshev prototypes. We observe that 60 dB sidelobe suppression in broad vicinity of the main lobe is possible in this example. This is a substantial improvement compared to the radiation pattern of a single disc radiator of the same size shown in Fig. 2.2. The corresponding normalized weighting coefficients and ring sizes are tabulated in Table 2.1.

2.4 Summary

An equivalent linear array approach is developed for the design of an array with ring radiators which is capable of producing a search-light-type beam with greatly suppressed sidelobes. A design procedure is proposed which benefits from the existing design techniques developed for linear arrays. The results indicate that radiation patterns with arbitrary sidelobe suppression can be achieved.

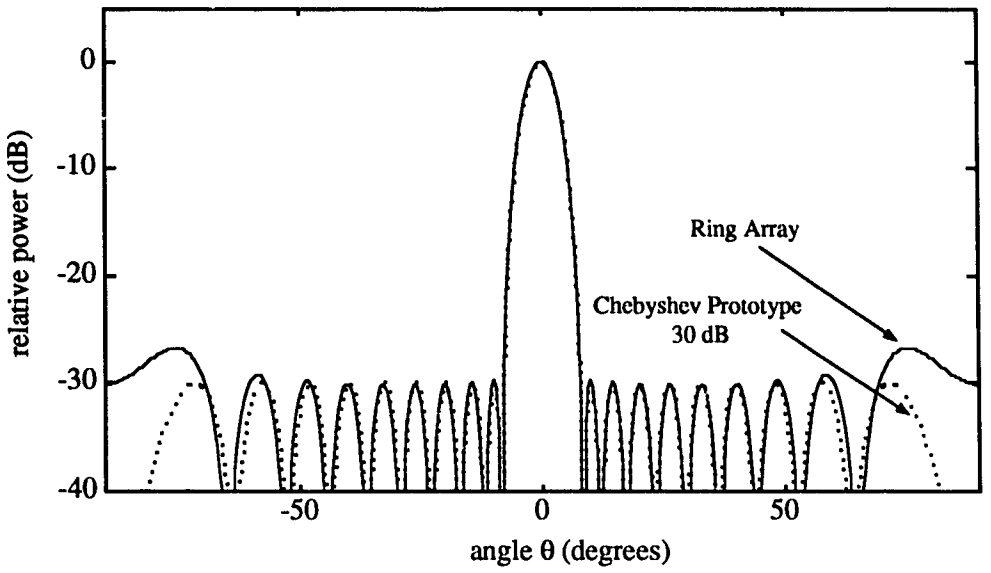

(a)

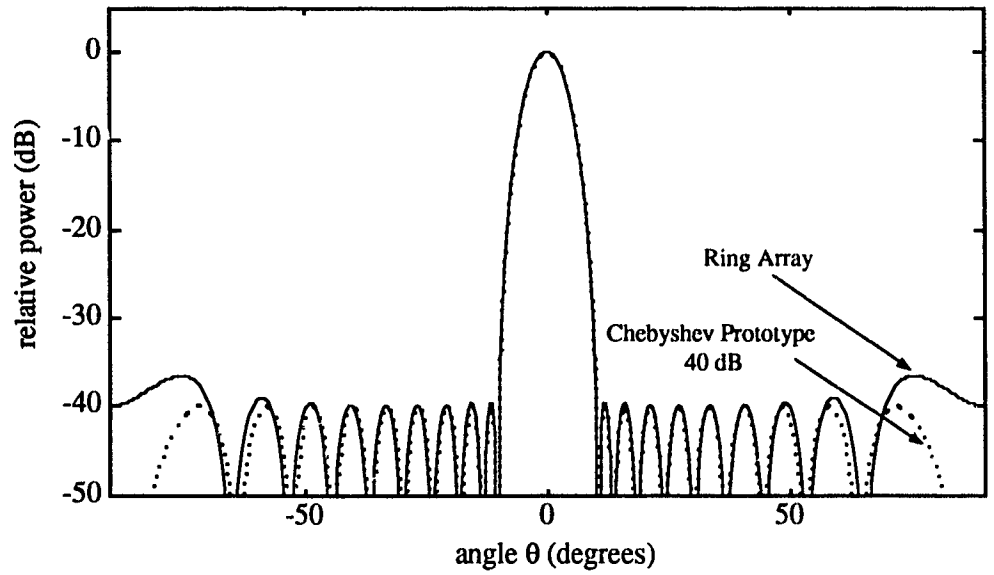

(b)

Figure 2.6: Beam patterns of an array of 10 ring radiators compared with Chebyshev prototypes (dotted line). (a) Postulated 30 dB sidelobe suppression in the prototype. (b) Postulated 40 dB sidelobe suppression in the prototype. (c) Postulated 50 dB sidelobe suppression in the prototype. (d) Postulated 60 dB sidelobe suppression in the prototype.

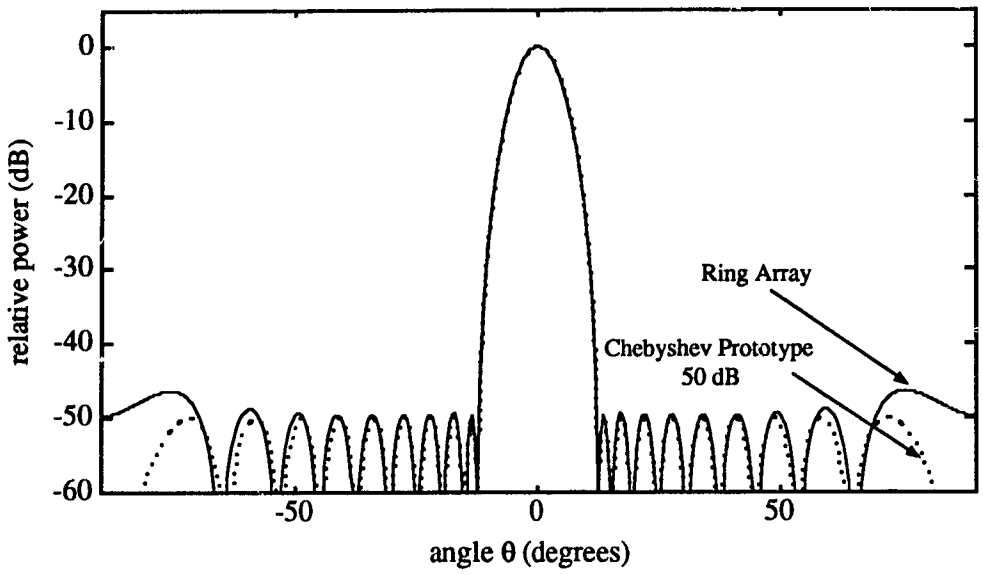

(c)

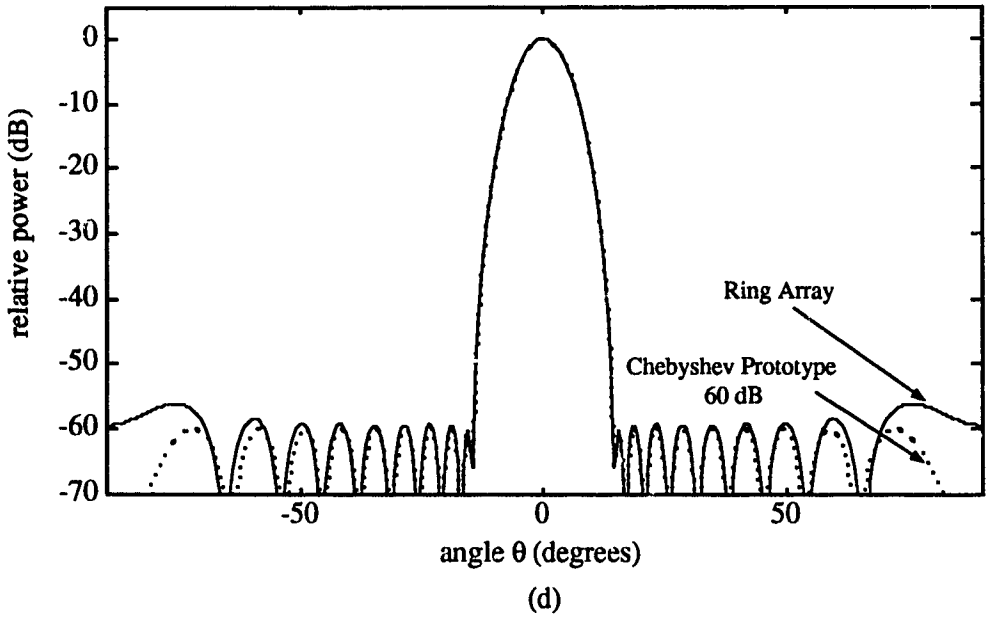

(d)

Figure 2.6: (Continued)

Table 2.1: Weighting coefficients of a array of ring radiators for different sidelobe suppression levels

Ring No.	Radius	Weighting Coefficient			
i	a_i/λ	30 dB	40 dB	50 dB	60 dB
1	0.5	0.8730	0.9994	1.0000	1.0000
2	1.0	1.0000	1.0000	0.9618	0.9446
3	1.5	0.7947	0.8874	0.8600	0.8319
4	2.0	0.8894	0.8275	0.7470	0.6913
5	2.5	0.6262	0.6629	0.5948	0.5305
6	3.0	0.7268	0.5830	0.4631	0.3811
7	3.5	0.3904	0.3971	0.3154	0.2449
8	4.0	0.5792	0.3500	0.2193	0.1462
9	4.5	0.0083	0.1374	0.1058	0.0683
10	5.0	0.7203	0.2445	0.0877	0.0353

Chapter 3

Design Considerations

In Chapter 2, we proposed novel acoustic arrays of circular ring radiators which can generate search-light-type beams with greatly reduced sidelobes. In this chapter we consider several aspects associated with the implementation of such an array.

3.1 Introduction

Recently developed piezoelectric polymeric materials, are now available in the form of film and wire, and enable construction of inexpensive and innovative acoustic arrays. The material KYNAR is one example. The use of arrays instead of single radiators makes it possible to tailor radiation patterns to almost any desired shape, and to increase the gain and power-handling capability.

A convenient procedure to design a novel array of ring radiators was described in Chapter 2. The array design example was shown to generate a symmetric search-light type narrow beam with greatly reduced sidelobes. Such a narrow beam can find several applications related to acoustic remote sensing, telemetry and specialized sonars.

In this chapter several practical aspects associated with the implementation of such an array are investigated. Specifically, the important aspect of sensitivity of the radiation pattern to finite tolerances associated with array implementation

is addressed. The results are presented in a tabular form convenient for designers. The proposed configuration can be readily implemented as a receiving array using piezoelectric film or as a transmitting/receiving array using concentric hollow cylinders operating in longitudinal mode. A compact receiving/transmitting configuration is also described in this chapter in which the transmitting element is a piston, while the receiving array consists of the same transmitting piston surrounded by several concentric rings made of piezoelectric film or several concentric hollow cylinders operating in longitudinal mode. It is shown that such a configuration allows for good sidelobe suppression in the combined transmitting/receiving radiation pattern even for simple arrays.

3.2 Modified Design Procedures

3.2.1 Principles of Circular Ring Array Design

A novel array configuration proposed in Chapter 2 consists of concentric ring transducers of different diameters, as illustrated in Fig. 3.1. Because of its radial symmetry, this array generates identical radiation pattern in any plane perpendicular to its face and passing through its centre. It was demonstrated in Chapter 2 that the radiation pattern in such a plane can be approximated to an arbitrary degree by the radiation pattern of a linear array placed on its face and passing through its centre, as illustrated in Fig. 3.1 (summing network for linear array is not shown). We call such an array an equivalent linear array. The above observation can be utilized for the design of a ring array with arbitrary radiation pattern. A similar consideration applies to an array of stacked concentric disc radiators; by applying it, one can take advantage of the theory developed for linear arrays.

The design procedure for obtaining the weighting coefficients and the size of the array of ring radiators with zero gap between rings consists of the following steps (the procedure presented here is a summary of design procedures described in Chapter 2):

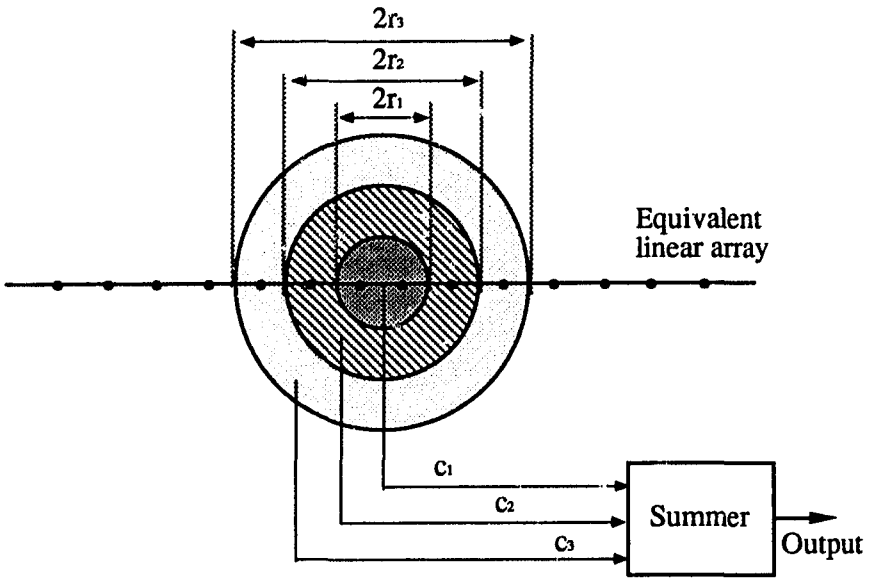

Figure 3.1: Front face of an array of ring radiators and its equivalent linear array.

1. Design a prototype linear array of point radiators which produces a desirable form of radiation pattern (for example, associated with Dolph-Chebyshev array). As a result, the vector of weighting coefficients **d**, the spacing which is half wavelength $\lambda/2$, and the size $2N$ (number of elements) of the array are obtained [3].

2. Consider a series of N disc radiators with diameters of $1\lambda, 2\lambda, \ldots, N\lambda$, and find their equivalent linear arrays with size of $2N$ by properly selecting their weighting coefficients.

3. Arrange the weighting coefficients of equivalent linear arrays to form a matrix of weighting coefficients as described in Chapter 2.

4. Find the weighting coefficients of the disc array by inverting the matrix formed in step 3 and multiplying it by the vector of weighting coefficients **d** of the prototype formed in step 1.

5. The weighting coefficients of a ring array are then derived from the weighting coefficients of the disc array by applying the superposition principle.

3.2.2 Design of Circular Ring Arrays with Nonzero Gaps between Rings

The design method proposed in Chapter 2 is restricted to the case of an array formed by several concentric contiguous (no gaps between) rings. However, this restriction can be removed by modifying the method. The modified design method contains the following steps:

1. Design a ring array with no gaps between ring radiators using the proposed method in Chapter 2 as outlined in Section 3.2.1.

2. Fix the outer radius of each ring radiator and reduce the inner radius to create a gap between rings.

3. Find the equivalent linear arrays of the ring radiators obtained in step 2 and use their weighting coefficients to reform the matrix of the weighting coefficients.

4. Solve the matrix equation and obtain the weighting coefficients of a ring array with gaps between rings.

Allowing a gap between the rings gives an additional degree of freedom in the design. By varying the gap we can reduce the truncation error and obtain a better approximation of the required radiation pattern than that of a ring array without gap between rings.

To illustrate these points, we performed an array design by applying the above technique to a Dolph-Chebyshev linear array as a prototype [35]. We assumed a prototype of 20 elements spaced by $d = \lambda/2$ with 30 dB postulated sidelobe suppression. We then followed the design example from Chapter 2 which resulted in a 10-ring array without gaps and with outer diameter of 10λ. We next proceed with the modified procedure described in Section 3.2.2. (step 2 through 4) for various gap sizes but equal to all rings. The resulting radiation patterns are shown in Fig. 3.2(a)-(c) for various gap sizes between rings.

We see that the resulting radiation patterns are almost identical to those of postulated Dolph-Chebyshev prototypes. We also observe the improvement in sidelobe suppression compared to that in the radiation pattern of a single disc radiator of the same size. The corresponding normalized weighting coefficients and ring sizes are tabulated in Table 3.1.

We also investigated the sensitivity of weighting coefficients to the width of the gap between rings. The results for a 10-ring array are shown in Fig. 3.3(a)-(d) for different postulated sidelobe suppression in the prototype linear array. The flatness of the curves suggests that the radiation pattern of a ring array is not sensitive to the manufacture tolerance for radii of ring radiators.

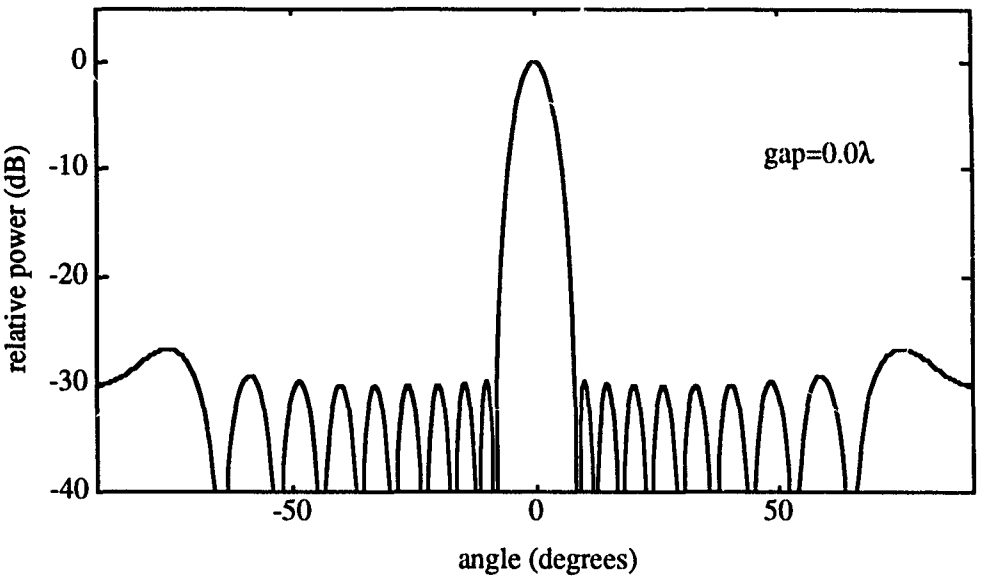

(a)

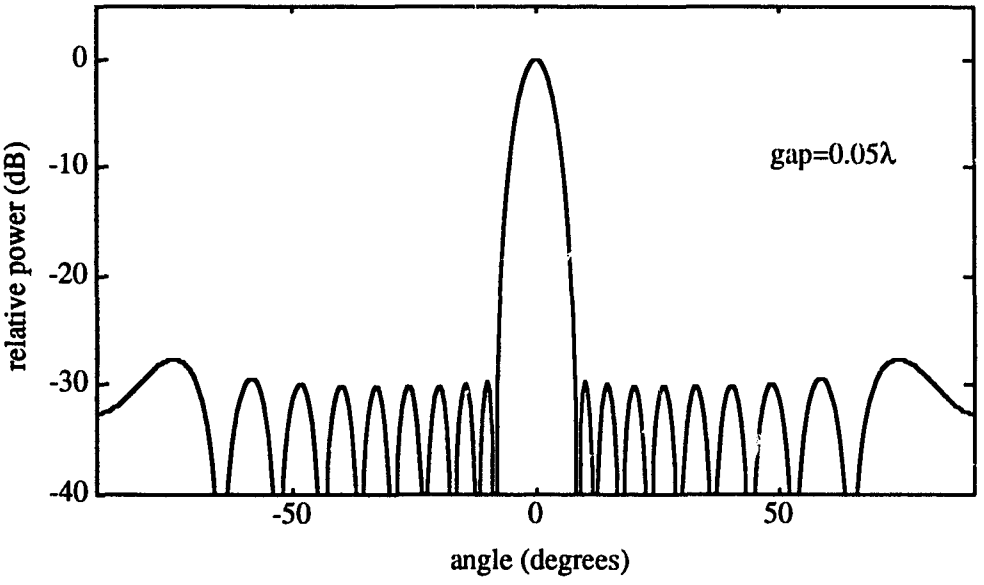

(b)

Figure 3.2: Radiation patterns of an array of 10 ring radiators with various gap sizes and postulated 30 dB sidelobe suppression in Dolph-Chebyshev prototype. (a) Gap = 0.0λ. (b) Gap = 0.05λ. (c) Gap = 0.1λ. (d) Gap = 0.15λ. (e) Gap = 0.2λ. (f) Gap = 0.25λ.

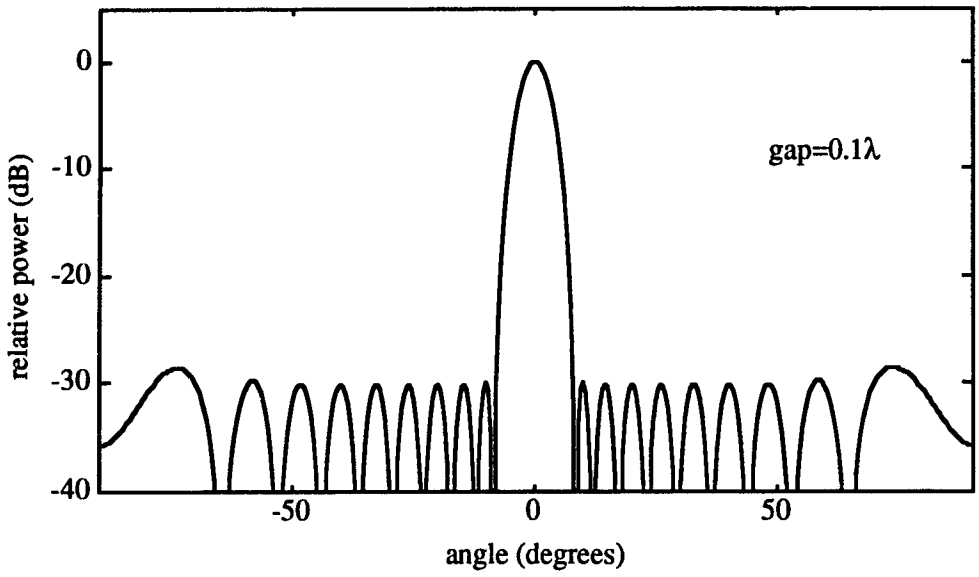

(c)

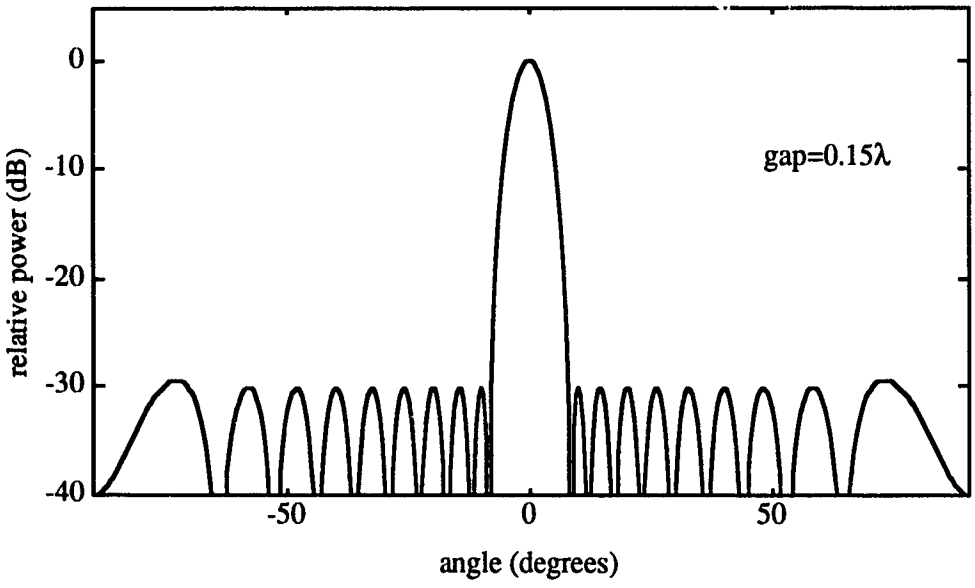

(d)

Figure 3.2: (Continued)

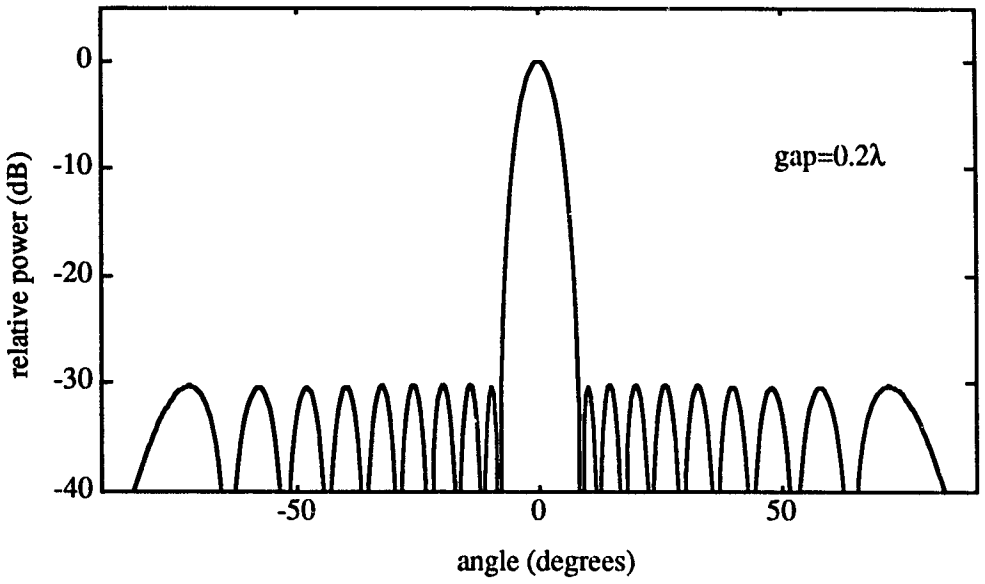

(e)

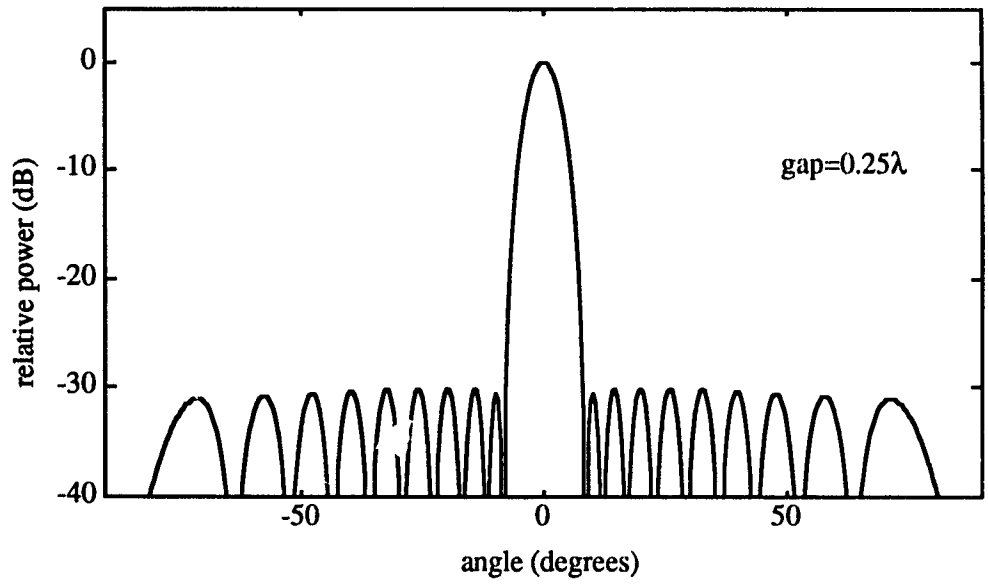

(f)

Figure 3.2: (Continued)

Table 3.1: Weighting coefficients of a circular ring array for different gap widths between rings

Radius	Weighting Coefficient for different gap					
r_i/λ	0.0λ	0.05λ	0.10λ	0.15λ	0.20λ	0.25λ
0.5	0.8730	0.9129	0.9423	0.9691	0.9982	1.0000
1.0	1.0000	1.0000	1.0000	1.0000	1.0000	0.9682
1.5	0.7947	0.8441	0.8774	0.9010	0.9199	0.9082
2.0	0.8894	0.8808	0.8727	0.8663	0.8620	0.8326
2.5	0.6262	0.6716	0.7032	0.7256	0.7427	0.7334
3.0	0.7268	0.7082	0.6906	0.6756	0.6637	0.6340
3.5	0.3904	0.4347	0.4679	0.4929	0.5122	0.5115
4.0	0.5792	0.5443	0.5107	0.4800	0.4528	0.4154
4.5	0.0083	0.0533	0.0929	0.1276	0.1581	0.1796
5.0	0.7203	0.7072	0.6900	0.6718	0.6545	0.6190

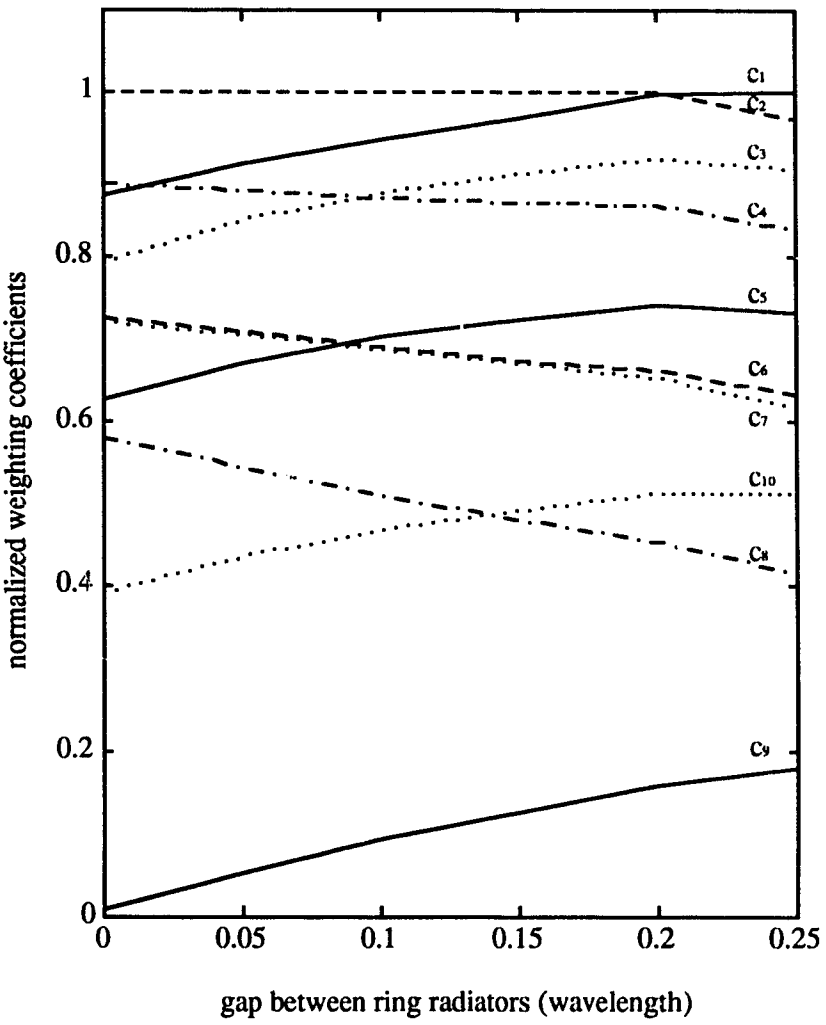

(a)

Figure 3.3: Weighting coefficients as a function of ring gap for a 10-ring array. (a) Postulated 30 dB sidelobe suppression. (b) Postulated 40 dB sidelobe suppression. (c) Postulated 50 dB sidelobe suppression. (d) Postulated 60 dB sidelobe suppression.

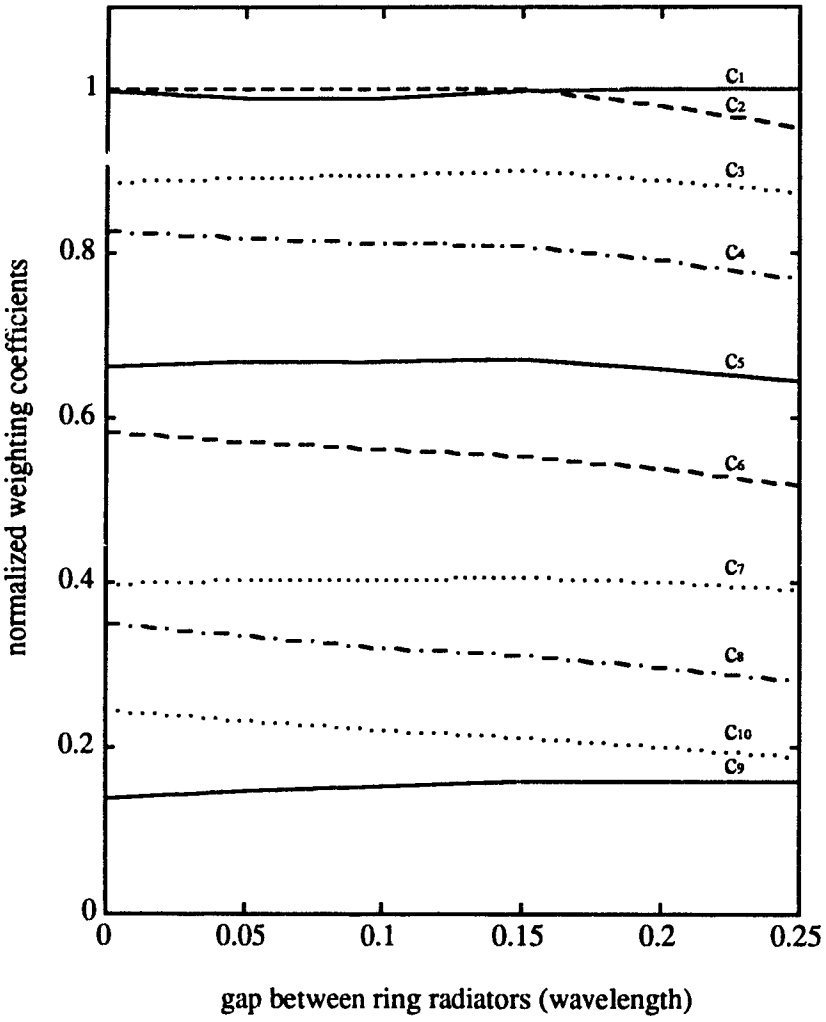

(b)

Figure 3.3: (Continued)

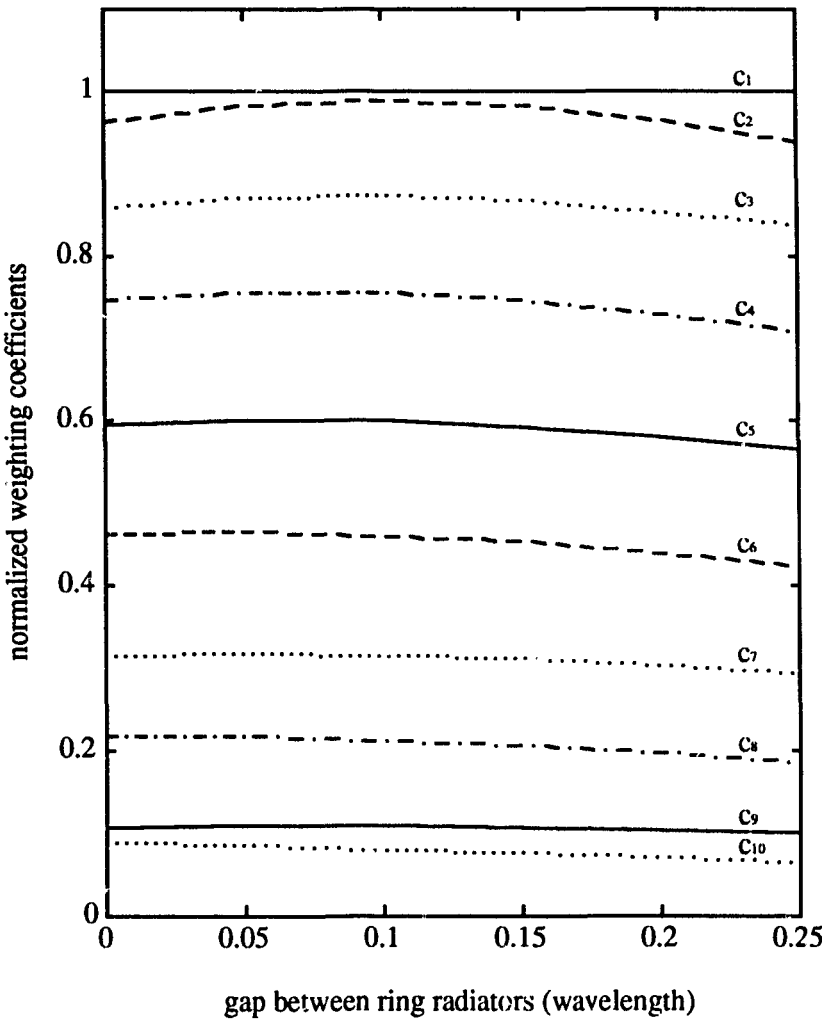

(c)

Figure 3.3: (Continued)

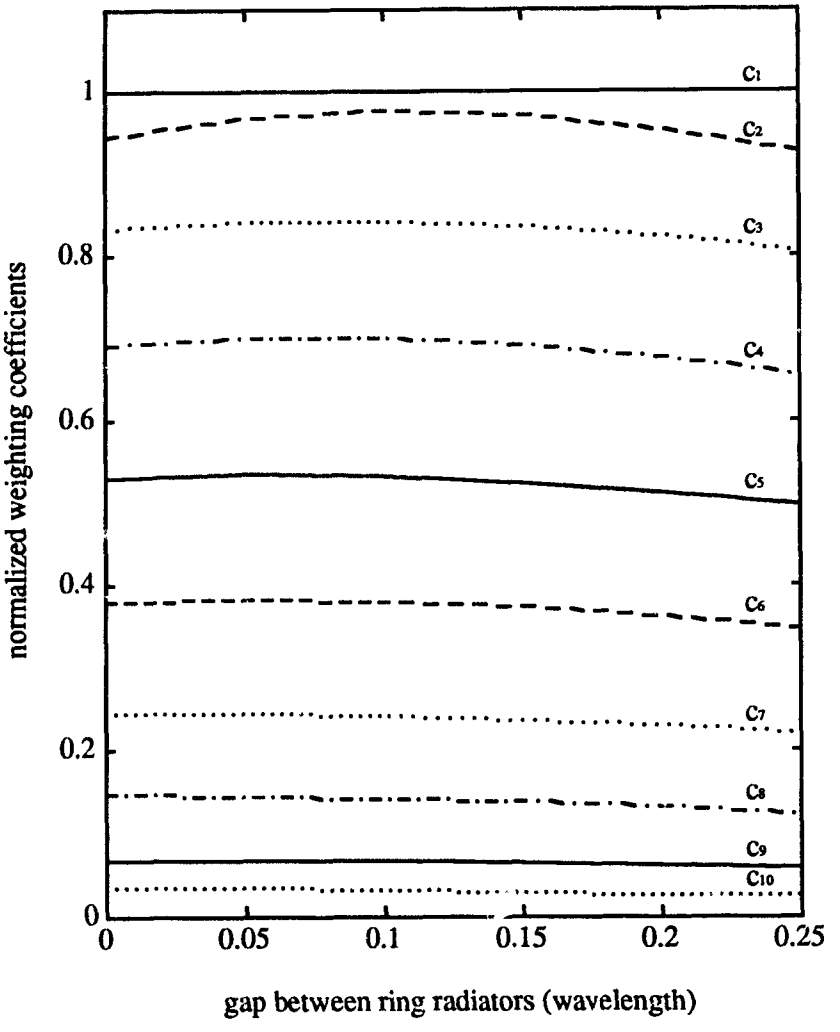

(d)

Figure 3.3: (Continued)

3.2.3 Design of Circular Ring Arrays with Reduced Number of Rings

Any radiation pattern achievable by a prototype array can be approximated by a properly designed ring array. It was shown in Chapter 2 that the minimum number of rings required for the best approximation in the sense of minimum mean square error is equal to half the number of elements in the prototype array. Any further increase in the number of rings will not reduce the approximation error. On the other hand, it is possible to reduce the number of rings in the array and still maintain an acceptable radiation pattern. This reduction must be done gradually and must be accompanied with suitable readjustment of the weighting coefficients.

To this effect we have modified the design procedure described in Chapter 2 to the following steps:

1. Design a prototype linear array of point radiators which produces a desired radiation pattern (for example associated with a Dolph-Chebyshev array). Therefore, the vector of weighting coefficients $\mathbf{w}_p$, spacing which is half wavelength $\lambda/2$, and size $2N$ (number of elements) of the array are obtained [3].

2. Select an arbitrary number $M(M < N)$ of ring radiators with outer diameters of $n_1\lambda$, $n_2\lambda, \ldots$, $n_{M-1}\lambda$, $N\lambda$, where $n_i < n_{i+1} < N$, and $i = 1, 2, \ldots, M-2$, are arbitrary integers. The rings have arbitrary widths of t_1, $t_2, \ldots$, t_M, such that there is no overlap between rings. Using the formula given in Chapter 2 we can find a truncated linear array equivalent to each ring and its associated vectors of weighting coefficients $\mathbf{w}_1$, $\mathbf{w}_2$, ..., $\mathbf{w}_M$. The selection of outer diameters $n_i\lambda$ of ring radiators involved in this step ensures that M vectors of weighting coefficients $\mathbf{w}_1$, $\mathbf{w}_2$, ..., $\mathbf{w}_M$ are linearly independent.

3. Form the matrix of the weighting coefficients $\mathbf{W}$ as

$$\mathbf{W} = [\mathbf{w}_1, \mathbf{w}_2 \ldots \mathbf{w}_M]. \tag{3.1}$$

4. Solve the matrix equation

$$\mathbf{W}^T\mathbf{W}\mathbf{w}_r = \mathbf{W}^T\mathbf{w}_p \tag{3.2}$$

to obtain the vector of weighting coefficients $\mathbf{w}_r$ of the ring array, where $\mathbf{W}^T$ is the transpose of matrix $\mathbf{W}$ and

$$\mathbf{w}_r = (\mathbf{W}^T\mathbf{W})^{-1}\mathbf{W}\mathbf{w}_p. \tag{3.3}$$

Since the vectors of weighting coefficients $\mathbf{w}_1$, $\mathbf{w}_2$, ..., $\mathbf{w}_M$, are linearly independent, $\mathbf{W}^T\mathbf{W}$ in Eq. (3.2) is nonsingular.

The vector $\mathbf{w}_r$ is the optimum solution in the sense of minimum mean square error ϵ^2 between the radiation pattern of the prototype obtained in step 1 and that of the ring array; the mean square error ϵ^2 is given by

$$\epsilon^2 = (\mathbf{W}\mathbf{w}_r - \mathbf{w}_p)^T(\mathbf{W}\mathbf{w}_r - \mathbf{w}_p) \tag{3.4}$$

The derivation of Eqs. (3.3) and (3.4) is given in Appendix A.

We will next apply the above procedure and monitor the error as well as the resulting radiation patterns for different parameters chosen. In all examples in this section contiguous rings have been assumed, that is $t_1 = t_2 = \cdots = t_M = \lambda/2$. The assumed prototype is a 20-element Dolph-Chebyshev linear array. Shown in Fig. 3.4 is the relative error $\epsilon^2/\mathbf{w}_p^T\mathbf{w}_p$ as a function of the number of ring radiators for postulated sidelobe suppression of 30 dB, 40 dB, 50 dB and 60 dB in the prototype. The graph illustrates the earlier statement that the minimum number of ring radiators is 10. Further increase of this number to 11 and 12 will not reduce the error. For the same prototype, the effect of reducing the number of

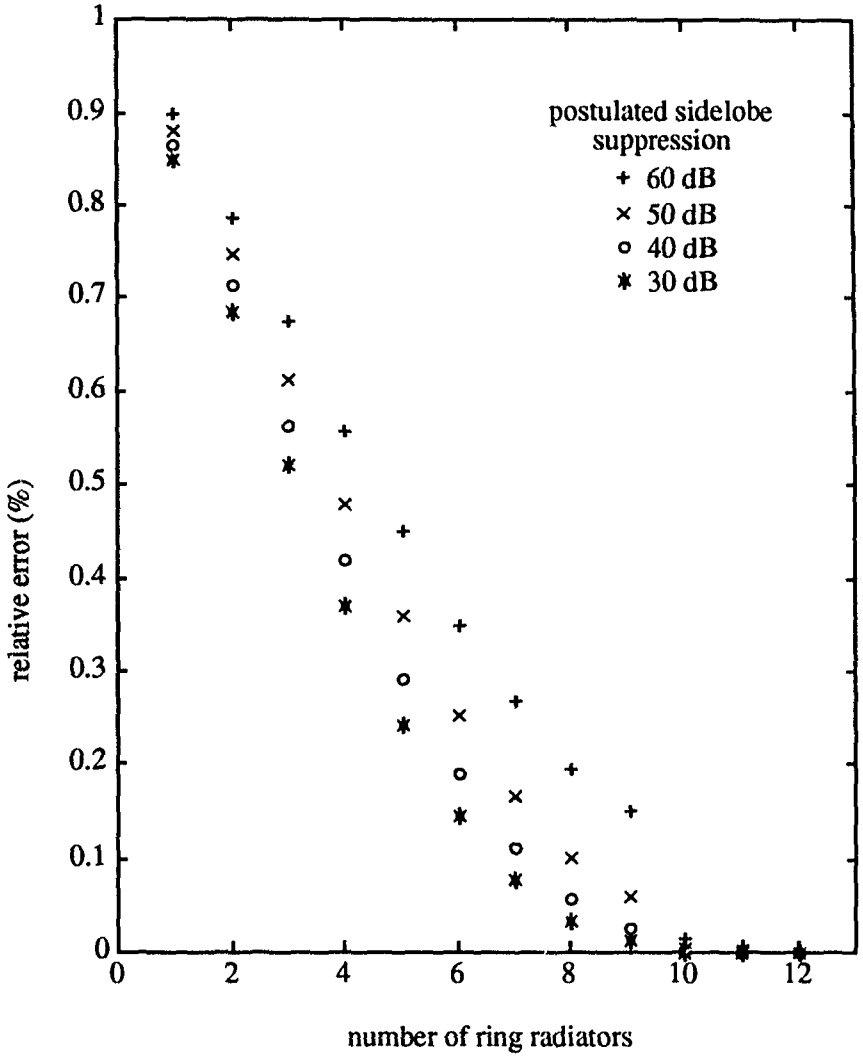

Figure 3.4: Relative error as a function of the number of ring radiators for different postulated sidelobe suppression levels.

rings was investigated. Specifically, we removed the central circular ring (9 rings left) and then removed the central circular ring plus a neighboring ring (8 rings left). The design procedure described earlier was followed to calculate weighting coefficients in each case. The resultant radiation pattern is shown in Fig. 3.5(a) (9-ring array) and Fig. 3.5(b) (8-ring array). For comparison the radiation pattern of the complete 10-ring array is plotted in a dotted line. As shown in Fig. 3.5, the radiation pattern deteriorates rapidly with the number of rings removed from the centre of the array.

However, by investigating several other possible cases it was found that by increasing n_1 and t_1, i.e., by increasing the diameter of the central circular ring, we can greatly reduce the number M of rings and still maintain an acceptable resulting radiation pattern. This reduction in the number of rings must be done on a gradual basis and must be accompanied with suitable readjustment of the weighting coefficients. The proper procedure is to reduce M by one at a time (increase n_1 by one) and for each case find $\mathbf{w}_r$ as well as the associated radiation pattern. This process is repeated until a minimum M is reached which still yields an acceptable radiation pattern. The beamwidth of the radiation pattern of the array is determined by the ring with the largest diameter. When a second largest ring is added to the array its first nulls contribute to the radiation pattern in such a way as to reduce the original first sidelobes. The central ring with the smallest diameter, however, contributes only to the high order sidelobe reducing in the region far away from the main lobe. Since the radiation pattern of a ring array has much lower sidelobes in this region we can increase the diameter of the central ring (reduce the number of rings) and still obtain an acceptable radiation pattern. We will illustrate this process with the design examples to be discussed in Section 3.4.

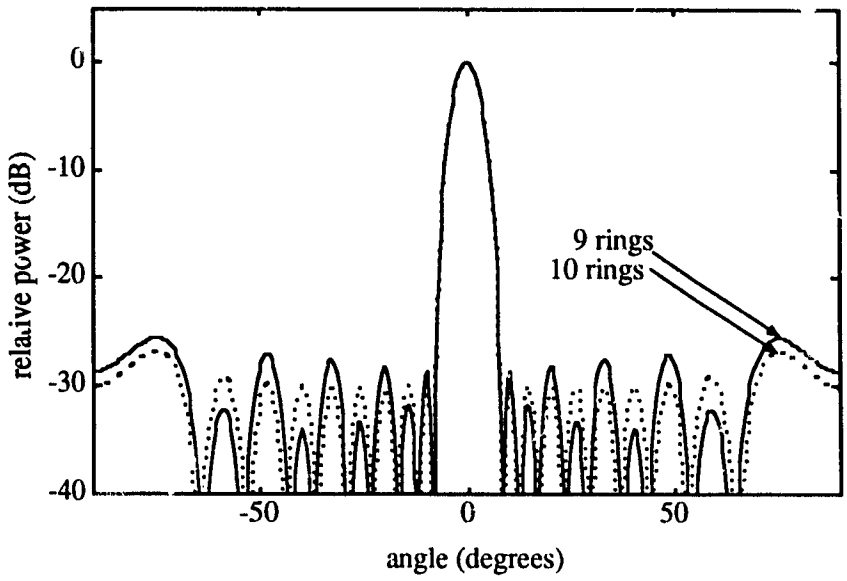

(a)

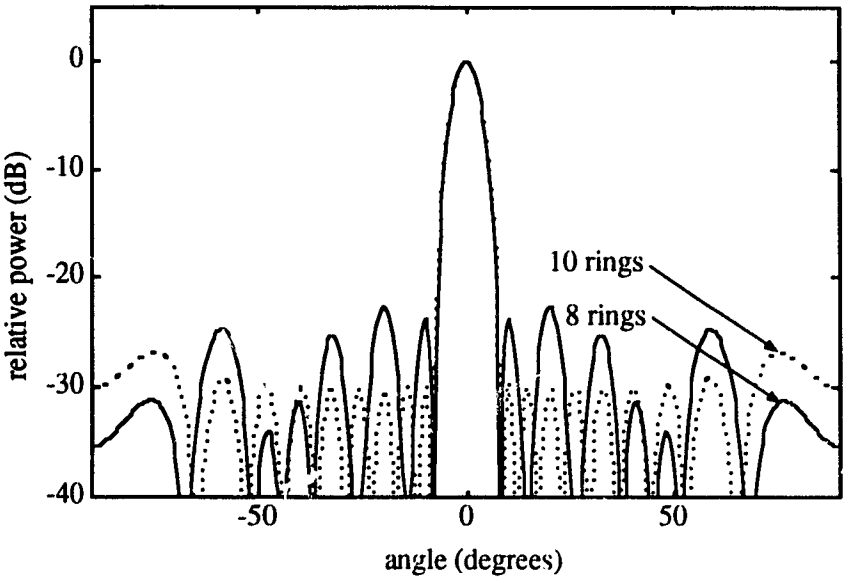

(b)

Figure 3.5: Radiation patterns of ring arrays with removed central elements.

3.3 Aspects of Implementation of Acoustic Ring Arrays

We discuss here several practical aspects associated with implementation of an acoustic ring array. Specifically, the sensitivity of the radiation pattern to finite tolerances associated with array implementation is addressed. The results are presented in a tabular form convenient for a designer.

3.3.1 Design Table

Based on the modified design procedure described in Section 3.2.2, the weighting coefficients of the equivalent linear array of a ring radiator for different outer radii r_i and different gap widths are tabulated in Table 3.2-3.4. The use of this table is illustrated in the following example.

We start with a desired radiation pattern of beamwidth $\psi = 15°$ and sidelobe suppression of 26 dB. We find that the Chebyshev linear array prototype requires 10 elements with spacing $d = \lambda/2$ between the elements. The weighting coefficients of the prototype are found to be [32]

$$\begin{aligned} a_1 &= 5.8377 \\ a_2 &= 5.2073 \\ a_3 &= 4.1184 \\ a_4 &= 2.8308 \\ a_5 &= 2.0860. \end{aligned}$$

The radiation pattern of the prototype is presented in Fig. 3.6 with a dotted line. Using Table 3.3 we form the weighting coefficient matrix of the equivalent linear arrays by picking up the data at the most upper-left part of the table. Since the size of the prototype linear array is 10, only the data at the intersection of the first 5 rows and the first 5 columns in Table 3.3 (for an ring array with 0.1λ gap between rings) are needed to form the weighting coefficient matrix, which is

Table 3.2: Weighting coefficients of the equivalent linear array of a circular ring radiator with gap of 0.0λ for different outer radii

Term No.	Weighting Coefficient for Different Outer Radii						
	0.5λ	1.0λ	1.5λ	2.0λ	2.5λ	3.0λ	3.5λ
1	0.4010	0.5782	0.4940	0.5148	0.4969	0.5066	0.4981
2	-0.0175	0.6188	0.7202	0.5199	0.5519	0.5053	0.5248
3	0.0160	-0.0374	0.7719	0.8405	0.5567	0.5911	0.5216
4	-0.0122	0.0326	-0.0447	0.8993	0.9460	0.5949	0.6295
5	0.0097	-0.0255	0.0392	-0.0504	1.0108	1.0411	0.6323
6	-0.0081	0.0208	-0.0309	0.0440	-0.0553	1.1111	1.1283
7	0.0069	-0.0176	0.0254	-0.0347	0.0481	-0.0598	1.2032
8	-0.0060	0.0152	-0.0216	0.0286	-0.0378	0.0518	-0.0639
9	0.0053	-0.0134	0.0188	-0.0243	0.0311	-0.0406	0.0552
10	-0.0047	0.0120	-0.0167	0.0212	-0.0265	0.0333	0.0431
11	0.0043	-0.0108	0.0150	-0.0189	0.0231	-0.0283	0.0353
12	-0.0039	0.0099	-0.0136	0.0170	-0.0206	0.0248	-0.0300
13	0.0036	-0.0091	0.0124	-0.0155	0.0186	0.0220	0.0262
14	-0.0033	0.0084	-0.0115	0.0142	-0.0169	0.0199	0.0233
15	0.0031	-0.0078	0.0107	-0.0131	0.0156	-0.0181	0.0210
16	-0.0029	0.0073	-0.0100	0.0122	-0.0144	0.0167	-0.0192
17	0.0027	-0.0069	0.0093	-0.0114	0.0134	-0.0155	0.0177
18	-0.0026	0.0065	-0.0088	0.0107	-0.0126	0.0144	0.0164
19	0.0024	-0.0061	0.0083	-0.0101	0.0118	-0.0135	0.0153
20	-0.0023	0.0058	-0.0079	0.0096	-0.0112	0.0127	0.0143
21	0.0022	-0.0055	0.0075	-0.0091	0.0106	-0.0120	0.0135
22	-0.0021	0.0053	-0.0071	0.0087	-0.0101	0.0114	0.0128

$$\begin{bmatrix} 0.3812 & 0.4506 & 0.3969 & 0.4100 & 0.3984 \\ -0.0112 & 0.5608 & 0.5469 & 0.4182 & 0.4368 \\ 0.0122 & -0.0169 & 0.6961 & 0.6309 & 0.4476 \\ -0.0095 & 0.0196 & -0.0189 & 0.8094 & 0.7055 \\ 0.0076 & -0.0159 & 0.0229 & -0.0205 & 0.9088 \end{bmatrix}.$$

The weighting coefficients c_i of the ring array consisting of 5 rings can be determined by

Table 3.2: (Continued)

Term No.	Weighting Coefficient for Different Outer Radii						
	4.0λ	4.5λ	5.0λ	5.5λ	6.0λ	6.5λ	7.0λ
1	0.5039	0.4986	0.5026	0.4990	0.5019	0.4992	0.5014
2	0.5018	0.5149	0.5006	0.5101	0.5001	0.5074	0.4998
3	0.5460	0.5109	0.5284	0.5063	0.5196	0.5040	0.5144
4	0.5408	0.5680	0.5226	0.5431	0.5142	0.5302	0.5096
5	0.6665	0.5611	0.5903	0.5356	0.5584	0.5233	0.5414
6	0.6683	0.7020	0.5817	0.6123	0.5493	0.5738	0.5331
7	1.2092	0.7029	0.7361	0.6021	0.6339	0.5634	0.5893
8	1.2886	1.2851	0.7361	0.7688	0.6223	0.6550	0.5775
9	-0.9678	1.3688	1.3567	0.7681	0.8003	0.6422	0.6757
10	0.0584	-0.0714	1.4445	1.4248	0.7989	0.8307	0.6616
11	-0.0454	0.0613	-0.0749	1.5165	1.4898	0.8287	0.8601
12	0.0371	-0.0476	0.0642	-0.0782	1.5852	1.5520	0.8574
13	-0.0315	0.0388	-0.0497	0.0669	-0.0814	1.6510	1.6119
14	0.0275	-0.0329	0.0405	-0.0517	0.0695	-0.0844	1.7143
15	-0.0244	0.0287	-0.0343	0.0420	-0.0536	0.0719	-0.0873
16	0.0221	-0.0255	0.0298	-0.0355	0.0435	-0.0554	0.0744
17	-0.0201	0.0230	-0.0265	0.0309	-0.0367	0.0449	-0.0572
18	0.0185	-0.0210	0.0239	-0.0274	0.0319	-0.0379	0.0463
19	-0.0172	0.0193	-0.0218	0.0247	-0.0283	0.0329	0.0390
20	0.0161	-0.0179	0.0201	-0.0225	0.0255	-0.0292	0.0339
21	-0.0151	0.0167	-0.0186	0.0207	-0.0232	0.0263	-0.0300
22	0.0142	-0.0157	0.0174	-0.0192	0.0214	-0.0239	0.0270

Table 3.2: (Continued)

Term No.	Weighting Coefficient for Different Outer Radii						
	7.5λ	8.0λ	8.5λ	9.0λ	9.5λ	10.0λ	10.5λ
1	0.4993	0.5011	0.4994	0.5009	0.4995	0.5008	0.4996
2	0.5056	0.4997	0.5045	0.4997	0.5037	0.4996	0.5031
3	0.5026	0.5111	0.5018	0.5089	0.5012	0.5073	0.5009
4	0.5225	0.5068	0.5175	0.5050	0.5140	0.5038	0.5115
5	0.5163	0.5312	0.5120	0.5244	0.5091	0.5197	0.5071
6	0.5530	0.5238	0.5402	0.5178	0.5318	0.5138	0.5258
7	0.5435	0.5648	0.5317	0.5496	0.5212	0.5394	0.5190
8	0.6046	0.5541	0.5766	0.5400	0.5590	0.5308	0.5472
9	0.5916	0.6198	0.5648	0.5884	0.5485	0.5686	0.5378
10	0.6959	0.6057	0.6348	0.5756	0.6002	0.5571	0.5782
11	0.6807	0.7157	0.6196	0.6496	0.5864	0.6119	0.5658
12	0.8886	0.6993	0.7350	0.6333	0.6642	9.5972	0.6235
13	0.8853	0.9162	0.7175	0.7538	0.6469	0.6785	0.6079
14	1.6696	0.9124	0.9431	0.7354	0.7723	0.6603	0.6926
15	1.7753	1.7254	0.9387	0.9692	0.7529	0.7903	0.6735
16	-0.0902	1.8344	1.7794	0.9643	0.9947	0.7700	0.8080
17	0.0767	-0.0930	1.8915	1.8319	0.9893	1.0195	0.7868
18	-0.0589	0.0789	-0.0956	1.9470	1.8829	1.0137	1.0437
19	0.0476	-0.0605	0.0811	-0.0982	2.0010	1.9325	1.0375
20	-0.0401	0.0489	-0.0622	0.0833	-0.1008	2.0536	1.9809
21	0.0348	-0.0412	0.0502	-0.0637	0.0853	-0.1032	2.1048
22	-0.0308	0.0357	-0.0422	0.0514	-0.0653	0.0874	-0.1057

Table 3.3: Weighting coefficients of the equivalent linear array of a circular ring radiator with gap of 0.1λ for different outer radii

Ter	Weighting Coefficient for Different Outer Radii						
No.	0.5λ	1.0λ	1.5λ	2.0λ	2.5λ	3.0λ	3.5λ
1	0.3812	0.4506	0.3969	0.4100	0.3984	0.4045	0.3990
2	-0.0112	0.5608	0.5469	0.4182	0.4368	0.4060	0.4177
3	0.0122	-0.0169	0.6961	0.6309	0.4476	0.4658	0.4195
4	-0.0095	0.0196	-0.0189	0.8094	0.7355	0.4780	0.4945
5	0.0076	-0.0159	0.0229	-0.0205	0.9088	0.7731	0.5077
6	-0.0063	0.0131	-0.0187	0.0253	-0.0220	0.9984	0.8355
7	0.0054	-0.0111	0.0156	-0.0208	0.0275	-0.0234	1.0807
8	-0.0047	0.0097	-0.0134	0.0174	-0.0225	0.0294	-0.0247
9	0.0042	-0.0085	0.0117	-0.0149	0.0188	-0.0240	0.0312
10	-0.0037	0.0076	-0.0104	0.0130	-0.0161	0.0200	-0.0254
11	0.0034	-0.0069	0.0093	-0.0116	0.0141	-0.0172	0.0212
12	-0.0031	0.0063	-0.0085	0.0105	-0.0126	0.0151	-0.0181
13	0.0028	-0.0058	0.0078	-0.0096	0.0114	-0.0135	0.0159
14	-0.0026	0.0054	-0.0072	0.0088	-0.0104	0.0122	-0.0142
15	0.0025	-0.0050	0.0067	0.0081	0.0096	-0.0111	0.0128
16	-0.0023	0.0047	-0.0062	0.0076	-0.0089	0.0102	-0.0117
17	0.0022	-0.0044	0.0058	-0.0071	0.0083	-0.0095	0.0108
18	-0.0020	0.0041	-0.0055	0.0067	-0.0078	0.0089	-0.0100
19	0.0019	-0.0039	0.0052	-0.0063	0.0073	-0.0083	0.0094
20	-0.0018	0.0037	-0.0049	0.0060	-0.0069	0.0078	-0.0088
21	0.0017	-0.0035	0.0047	-0.0057	0.0065	-0.0074	0.0083
22	-0.0017	0.0034	-0.0045	0.0054	-0.0062	0.0070	-0.0078

Table 3.3: (Continued)

Term No.	Weighting Coefficient for Different Outer Radii						
	4.0λ	4.5λ	5.0λ	5.5λ	6.0λ	6.5λ	7.0λ
1	0.4026	0.3993	0.4017	0.3994	0.4012	0.3996	0.4009
2	0.4027	0.4106	0.4014	0.4071	0.4007	0.4052	0.4004
3	0.4334	0.4104	0.4207	0.4063	0.4142	0.4042	0.4101
4	0.4351	0.4500	0.4200	0.4318	0.4128	0.4222	0.4089
5	0.5224	0.4515	0.4669	0.4306	0.4434	0.4203	0.4308
6	0.5363	0.5492	0.4681	0.4837	0.4418	0.4552	0.4281
7	0.8935	0.5639	0.5751	0.4846	0.5003	0.4532	0.4671
8	1.1571	0.9480	0.5903	0.6000	0.5009	0.5165	0.4646
9	-0.0260	1.2287	0.9996	0.6158	0.6240	0.5168	0.5324
10	0.0329	-0.0272	1.2965	1.0486	0.6403	0.6472	0.5325
11	-0.0267	0.0345	-0.0283	1.3608	1.0955	0.6640	0.6696
12	0.0222	-0.0280	0.0360	-0.0294	1.4223	1.1405	0.6870
13	-0.0190	0.0232	-0.0291	0.0374	-0.0305	1.4812	1.1837
14	0 0167	-0.0198	0.0241	-0.0303	0.0388	-0.0315	1.5378
15	-0.0149	0.0174	-0.0206	0.0250	-0.0314	0.0402	0.0325
16	0.0134	-0.0155	0.0180	-0.0214	0.0259	-0.0324	0.0415
17	-0.0123	0.0140	-0.0161	0.0187	-0.0221	0.0267	0.0334
18	0.0113	-0.0128	0.0145	-0.0166	0.0193	-0.0227	0.0275
19	-0.0105	0.0118	-0.0133	0.0150	-0.0171	0.0198	0.0234
20	0.0098	-0.0110	0.0122	-0.0137	0.0155	-0.0176	0.0204
21	-0.0092	0.0102	-0.0114	0.0126	-0.0141	0.0159	0.0181
22	0.0087	-0.0096	0.0106	-0.0117	0.0130	0.0145	0.0164

Table 3.3: (Continued)

Term No.	Weighting Coefficient for Different Outer Radii						
	7.5λ	8.0λ	8.5λ	9.0λ	9.5λ	10.0λ	10.5λ
1	0.3996	0.4007	0.3997	0.4006	0.3997	0.4005	0.3998
2	0.4020	0.4002	0.4031	0.4001	0.4025	0.4000	0.4021
3	0.4029	0.4080	0.4021	0.4064	0.4016	0.4052	0.4012
4	0.4165	0.4065	0.4128	0.4049	0.4103	0.4038	0.4084
5	0.4145	0.4231	0.4108	0.4181	0.4083	0.4146	0.4066
6	0.4397	0.4206	0.4301	0.4156	0.4237	0.4122	0.4193
7	0.4368	0.4487	0.4271	0.4373	0.4208	0.4296	0.4164
8	0.4789	0.4454	0.4578	0.4338	0.4446	0.4262	0.4356
9	0.4760	0.4906	0.4541	0.4670	0.4408	0.4520	0.4319
10	0.5480	0.4874	0.5023	0.4629	0.4761	0.4478	0.4594
11	0.5478	0.5632	0.4986	0.5137	0.4716	0.4852	0.4548
12	0.6914	0.5628	0.5781	0.5097	0.5250	0.4803	0.4942
13	0.7092	0.7125	0.5774	0.5927	0.5206	0.5361	0.4890
14	1.2255	0.7308	0.7331	0.5918	0.6070	0.5314	0.5470
15	1.5925	1.2658	0.7518	0.7531	0.6058	0.6209	0.5420
16	-0.0335	1.6453	1.3050	0.7722	0.7726	0.6196	0.6346
17	0.0427	-0.0344	1.6965	1.3429	0.7921	0.7916	0.6331
18	-0.0344	0.0440	-0.0353	1.7462	1.3799	0.8115	0.8102
19	0.0283	-0.0353	0.0451	-0.0362	1.7945	1.4159	0.8305
20	-0.0240	0.0290	-0.0362	0.0463	-0.0371	1.8415	1.4509
21	0.0209	-0.0247	0.0298	-0.0371	0.0474	-0.0380	1.8874
22	-0.0186	0.0215	-0.0253	0.0305	-0.0380	0.0485	-0.0388

Table 3.4: Weighting coefficients of the equivalent linear array of a circular ring radiator with gap of 0.2λ for different outer radii

Term No.	Weighting Coefficient for Different Outer Radii						
	0.5λ	1.0λ	1.5λ	2.0λ	2.5λ	3.0λ	3.5λ
1	0.3240	0.3263	0.3009	0.3052	0.3002	0.3022	0.3001
2	0.0045	0.4641	0.3840	0.3195	0.3217	0.3076	0.3103
3	0.0029	0.0094	0.5733	0.4369	0.3130	0.3408	0.3187
4	-0.0029	0.0033	0.0131	0.6651	0.4847	0.3668	0.3602
5	0.0025	-0.0039	0.0032	0.0160	0.7459	0.5285	0.3899
6	-0.0021	0.0036	-0.0042	0.0031	0.0184	0.8188	0.5691
7	0.0018	-0.0032	0.0040	-0.0045	0.0031	0.0206	0.8858
8	-0.0016	0.0028	-0.0036	0.0043	-0.0047	0.0031	0.0226
9	0.0014	-0.0025	0.0033	-0.0039	0.0045	-0.0048	0.0031
10	-0.0013	0.0023	-0.0030	0.0036	-0.0042	0.0047	-0.0050
11	0.0012	-0.0021	0.0027	-0.0032	0.0038	0.0044	0.0049
12	-0.0011	0.0019	-0.0025	0.0030	-0.0035	0.0040	0.0046
13	0.0010	-0.0018	0.0023	-0.0027	0.0032	-0.0037	0.0042
14	-0.0009	0.0016	-0.0021	0.0025	-0.0029	0.0034	0.0038
15	0.0009	-0.0015	0.0020	-0.0024	0.0027	-0.0031	0.0035
16	-0.0008	0.0014	-0.0019	0.0022	-0.0026	0.0029	0.0033
17	0.0008	-0.0014	0.0017	-0.0021	0.0024	0.0027	0.0030
18	-0.0007	0.0013	-0.0016	0.0020	-0.0023	0.0025	0.0028
19	0.0007	-0.0012	0.0016	-0.0019	0.0021	-0.0024	0.0027
20	-0.0006	0.0011	-0.0015	0.0018	-0.0020	0.0023	0.0025
21	0.0006	-0.0011	0.0014	-0.0017	0.0019	-0.0022	0.0024
22	-0.0006	0.0010	-0.0013	0.0016	-0.0018	0.0020	0.0023

Table 3.4: (Continued)

Term No.	Weighting Coefficient for Different Outer Radii						
	4.0λ	4.5λ	5.0λ	5.5λ	6.0λ	6.5λ	7.0λ
1	0.3012	0.3000	0.3008	0.3000	0.3006	0.3000	0.3004
2	0.3040	0.3061	0.3024	0.3040	0.3016	0.3029	0.3011
3	0.3207	0.3105	0.3127	0.3067	0.3086	0.3047	0.3063
4	0.3312	0.3320	0.3184	0.3202	0.3121	0.3140	0.3086
5	0.3793	0.3442	0.3436	0.3268	0.3282	0.3182	0.3199
6	0.4122	0.3978	0.3571	0.3552	0.3356	0.3364	0.3246
7	0.6070	0.4335	0.4156	0.3700	0.3668	0.3445	0.3447
8	0.9480	0.6428	0.4540	0.4329	0.3826	0.3782	0.3534
9	0.0244	1.0065	0.6766	0.4737	0.4497	0.3950	0.3894
10	0.0031	0.0260	1.0617	0.7089	0.4927	0.4659	0.4071
11	-0.0052	0.0031	0.0276	1.1142	0.7398	0.5110	0.4816
12	0.0051	-0.0054	0.0032	0.0291	1.1643	0.7695	0.5287
13	-0.0047	0.0053	-0.0055	0.0032	0.0305	1.2123	0.7981
14	0.0043	-0.0049	0.0055	-0.0057	0.0032	0.0319	1.2586
15	-0.0040	0.0045	-0.0051	0.0056	-0.0059	0.0033	0.0331
16	0.0037	-0.0041	0.0046	-0.0052	0.0058	-0.0060	0.0033
17	-0.0034	0.0038	-0.0043	0.0048	-0.0054	0.0060	-0.0062
18	0.0032	-0.0035	0.0039	-0.0044	0.0049	-0.0055	0.0061
19	-0.0030	0.0033	-0.0036	0.0040	-0.0045	0.0051	-0.0057
20	0.0028	-0.0031	0.0034	-0.0037	0.0042	-0.0046	0.0052
21	-0.0026	0.0029	-0.0032	0.0035	-0.0039	0.0043	-0.0047
22	0.0025	-0.0027	0.0030	-0.0033	0.0036	-0.0040	0.0044

Table 3.4: (Continued)

Term No.	Weighting Coefficient for Different Outer Radii						
	7.5λ	8.0λ	8.5λ	9.0λ	9.5λ	10.0λ	10.5λ
1	0.3000	0.3003	0.3000	0.3003	0.3000	0.3002	0.3000
2	0.3022	0.3008	0.3017	0.3007	0.3014	0.3005	0.3011
3	0.3034	0.3048	0.3026	0.3038	0.3020	0.3031	0.3016
4	0.3104	0.3064	0.3080	0.3050	0.3061	0.3040	0.3052
5	0.3132	0.3149	0.3100	0.3116	0.3078	0.3093	0.3063
6	0.3261	0.3181	0.3197	0.3138	0.3155	0.3110	0.3125
7	0.3312	0.3324	0.3232	0.3248	0.3180	0.3196	0.3114
8	0.3531	0.3379	0.3389	0.3285	0.3299	0.3223	0.3238
9	0.3623	0.3614	0.3447	0.3454	0.3339	0.3352	0.3267
10	0.4004	0.3711	0.3696	0.3515	0.3518	0.3394	0.3404
11	0.4189	0.4112	0.3798	0.3777	0.3583	0.3583	0.3448
12	0.4968	0.4305	0.4218	0.3884	0.3858	0.3650	0.3648
13	0.5458	0.5116	0.4418	0.4321	0.3968	0.3937	0.3717
14	0.8256	0.5625	0.5260	0.4529	0.4422	0.4051	0.4015
15	1.3031	0.8523	0.5787	0.5401	0.4637	0.4522	0.4133
16	0.0344	1.3463	0.8782	0.5944	0.5538	0.4743	0.4619
17	0.0034	0.0356	1.3880	0.9034	0.6098	0.5672	0.4847
18	-0.0063	0.0034	0.0368	1.4286	0.9279	0.6248	0.5803
19	0.0063	-0.0064	0.0035	0.0379	1.4680	0.9517	0.6394
20	-0.0058	0.0064	-0.0066	0.0035	0.0390	1.5064	0.9750
21	0.0053	-0.0059	0.0066	-0.0067	0.0035	0.0401	1.5439
22	-0.0049	0.0054	-0.0061	0.0067	-0.0069	0.0036	0.0411

$$\begin{bmatrix} 0.3812 & 0.4506 & 0.3969 & 0.4100 & 0.3984 \\ -0.0112 & 0.5608 & 0.5469 & 0.4182 & 0.4368 \\ 0.0122 & -0.0169 & 0.6961 & 0.6309 & 0.4476 \\ -0.0095 & 0.0196 & -0.0189 & 0.8094 & 0.7055 \\ 0.0076 & -0.0159 & 0.0229 & -0.0205 & 0.9088 \end{bmatrix}^{-1} \begin{bmatrix} a_1 \\ a_2 \\ a_3 \\ a_4 \\ a_5 \end{bmatrix}.$$

The c_i coefficients obtained are (in normalized form)

$$\begin{aligned} c_1 &= 1.0000 \\ c_2 &= 0.8620 \\ c_3 &= 0.7655 \\ c_4 &= 0.3861 \\ c_5 &= 0.5697. \end{aligned}$$

The radiation pattern corresponding to the above example is shown in Fig. 3.6 by solid line. The outer radii of rings are 2.5λ, 2.0λ, 1.5λ, 1.0λ and 0.5λ, respectively, while the width of rings is 0.4λ. To illustrated the symmetry of the radiation pattern, the three-dimensional radiation pattern is plotted in Fig. 3.7.

3.3.2 Effect of Array Finite Tolerance on the Beam Pattern of a Ring Array

Another practical aspect which needs to be investigated is the effect of finite tolerance of the weighting coefficients in the summing network producing array output and the finite tolerance of the dimension of rings.

If we ignore the approximation error in the radiation patterns between the prototype linear array and the resultant ring array, we may represent the directivity function of the ring array by that of the linear array, that is

$$D(\theta) = \sum_{j=1}^{N} d_j \cos((2j-1)\frac{\pi}{2}\sin\theta) \tag{3.5}$$

where d_j are the weighting coefficients of the prototype linear array.

The vector $\mathbf{d}$ of the weighting coefficients of the prototype linear array can be

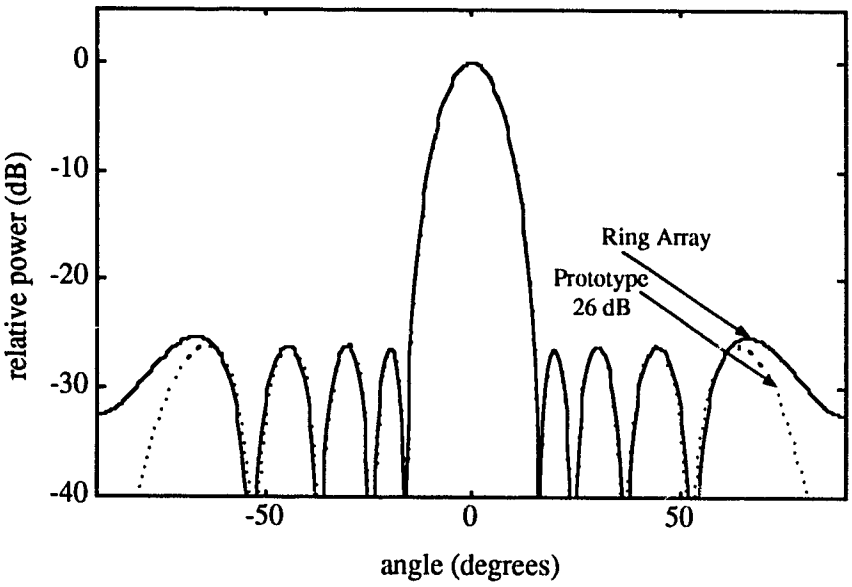

Figure 3.6: Radiation pattern of a 5-ring array with postulated 26 dB sidelobe suppression in Dolph-Chebyshev prototype.

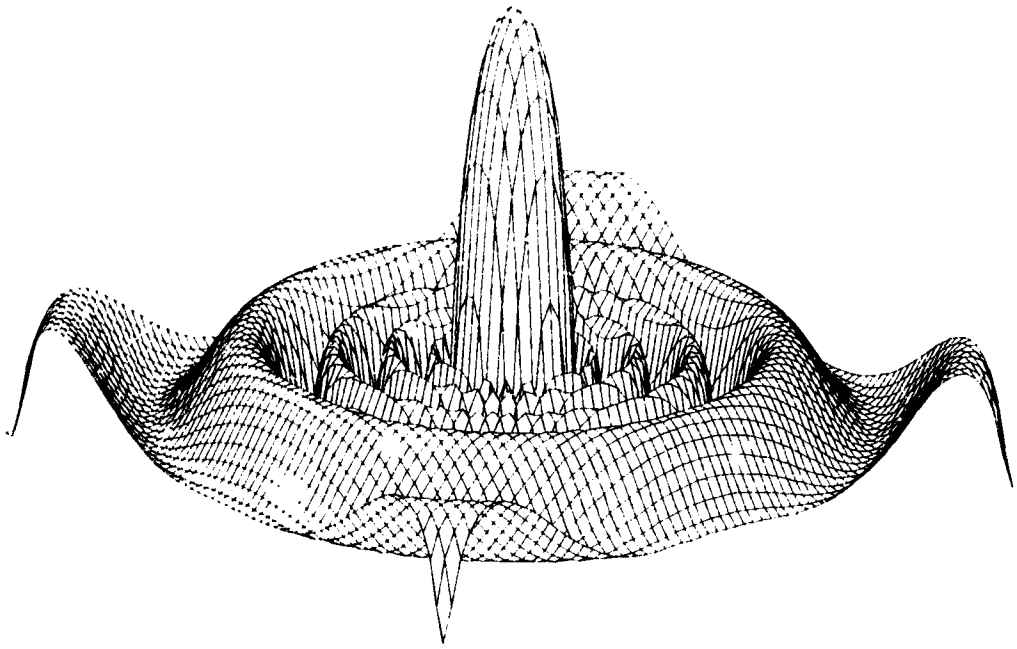

Figure 3.7: Three-dimensional plot of the radiation pattern of the 5-ring array.

represented as

$$\mathbf{d} = [\mathbf{w_1}, \mathbf{w_2}, \ldots, \mathbf{w_N}]\mathbf{c} \tag{3.6}$$

where $[\mathbf{w_1}, \mathbf{w_2}, \ldots, \mathbf{w_N}]$ is the matrix of weighting coefficients of the equivalent linear arrays of a ring array, and $\mathbf{c}$ is the vector of the weighting coefficients of the ring array.

Because of practical considerations the weighting coefficients c_i can only be generated with finite accuracy. If the statistical characteristic of c_i is given, we may find the statistical characteristic of d_i by applying Eq. (3.6). Therefore, the effects of finite tolerance on sidelobe level and directivity can be treated by any method available for linear arrays [3].

Shown in Fig. 3.8(a)-(b) are the 20 samples of radiation patterns of a 10 ring array for randomized weighting coefficients with tolerances of 5% and 10% uniformly distributed, respectively. Plotted in Fig. 3.9(a)-(b) are the 10 samples of radiation patterns of a 10-ring array with a 0.1λ gap between rings for randomized outer and inner radii with tolerances of 5% and 10%, respectively.

3.4 Compact Receiving/Transmitting Configurations

We consider a compact receiving/transmitting array where the transmitting element is a piston, while the receiving array consists of the same transmitting piston surrounded by several concentric rings made of piezoelectric film or several concentric hollow cylinders operating in longitudinal mode.

We investigate the transmitting/receiving pattern of such a configuration and apply the design procedure described in Section 3.2.3 to this situation. We use again the Dolph-Chebyshev linear array as a prototype [35]. It is assumed that the prototype has 20 elements ($N = 10$) spaced by $d = \lambda/2$, with 30 dB and 40 dB postulated sidelobe suppression and with corresponding 7° and 8° beamwidths

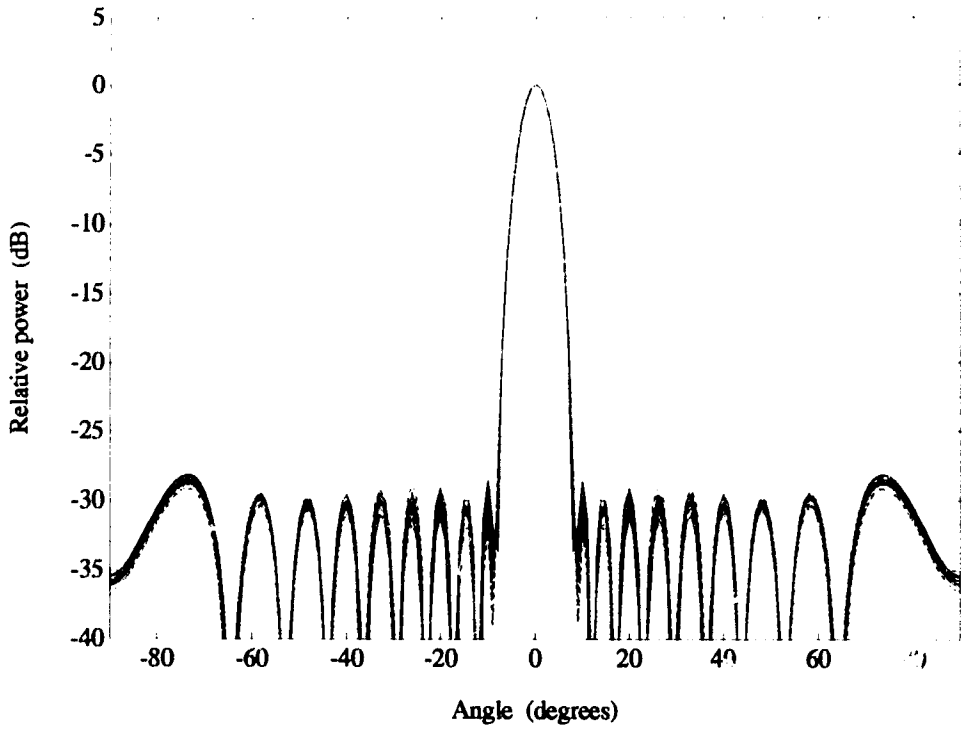

(a)

Figure 3.8: Radiation patterns of a 10-ring array for different postulated sidelobe suppression levels in Dolph-Chebyshev prototype. (a) 5 % weighting coefficient tolerance with postulated 30 dB sidelobe suppression. (b) 5 % weighting coefficient tolerance with postulated 40 dB sidelobe suppression. (c) 10 % weighting coefficient tolerance with postulated 30 dB sidelobe suppression. (d) 10 % weighting coefficient tolerance with postulated 40 dB sidelobe suppression.

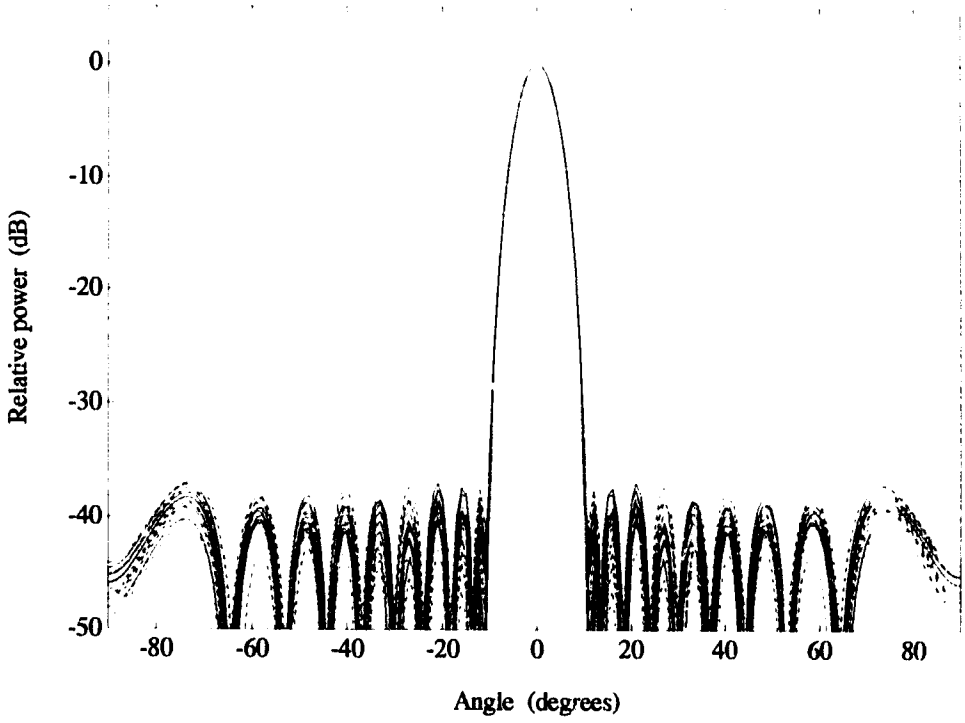

(b)

Figure 3.8: (Continued)

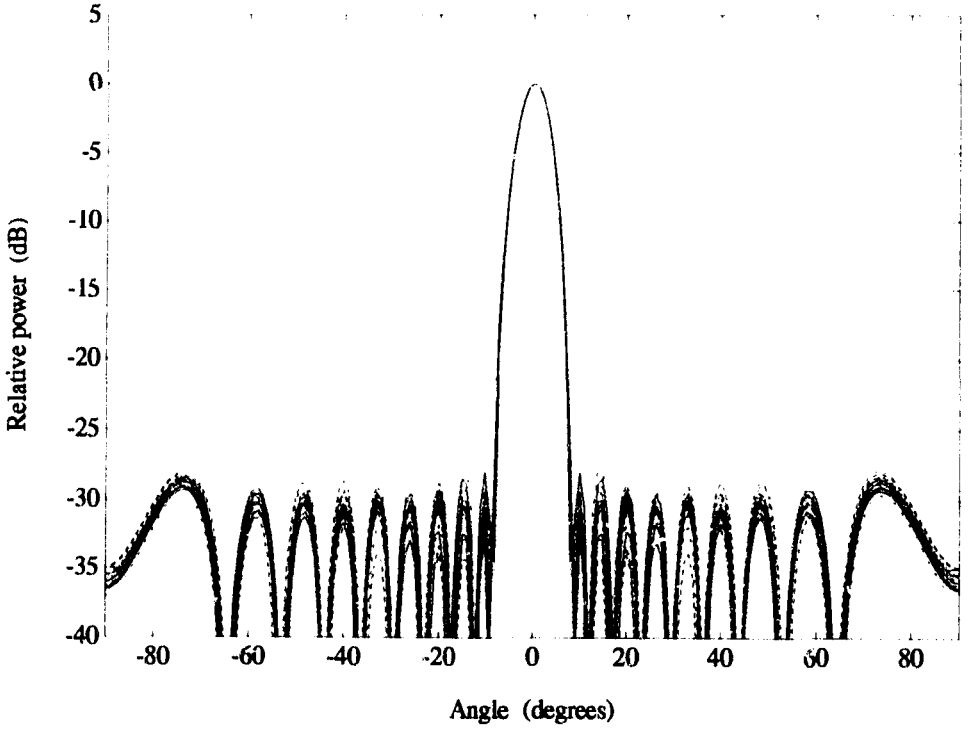

(c)

Figure 3.8: (Continued)

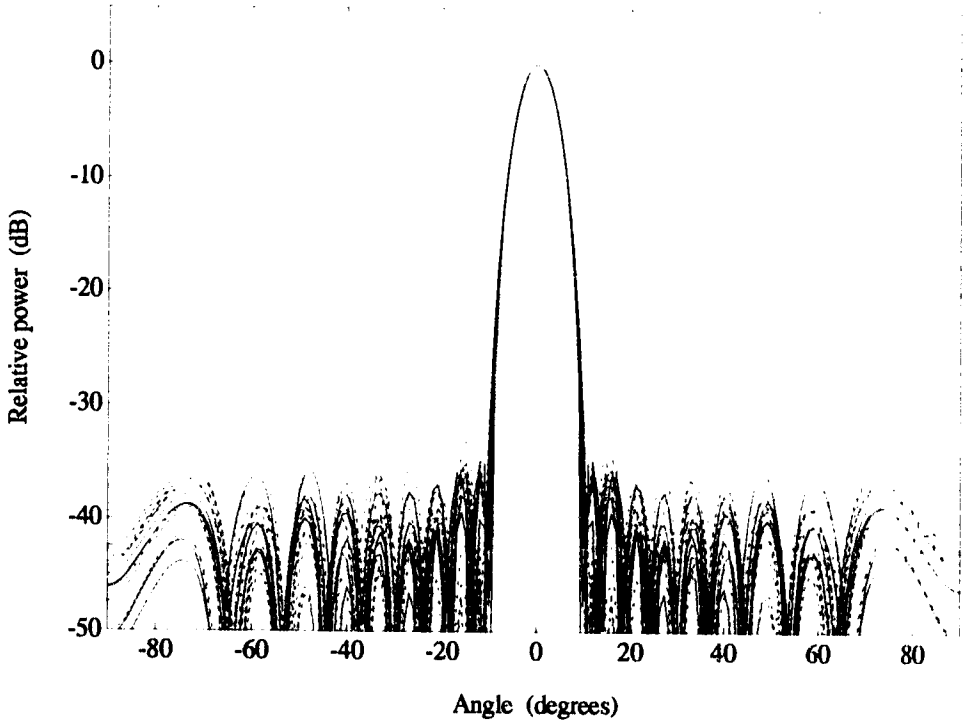

(d)

Figure 3.8: (Continued)

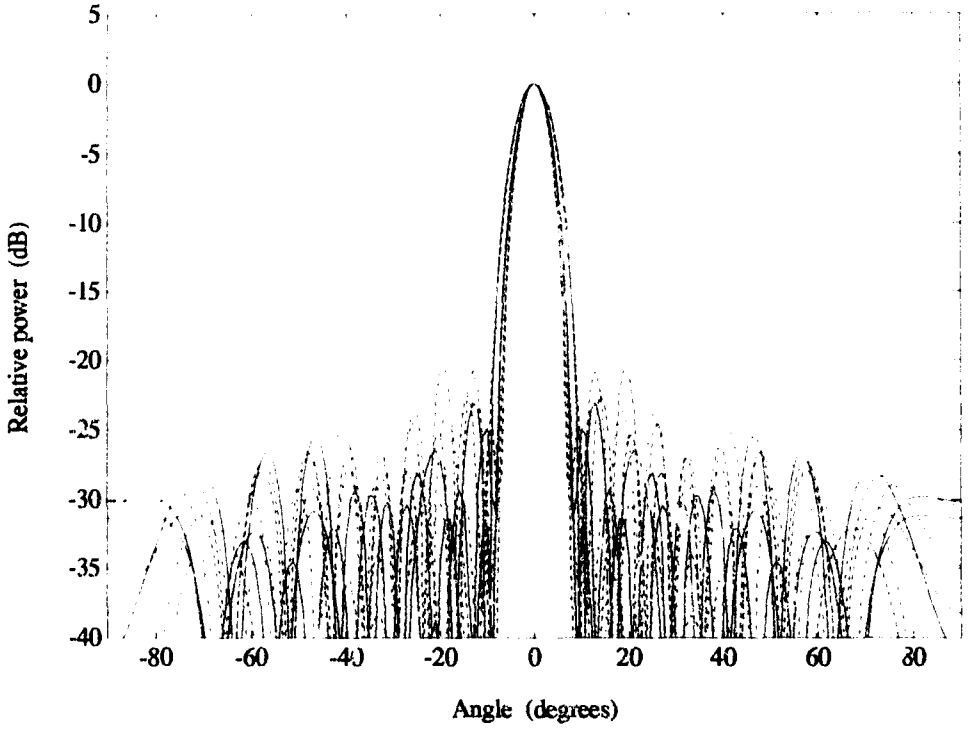

(a)

Figure 3.9: Radiation patterns of a 10-ring array postulated 30 dB sidelobe suppression in Dolph-Chebyshev prototype. (a) 5 % outer and inner radii tolerance. (b) 10 % outer and inner radii tolerance.

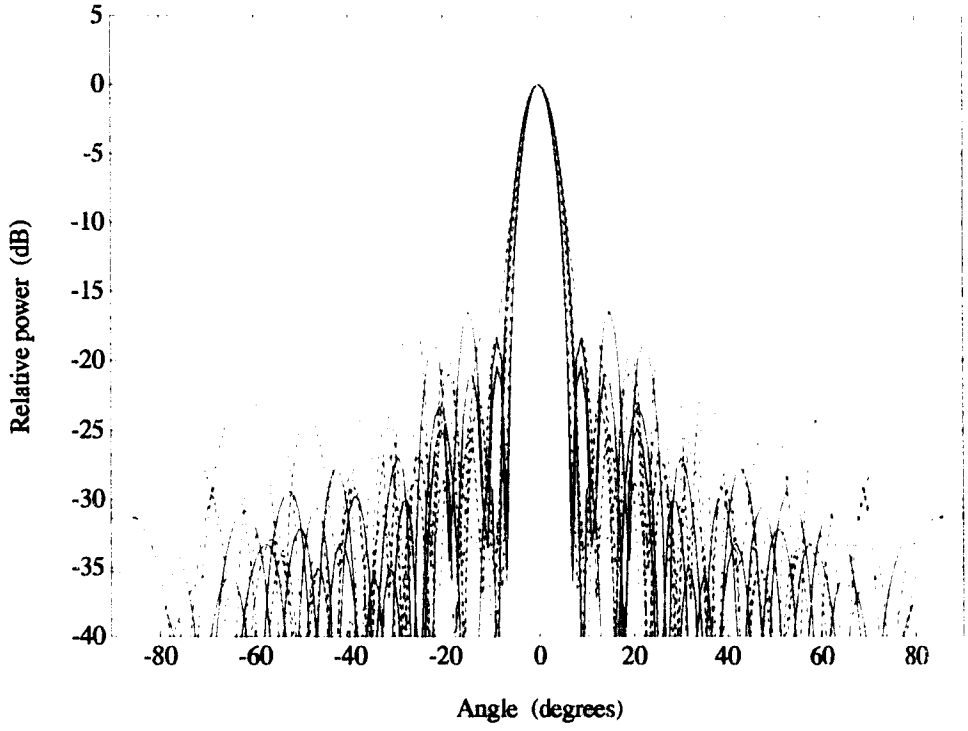

(b)

Figure 3.9: (Continued)

(3 dB), respectively. We first assume that the central piston of the ring array has a diameter of 2λ. We then follow the design step 2 which results in a 9-ring array (assumed $M = 9$) with outer ring diameters of 10λ, 9λ, 8λ, 7λ, 6λ, 5λ, 4λ, 3λ, 2λ. The last element is the central piston with diameter of 2λ. The widths t_i of rings are selected such that there is no overlap between rings. Once the physical size of rings is determined, we proceed with the method described in Chapter 2 to find the equivalent linear arrays of these rings and the associated vectors of weighting coefficients $\mathbf{w}_1$, $\mathbf{w}_2$, ..., $\mathbf{w}_9$. The weighting coefficients of rings can be found by forming the matrix (step 3) and solving the matrix equation (step 4). The resulting radiation patterns for ring widths $t_i = 0.4\lambda$, $i = 1, 2, \ldots, 8$ (gap of 0.1λ between rings) of this example are shown in Fig. 3.10(a)-(b).

We see that the resulting radiation pattern is still close to that of the postulated Dolph-Chebyshev prototype (shown in dotted line). Referring to Fig. 3.5 we note that the presence of the central piston in the receiving array assures a more satisfactory radiation pattern. We proceed to gradually reduce the number M of rings (i.e., increase the diameter of the central piston) and repeat Steps 2-4. The resulting radiation patterns are shown in Figs. 3.10-3.14 with the number of elements of 9, 8, 7, 6 and 5. The corresponding normalized weighting coefficients and ring sizes are tabulated in Table 3.5.

In all cases the transmitting element is the central piston with its well known radiation pattern. The total transmitting/receiving radiation pattern is obtained by multiplying the transmitting and receiving radiation patterns. We use a 6-element array with receiving radiation pattern shown in Fig. 3.13 as the transmitting/receiving array. The combined transmitting/receiving radiation pattern is shown in Fig. 3.15 for various sidelobe suppression. The dotted line shows the transmitting radiation pattern of the central piston with diameter of 5λ. We see from Fig. 3.15(b) that the narrow beam of 8° and sidelobes more than 48 dB down can be obtained using only a 6-element array.

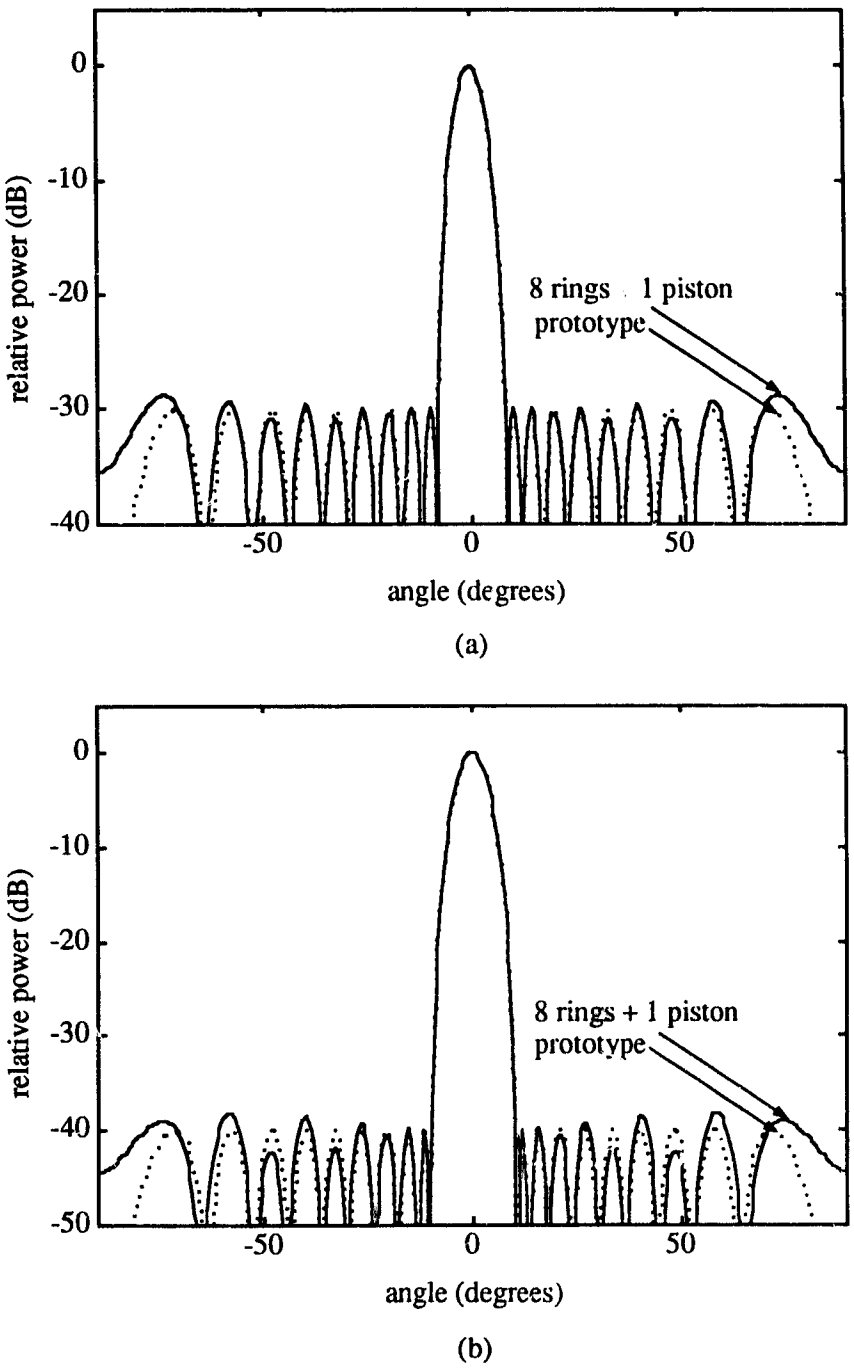

Figure 3.10: Radiation patterns of an array of 8 rings and 1 central piston. (a) Postulated 30 dB sidelobe suppression. (b) Postulated 40 dB sidelobe suppression.

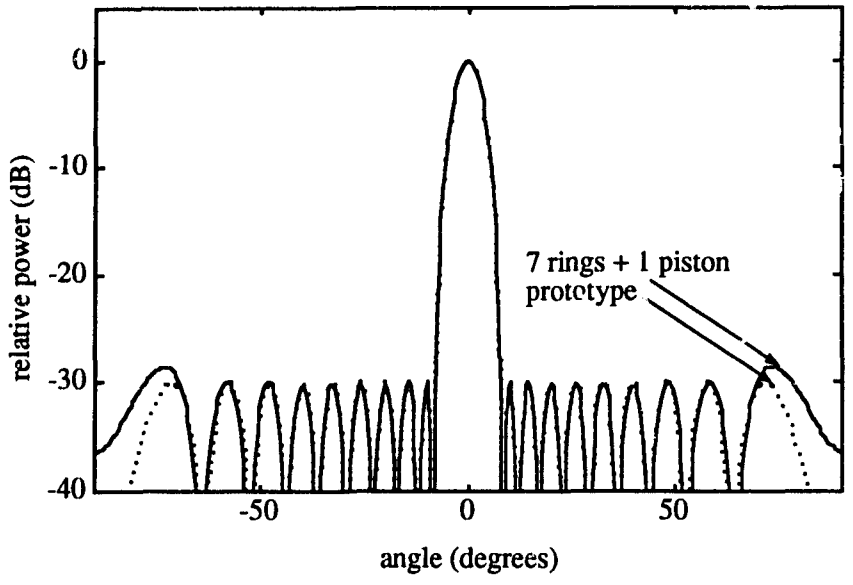

(a)

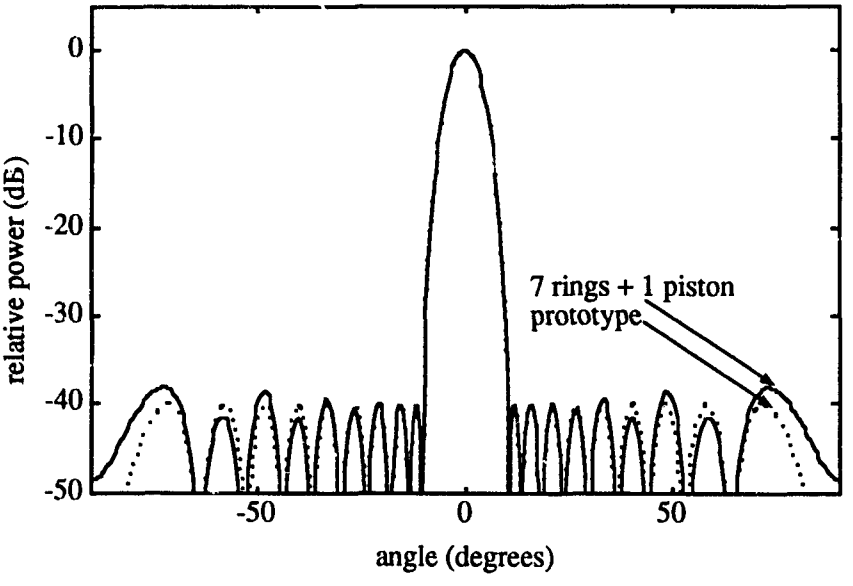

(b)

Figure 3.11: Radiation patterns of an array of 7 rings and 1 central piston. (a) Postulated 30 dB sidelobe suppression. (b) Postulated 40 dB sidelobe suppression.

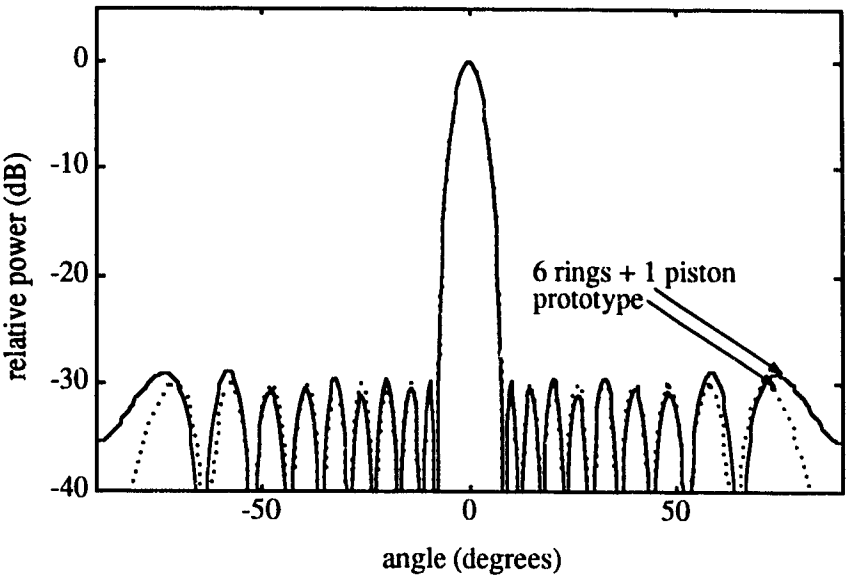

(a)

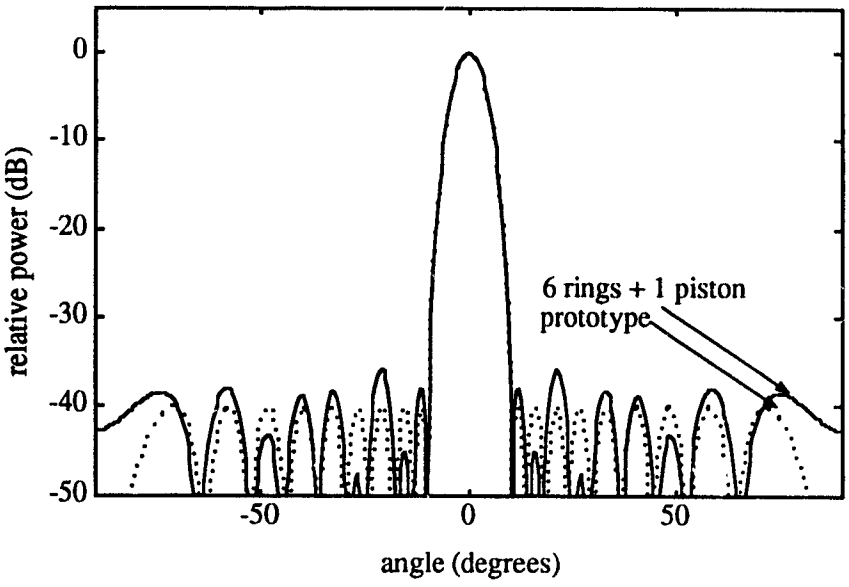

(b)

Figure 3.12: Radiation patterns of an array of 6 rings and 1 central piston. (a) postulated 30 dB sidelobe suppression. (b) postulated 40 dB sidelobe suppression.

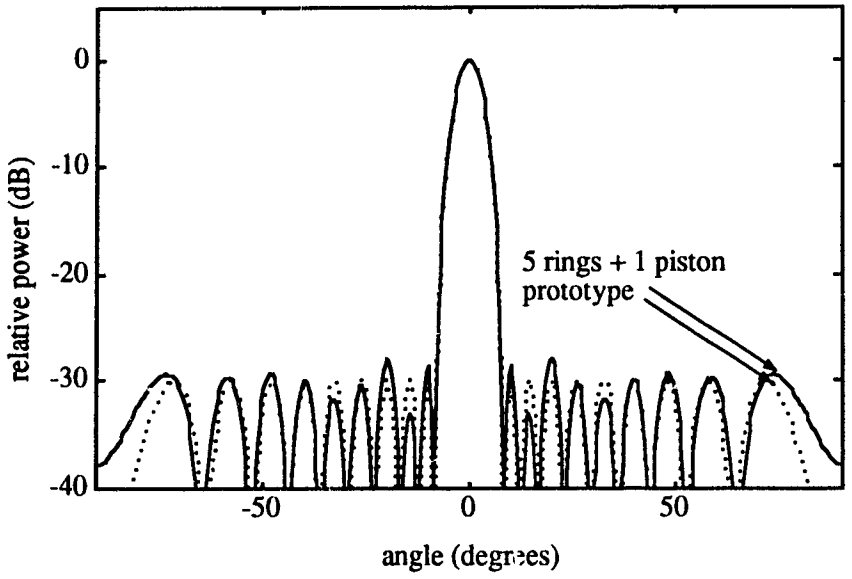

(a)

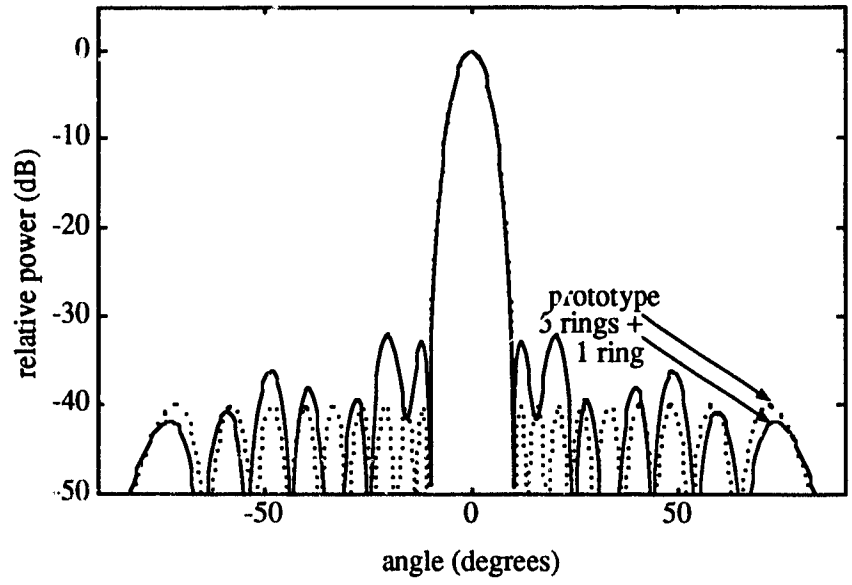

(b)

Figure 3.13: Radiation patterns of an array of 5 rings and 1 central piston. (a) Postulated 30 dB sidelobe suppression. (b) Postulated 40 dB sidelobe suppression.

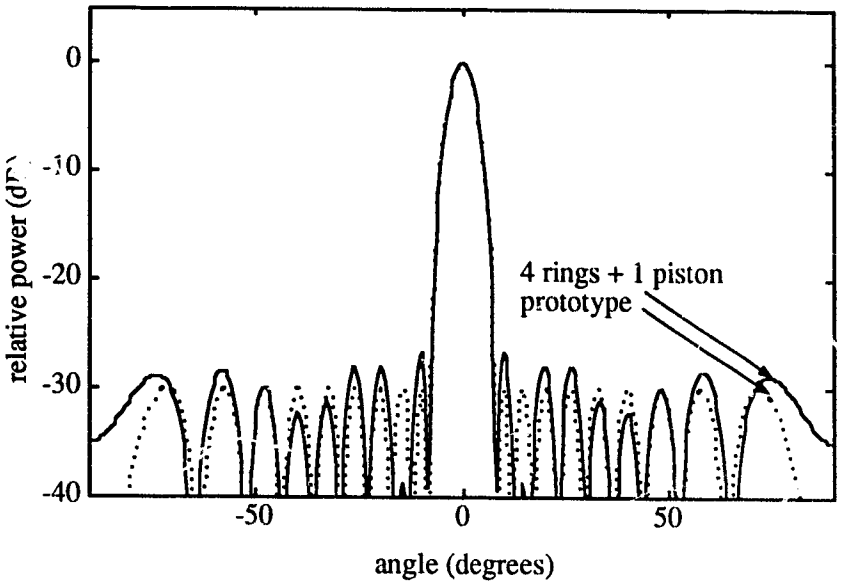

(a)

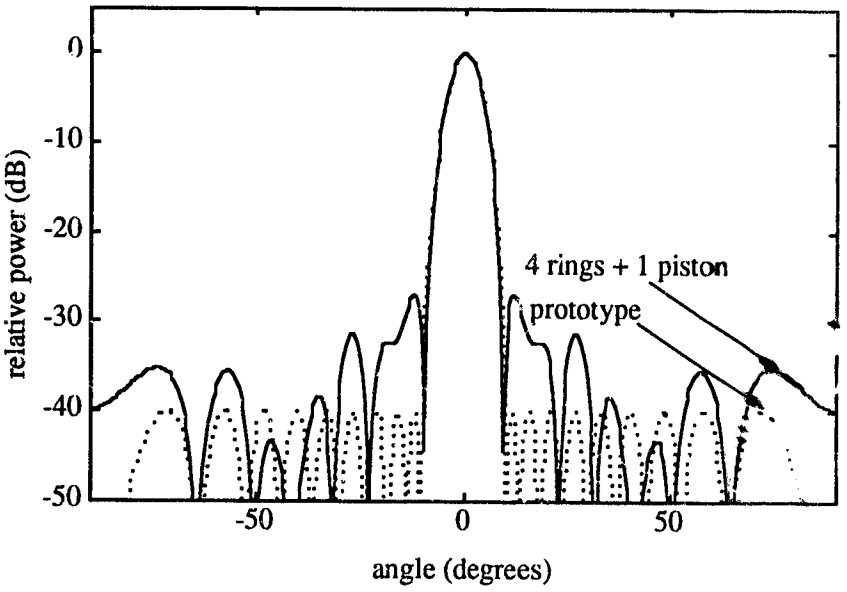

(b)

Figure 3.14: Radiation patterns of an array of 4 rings and 1 central piston. (a) Postulated 30 dB sidelobe suppression. (b) Postulated 40 dB sidelobe suppression.

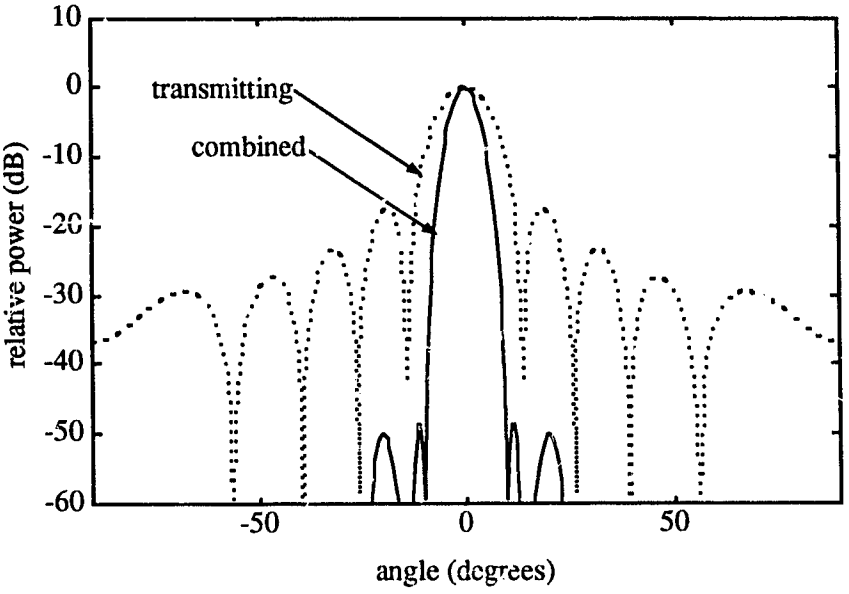

(a)

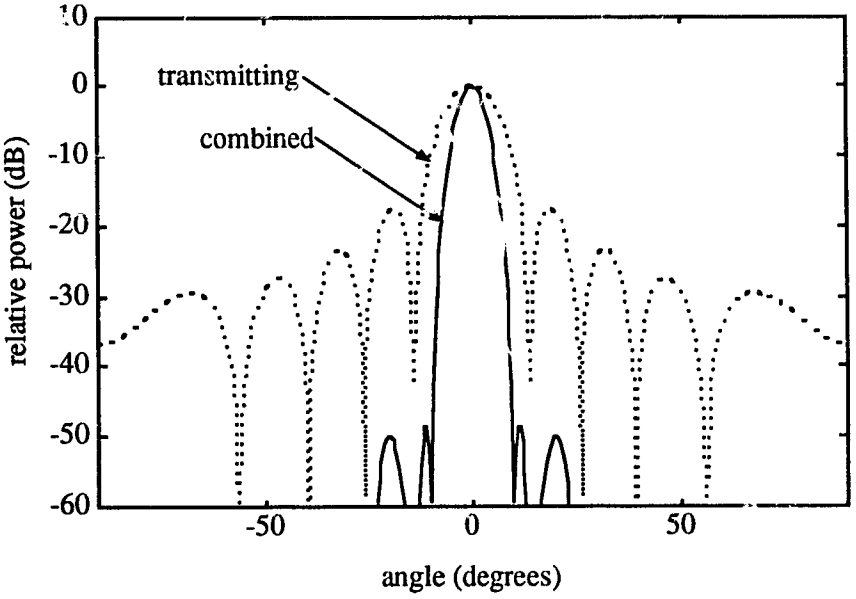

(b)

Figure 3.15: Transmitting/receiving two-way radiation patterns of a 6-ring array. (a) Postulated 30 dB sidelobe suppression in receiving. (b) Postulated 40 dB sidelobe suppression in receiving.

Table 3.5: Weighting coefficients of ring array for different piston diameters

(a) postulated 30 dB sidelobe suppression

Radius	Weighting Coefficient for Different Piston					
r_i/λ	1.0λ	2.0λ	3.0λ	4.0λ	5.0λ	6.0λ
0.5	0.9423	–	–	–	–	–
1.0	1.0000	0.8988	–	–	–	–
1.5	0.8774	1.0000	0.8638	–	–	–
2.0	0.8727	0.9244	1.0000	1.0000	–	–
2.5	0.7032	0.7712	0.7656	0.9878	1.0000	–
3.0	0.6906	0.7403	0.7750	0.9002	0.9616	0.9688
3.5	0.4679	0.5105	0.5135	0.6387	0.6539	0.6515
4.0	0.5107	0.5491	0.5705	0.6741	0.7334	0.7276
4.5	0.0929	0.1027	0.1003	0.1299	0.1257	0.1409
5.0	0.6900	0.7451	0.7670	0.9196	0.9851	1.0000

(b) postulated 40 dB sidelobe suppression

Radius	Weighting Coefficient for Different Piston					
r_i/λ	1.0λ	2.0λ	3.0λ	4.0λ	5.0λ	6.0λ
0.5	0.9894	–	–	–	–	–
1.0	1.0000	0.9002	–	–	–	–
1.5	0.8957	1.0000	0.9393	–	–	–
2.0	0.8134	0.8466	1.0000	1.0000	–	–
2.5	0.6691	0.7227	0.7780	0.9219	1.0000	–
3.0	0.5617	0.5909	0.6757	0.7365	0.7748	1.0000
3.5	0.4048	0.4354	0.4743	0.5561	0.5772	0.5329
4.0	0.3224	0.3398	0.3866	0.4255	0.4725	0.5003
4.5	0.1528	0.1649	0.1784	0.2112	0.2158	0.2395
5.0	0.2221	0.2352	0.2649	0.2960	0.3243	0.3442

3.5 Summary

This chapter considers several practical aspects associated with the implementation of a novel array of ring radiators. Modified design methods are developed to include the variability of the gap between rings and to reduce the number of rings. A simplified design procedure is proposed and the results are presented in a tabular form convenient for designers. The effect of finite tolerance of weighting coefficients and the radii of rings on the radiation pattern of a ring array is also discussed. The proposed configuration can be implemented as a receiving array using piezoelectric film or as a transmitting/receiving array using concentric hollow cylinders operating in longitudinal mode.

A compact receiving/transmitting configuration is also proposed in which the transmitting element is a piston, while the receiving array consists of the same transmitting piston surrounded by several concentric rings made of piezoelectric film or several concentric hollow cylinders operating in longitudinal mode. By applying the proposed design method to a compact transmitting/receiving array, it is found that the reduction of the number of elements can still yield an acceptable radiation pattern. A design example shows that a narrow beam of 8° beamwidth (3 dB) with more than 48 dB sidelobe suppression in the transmitting/receiving pattern can be achieved with an array using only 6 receiving elements and one transmitting element.

Chapter 4

Novel Acoustic Arrays of Elliptic Ring Radiators

In Chapter 2 and 3 we dealt with novel arrays of circular ring radiators. These arrays can produce search-light-type beams with greatly reduced sidelobes. In this chapter we propose another novel acoustic array of elliptic ring radiators and discuss the relation between this novel array and the circular ring array.

4.1 Introduction

Fan-type acoustic beams are widely used in specialized sonars such as sidescan sonars, sonars for fish finding and stock assessment, and other systems [2]. Such beams are relatively broad (20° - 45°) in one direction and narrow (1° - 5°) in the direction orthogonal to the broad beam direction. The systems usually consist of linear arrays made from rectangular elements. It is possible to control the radiation pattern in the narrow beam direction by the application of proper weights to each array element. In the broad beam direction, however, the radiation pattern is determined by the width of the rectangular elements and has large first sidelobes (13.5 dB). Existence of such sidelobes adversely affects sonar performance.

In this chapter we propose a novel array consisting of several concentric elliptic ring radiators, and capable of generating a superior radiation pattern. Two approaches to the design are presented. One approach utilizes a mapping to trans-

form a radiation pattern designed for circular ring array by previously developed methodology to that of elliptic ring array. The other approach uses the concept of equivalent linear arrays. This approach benefits from the existing design techniques developed for linear arrays. It requires only simple matrix operations and does not involve any optimization.

The design examples are presented which show that 40 dB or more sidelobe suppression in all possible angular directions in the radiation pattern is achievable. The proposed configuration can be implemented as a receiving array using piezoelectric film and as a transmitting/receiving array using concentric hollow elliptic cylinders operating in longitudinal mode.

4.2 Directivity Function of an Elliptic Piston

In general the directivity function of an arbitrary piston can be obtained as a suitable integral over its face [38]. The face of an elliptic piston is shown in Fig. 4.1. The directivity function (radiation pattern) of such a planar elliptic radiator of uniform sensitivity, with major and minor axes of $2a$ and $2b$, respectively, placed in an infinite rigid baffle, is given by

$$D_e(\theta,\phi) = \int\int_s e^{j\frac{2\pi}{\lambda}(x\sin\theta\cos\phi + y\sin\theta\sin\phi)}dxdy \tag{4.1}$$

where λ is the wavelength of radiated signal, s is the area of integration (surface of the elliptic piston), and θ, ϕ are the angular coordinates shown in Fig. 4.1.

We introduce implicitly the new variables ρ and ψ by the following transformation:

$$x = a\rho\cos\psi, \quad 0 \le \rho \le 1; \tag{4.2}$$

$$y = b\rho\sin\psi, \quad 0 \le \psi \le 2\pi. \tag{4.3}$$

For these new variables we have

$$dxdy = |J|d\rho d\psi$$

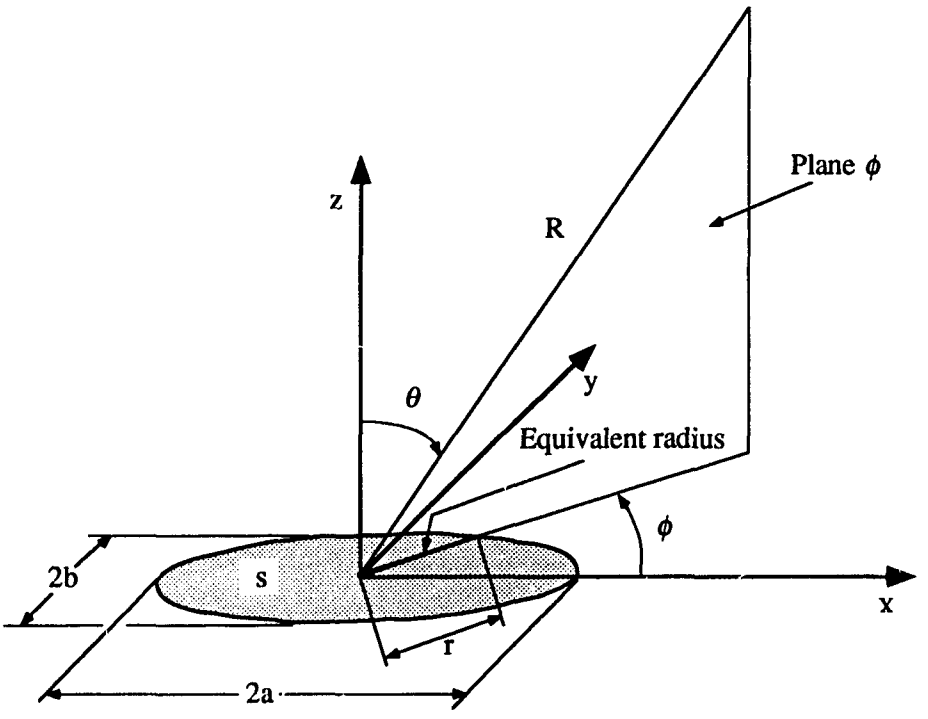

Figure 4.1: Geometry of an elliptic piston and its equivalent radius.

$$= \quad ab\rho d\rho d\psi \tag{4.4}$$

where $|J|$ is the Jacobian of the transformation defined as

$$|J| = \left| \frac{\partial x}{\partial \rho}\frac{\partial y}{\partial \psi} - \frac{\partial x}{\partial \psi}\frac{\partial y}{\partial \rho} \right| = ab\rho. \tag{4.5}$$

Now we rearrange the integral in Eq. (4.1) to obtain the following form:

$$D_e(\theta,\phi) = \int_0^{2\pi}\int_0^1 e^{j\frac{2\pi}{\lambda}\sin\theta(a\cos\psi\cos\phi + b\sin\psi\sin\phi)} ab\rho d\rho d\psi. \tag{4.6}$$

Furthermore, if we let

$$\cos\phi' = \frac{a\cos\phi}{\sqrt{a^2\cos^2\phi + b^2\sin^2\phi}} \tag{4.7}$$

and

$$\sin\phi' = \frac{b\sin\phi}{\sqrt{a^2\cos^2\phi + b^2\sin^2\phi}} \tag{4.8}$$

then we express Eq. (4.6) as

$$D_e(\theta,\phi) = \int_0^{2\pi}\int_0^1 e^{j\frac{2\pi}{\lambda}\sin\theta\sqrt{a^2\cos^2\phi + b^2\sin^2\phi}\cos(\psi-\phi')} ab\rho d\rho d\psi. \tag{4.9}$$

We note that the integral (4.9) has the form of the integral expression of the zero-order Bessel function of the first kind $J_0(z)$, which is

$$2\pi J_0(z) = \int_0^{2\pi} e^{jz\cos\psi} d\psi. \tag{4.10}$$

Using this observation we can write Eq. (4.9) as

$$D_e(\theta,\phi) = 2\pi ab\int_0^1 J_0\left(\frac{2\pi}{\lambda}\sqrt{a^2\cos^2\phi + b^2\sin^2\phi}\sin\theta\right)\rho d\rho. \tag{4.11}$$

By making use of the identity

$$\int_0^x zJ_0(z)dz = xJ_1(x) \tag{4.12}$$

we finally write Eq. (4.11) as

$$D_e(\theta\ \phi) = ab\frac{J_1(2\pi\sqrt{a^2\cos^2\phi + b^2\sin^2\phi}\sin\theta/\lambda}{\sqrt{a^2\cos^2\phi + b^2\sin^2\phi}\sin\theta/\lambda} \tag{4.13}$$

where $J_1(\cdot)$ is the first-order Bessel function of the first kind. For a circular piston transducer for which $a = b$, the above result reduces to that derived in [33].

The radiation patterns of an elliptic piston transducer with $a = 5\lambda$ and $b = 0.175a$ are shown in Fig. 4.2(a)-(d) on a plane perpendicular to its surface and passing through its center. We refer to this plane as plane ϕ. An elliptic piston can generate a fan-type beam, broad on the plane $\phi = 90°$ and narrow on the plane $\phi = 0°$. As will be explained later, the radiation pattern of the elliptic transducer can be obtained through a suitable transformation of a radiation pattern of a circular piston. Such a transformation preserves the relative levels of sidelobes. For this reason the maximum sidelobe level associated with an elliptic piston is 17.6 dB below the main lobe maximum, the same as that of a circular piston.

4.3 Circular to Elliptic Piston Transformation

We introduce here a concept of angle mapping which transforms the two-dimensional (2-D) radiation pattern generated by a circular piston to a three-dimensional (3-D) radiation pattern generated by an elliptic piston. For this purpose we rewrite Eq. (4.13) as

$$D_e(\theta, \phi) = 2\pi ab\frac{J_1(kr\sin\theta)}{kr\sin\theta} \tag{4.14}$$

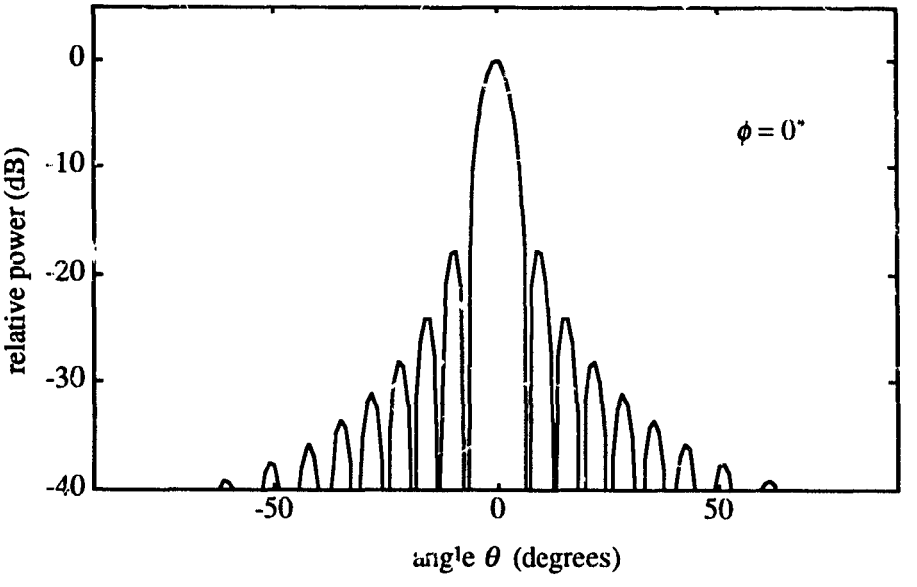

(a)

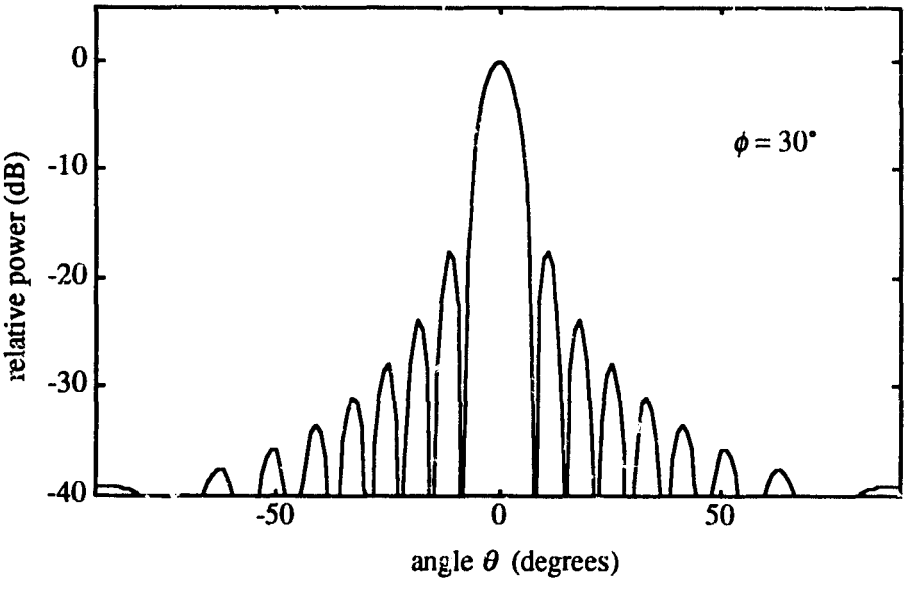

(b)

Figure 4.2: Radiation patterns of an elliptic piston transducer with $a = 5\lambda$ and $b = 0.175a$ on different planes perpendicular to its surface. (a) $\phi = 0°$. (b) $\phi = 30°$. (c) $\phi = 60°$. (d) $\phi = 90°$.

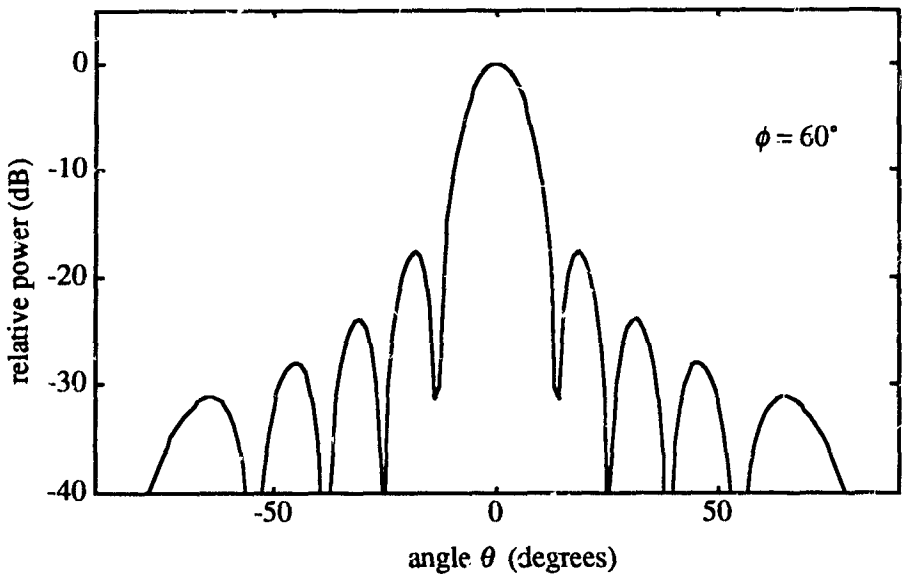

(c)

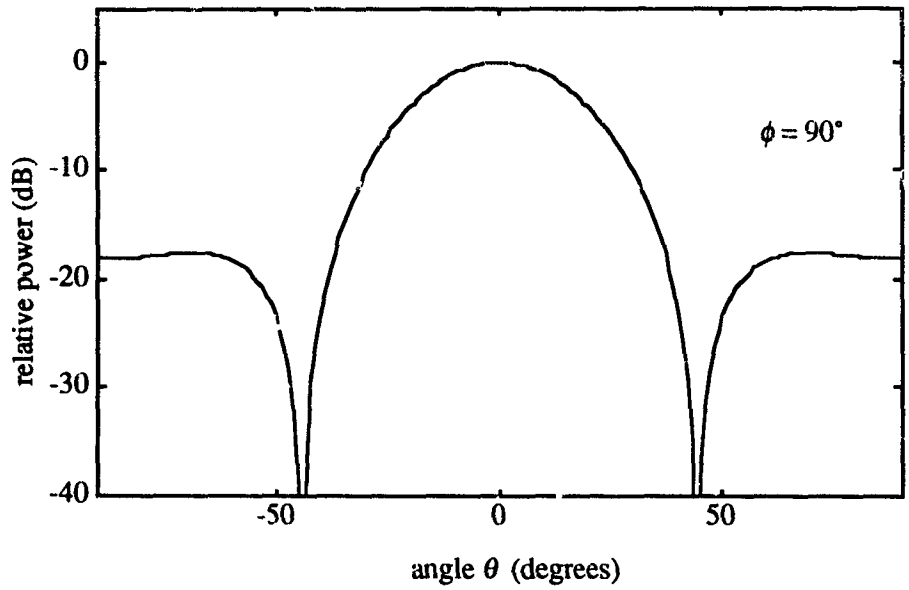

(d)

Figure 4.2: (Continued)

where

$$r = \sqrt{a^2 \cos^2 \phi + b^2 \sin^2 \phi}; \qquad a \leq r \leq b \tag{4.15}$$

is defined as the equivalent radius of an elliptic piston at the angle ϕ shown in Fig. 4.1, and $k = 2\pi/\lambda$ is the wavenumber of the radiated signal. This equivalent radius r will play an important role in the analysis of the radiation pattern of an elliptic piston.

A circular piston of radius r has a directivity function given by

$$D_c(\theta, \phi) = 2\pi r^2 \frac{J_1(kr \sin\theta)}{kr \sin\theta}. \tag{4.16}$$

We note that for a given ϕ the directivity function $D_e(\theta, \phi)$ given by Eq. (4.14) is equal to $D_c(\theta, \phi)$ given by Eq. (4.16) except for a constant factor. Based on this observation, we conclude that the normalized radiation pattern of an elliptic piston on the plane ϕ is identical to the beam pattern of a circular piston with the radius given by Eq. (4.15) on the same plane.

We define a piston angle u by

$$u = kr \sin\theta. \tag{4.17}$$

Using Definition (4.17), the directivity function of the elliptic piston in u domain becomes

$$D_e(\theta, \phi) = D_e(u) = 2\pi ab \frac{J_1(u)}{u}. \tag{4.18}$$

Similarly, the directivity function given by Eq. (4.16) for a circular piston in u domain becomes

$$D_c(\theta, \phi) = D_c(u) = 2\pi r^2 \frac{J_1(u)}{u}. \tag{4.19}$$

both directivity functions of Eqs. (4.18) and (4.19) are identical in the u-domain except for a proportionality constant. Consequently we will deal with only one normalized directivity function

$$D(u) = \frac{D_e(u)}{2\pi ab} = \frac{D_c(u)}{2\pi r^2} = \frac{J_1(u)}{u}. \tag{4.20}$$

Since $D(u)$ is the function of only one variable and is invariant to ϕ in u-domain, we can generate a 3-D radiation pattern of an elliptic piston through a 2-D radiation pattern $D(u)$ or $D_c(u)$ of a circular piston by using the transformations defined by Eqs. (4.15) and (4.17). These transformations can be considered as the mapping of the space angle (θ, ϕ)-domain into the u-domain and vice-versa. We call this approach an *angle mapping approach.* To visualize this transformation we constructed a suitable nomogram shown in Fig. 4.3 which will later prove useful in synthesizing a radiation pattern.

Shown in Fig. 4.3(a) is a plot of $D(u)$ as given by Eq. (4.20) which represents a normalized directivity function in the u-domain for both circular and elliptic pistons. We use this 2-D plot to generate a 3-D radiation pattern in any (θ, ϕ) direction for an elliptic piston. For a given a and b (in this example $a = 5\lambda$ and $b = 1\lambda$) we use Eq. (4.15) to find the equivalent radius $r(\phi)$ at a certain angle ϕ. This value is used to construct a semicircle with diameter $2kr$ as shown in Fig. 4.3(b). The diameter of the semicircle determines the visible range in the u-domain by its projection onto the u-axis shown by the dotted lines in Fig. 4.3(a) for semicircles corresponding to $\phi = 0°$, $60°$ and $90°$. When the equivalent radius r equals the major axis a (this occurs for $\phi = 0°$), u has a maximum visible range; this corresponds to the narrowest beamwidth in the radiation pattern. When the equivalent radius r equals the minor axis b (this occurs for $\phi = 90°$), u has a minimum visible range, which corresponds the broadest beamwidth in the radiation pattern. To complete the transformation we construct a curve shown in Fig. 4.3(c). The curve is constructed from points obtained in the following steps:

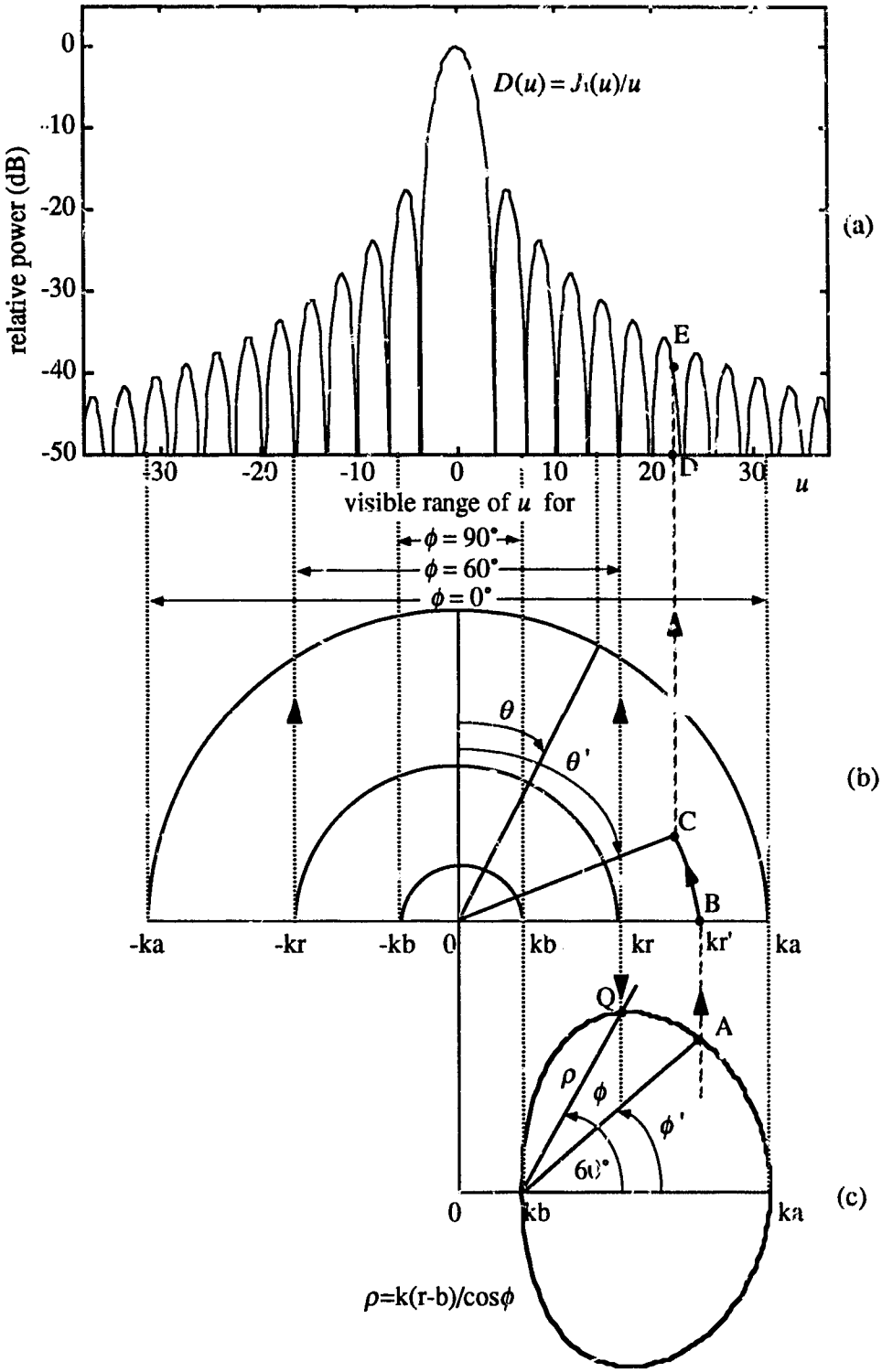

Figure 4.3: Transformations from space angles ϕ, θ to piston angle u for an elliptic piston transducer. (a) Radiation pattern in the u-domain. (b) Transformation from θ, r to u. (c) Transformation from ϕ to r.

1. For a given ϕ find the corresponding radius kr as shown in Fig. 4.3(b).

2. Construct a ray as shown in Fig. 4.3(c) pointing in the ϕ direction and starting from the point $(kb, 0)$. We use $\phi = 60°$ as an illustration.

3. Project kr shown in Fig. 4.3(b) towards the above ray to obtain an intersection point Q.

4. Repeat the above steps for different ϕ to obtain the whole curve.

It can be shown that the equation of the curve in polar coordinates (ρ, ϕ) obtained in such a way is given by

$$\rho = \frac{k(r(\phi) - b)}{\cos\phi}; \qquad 0° \leq \phi \leq 360° \tag{4.21}$$

with the origin as shown in Fig. 4.3(c).

Now we use the nomogram to find a 3-D radiation pattern in any given space angle (θ', ϕ'). First we map the angle ϕ' to the equivalent radius r' using Eq. (4.15). This is done graphically by mapping of the point A corresponding to ϕ in Fig. 4.3(c) onto the point B in Fig. 4.3(b). We then map the angle θ' to the piston angle u by Eq. (4.17). This is graphically accomplished by moving the point B along the semicircle of the radius kr' to the point C in Fig. 4.3(b) and projecting it to the point D in Fig. 4.3(a). Finally, we calculate the beam amplitude at (θ', ϕ') from Eq. (4.20) or obtain it graphically as the point E in Fig. 4.3(a).

Fig. 4.3 also illustrates the manner in which the major and minor axes affect the radiation pattern of an elliptic piston. As the axes a and b increase, the visible range of u increases. As a result the number of zeros and lobes appearing in the radiation pattern increases, and this in turn results in a narrower main lobe in the radiation pattern. 3-D plots of radiation patterns showing these effects are presented in Fig. 4.4(a)-(c).

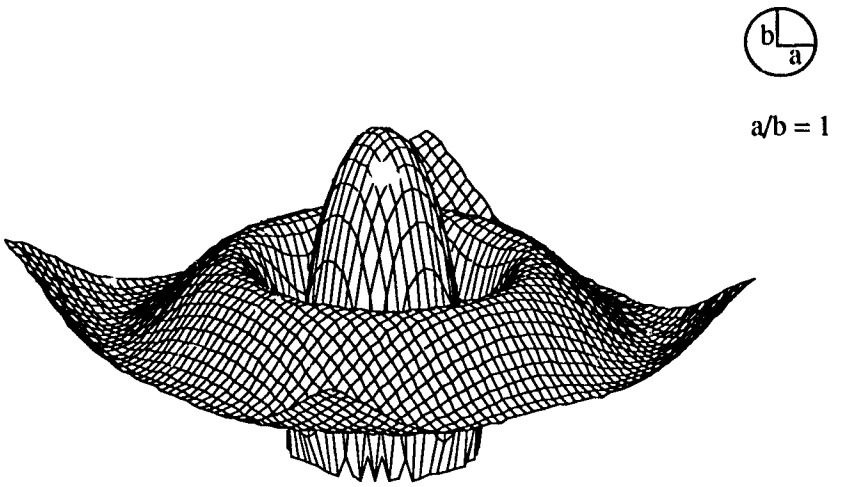

(a)

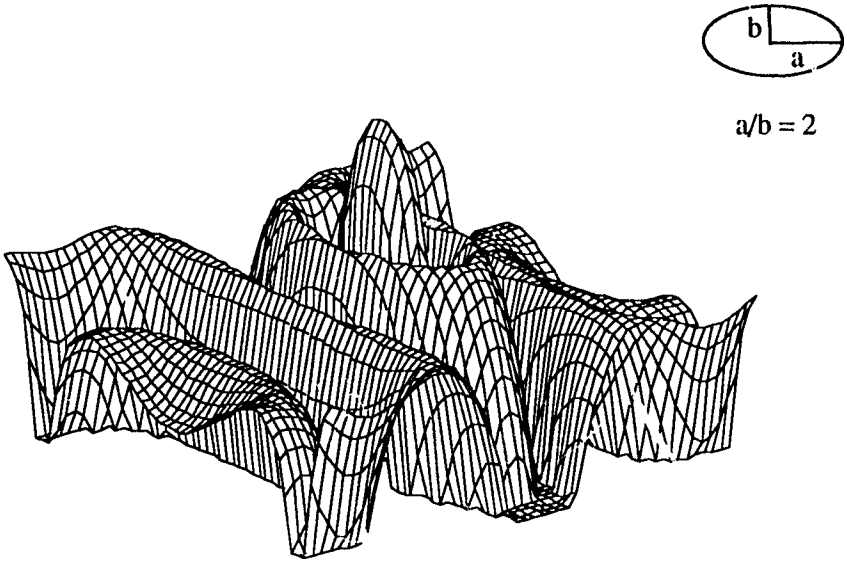

(b)

Figure 4.4: Perspective plots of radiation patterns of an elliptic piston transducer. (a) $a = 1\lambda$, $b = 1\lambda$. (b) $a = 2\lambda$, $b = 1\lambda$. (c) $a = 5\lambda$, $b = 1\lambda$.

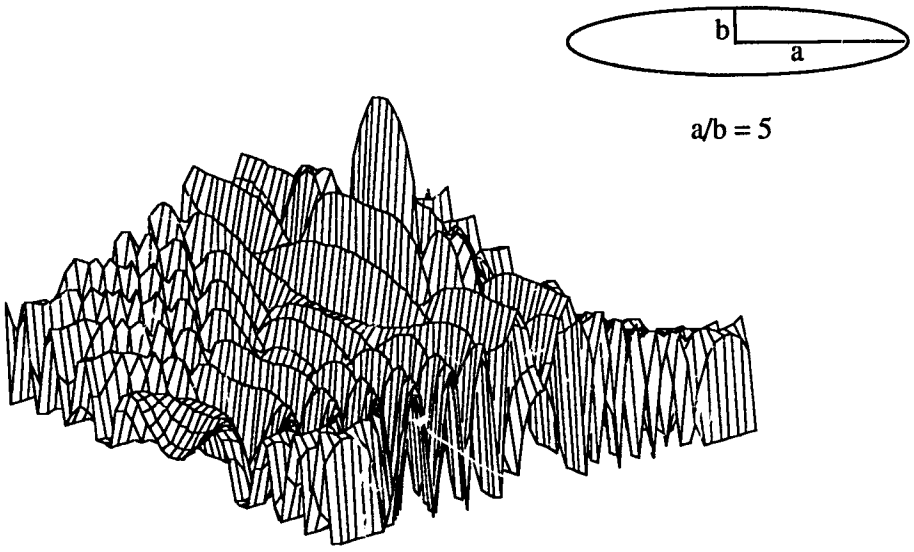

(c)

Figure 4.4: (Continued)

4.4 An Array of Elliptic Ring Radiators

The directivity function of an elliptic ring radiator shown in Fig. 4.5 with major axes a_i, a_{i-1}, minor axes b_i, b_{i-1}, uniform sensitivity, and placed in an infinite rigid baffle can be readily obtained by subtracting directivity functions of two elliptic piston radiators given by Eq. (4.14), that is:

$$D_r(\theta,\phi) = 2\pi a_i b_i \frac{J_1(kr_i \sin\theta)}{kr_i \sin\theta} - 2\pi a_{i-1} b_{i-1} \frac{J_1(kr_{i-1} \sin\theta)}{kr_{i-1} \sin\theta} \tag{4.22}$$

where

$$r_i = \sqrt{a_i^2 \cos^2\phi + b_i^2 \sin^2\phi} \tag{4.23}$$

and

$$r_{i-1} = \sqrt{a_{i-1}^2 \cos^2\phi + b_{i-1}^2 \sin^2\phi} \tag{4.24}$$

are defined as the equivalent outer and inner radii, respectively, of an elliptic ring at angle ϕ.

We now consider an array formed by several concentric, contiguous (no gaps between rings) elliptic ring radiators, each contributing to the overall directivity function with weighting coefficients c_i as illustrated in Fig. 4.6 for the case of three elliptic rings (for the sake of consistency we will also call the central, elliptic portion of the array a ring).

The directivity function of an array with N elliptic ring radiators arranged in such a way can be written as

$$\begin{aligned} D(\theta,\phi) &= 2\pi a_1 b_1 c_1 \frac{J_1(kr_1 \sin\theta)}{kr_1 \sin\theta} + \\ &\sum_{i=2}^{N} c_i \left\{ 2\pi a_i b_i \frac{J_1(kr_i \sin\theta)}{kr_i \sin\theta} - 2\pi a_{i-1} b_{i-1} \frac{J_1(kr_{i-1} \sin\theta)}{kr_{i-1} \sin\theta} \right\} \end{aligned} \tag{4.25}$$

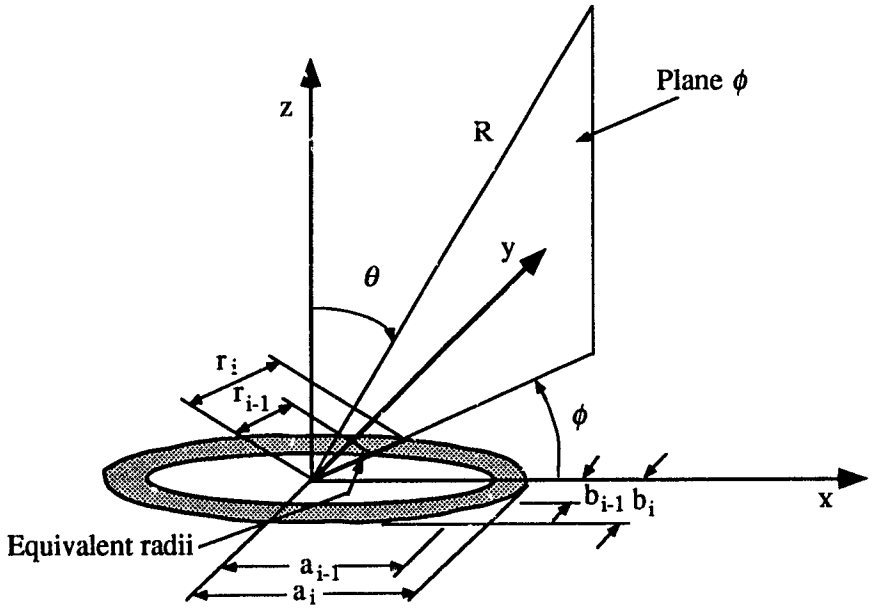

Figure 4.5: Geometry of an elliptic ring radiator and its equivalent radii.

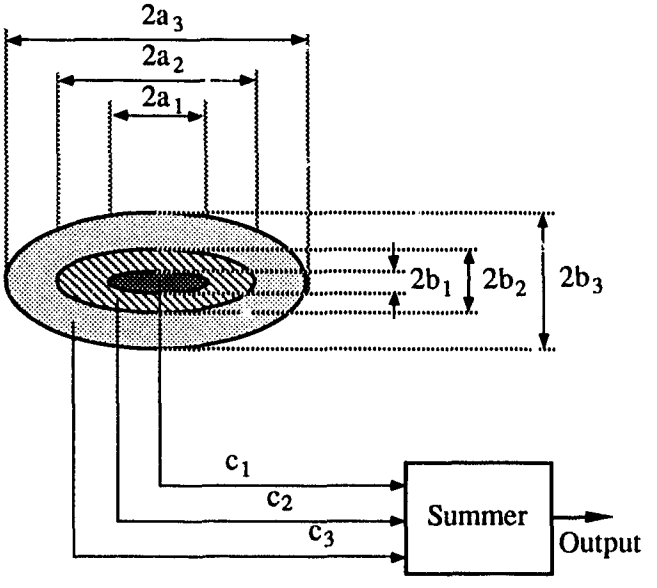

Figure 4.6: Front face of an array of elliptic ring radiators.

where r_i is the equivalent outer radius of the ith elliptic ring given by Eq. (4.23). By varying the weighting coefficients c_i, and the major and minor axes a_i and b_i, one can modify the overall function D to approximate a certain desired function D_d.

4.5 Design of an Array of Elliptic Ring Radiators

There are two possible approaches to the design of elliptic ring arrays. One approach takes advantage of a radiation pattern already designed for a circular ring array. Such a pattern typically has the form of a search-light beam with sidelobes suitably suppressed [18]. A transformation method called angle mapping is presented which transforms such a beam into a fan-type beam and yet maintains the same level of sidelobe suppression. While simple to apply, this approach lacks certain flexibility inherent to the second approach based on the equivalent linear array (ELA) concept. We will use the ELA concept described in [18] and extend it to the design of an array of elliptic ring radiators with the radiation pattern which closely approximates a prescribed radiation pattern. The technique takes advantage of the theory developed for linear arrays. Since linear array design is a mature and well-developed field, such an approach offers obvious advantage.

4.5.1 Angle Mapping Approach

4.5.1.1 Validity of Angle Mapping Approach

We consider radiation patterns of an array on plane ϕ defined in Section 4.2. Comparing the directivity function of an elliptic ring array given by Eq. (4.25) with Eq. (2.2) of that given in Chapter 2, which describes the directivity function of an array of circular ring radiators, we see that both equations have the same form. Therefore, the radiation pattern of an array of elliptic ring radiators on plane ϕ is equal to the radiation pattern of the array of circular ring radiators

with the outer and inner radii given by Eq. (4.23) for any given angle ϕ. That is, the radiation pattern of an elliptic ring array on the plane ϕ is identical to the radiation pattern generated by a circular ring array whose outer and inner radii are equal to the equivalent radii of the elliptic ring array.

In the following developments we investigate the validity of angle mapping approach for the case of the elliptic ring array. We consider a radiation pattern on the plane ϕ shown in Fig. 4.1. We observed earlier that as ϕ changes the radiation pattern remains the same in the u-domain and only the visible range of the radiation pattern is affected. That is, the radiation pattern of the elliptic piston is invariant to different ϕ. In general, this property does not apply to the radiation pattern in the u-domain of an elliptic ring array since its directivity function is not in the form of $D(u)$ as given by Eq. (4.20). We will, however, show that under certain conditions the radiation pattern in the u-domain of an elliptic ring array is invariant to ϕ. To this effect we introduce the concept of *scale-invariance* which will be useful for an array of elliptic ring radiators.

Definition: A radiation pattern is said to be scale-invariant if

$$D(v_1)|_{\phi=\phi_1} = D(v_2)|_{\phi=\phi_2} \tag{4.26}$$

where v_1, v_2, ϕ_1 and ϕ_2 are parameters.

We now show that the scale-invariance defined above guarantees the validity of the angle mapping approach in the analysis of the array of elliptic ring radiators.

Theorem 1: A sufficient condition for the radiation pattern of an array of N elliptic ring radiators to be scale-invariant is

$$b_i = \delta a_i \quad \text{for} \quad i = 1, 2, \ldots, N \tag{4.27}$$

where a_i and b_i are the major and minor axes of the ith elliptic ring, respectively, and δ is a constant.

Proof: Substituting $b_i = \delta a_i$ into Eq. (4.23) we can rewrite Eq. (4.25) as

$$D_a(u) = 2\pi\delta a_1^2 c_1 \frac{J_1(Tua_1/a_N)}{Tua_1/a_N}$$

$$+\sum_{i=2}^{N} c_i \left\{ 2\pi\delta a_i^2 \frac{J_1(Tua_i/a_N)}{Tua_i/a_N} \right.$$

$$\left. -2\pi\delta a_{i-1}^2 \frac{J_1(Tua_{i-1}/a_N)}{Tua_{i-1}/a_N} \right\} \tag{4.28}$$

where

$$u = ka_N \sin\theta \tag{4.29}$$

is called the array angle, a_N is the major axis of the Nth ring (biggest one), and

$$T = \sqrt{\cos^2\phi + \delta^2 \sin^2\phi}. \tag{4.30}$$

For given angles $\phi = \phi_i$; $i = 1, 2$ we introduce the variables

$$v_i = u\sqrt{\cos^2\phi_i + \delta^2 \sin^2\phi_i} \quad \text{for} \quad i = 1, 2. \tag{4.31}$$

Substituting Eq. (4.31) to Eq. (4.28), we find that

$$D(v_1)|_{\phi=\phi_1} = D(v_2)|_{\phi=\phi_2}. \tag{4.32}$$

Thus, Theorem 1 is true. □

We note from Eq. (4.26) that the shape of the radiation pattern is not affected by the variation of angle ϕ. As in the case of the elliptic piston, the visible range of the radiation pattern of an elliptic ring array changes with ϕ. This visible range is determined by

$$-\frac{2\pi}{\lambda} Ta_N \leq u \leq \frac{2\pi}{\lambda} Ta_N. \tag{4.33}$$

We conclude that for scale-invariant beams the radiation pattern is invariant to ϕ and therefore the angle mapping approach which transforms the space angles ϕ and θ to array angle u is valid.

With some minor modification of Eq. (4.25), we can derive the same sufficient condition for an array of elliptic ring radiators with gaps between rings.

4.5.1.2 Design of an Array of Elliptic Ring Radiators by the Angle Mapping Approach

We now discuss how to transform a circular ring array into an elliptic ring array which generates a fan-type beam with a beamwidth of $\Theta_h \times \Theta_v$, while preserving the same sidelobe level as for the radiation pattern of the circular ring array. Here Θ_h is the beamwidth on the plane $\phi = 0°$ and Θ_v is the beamwidth on the plane $\phi = 90°$. We assume that $\Theta_h < \Theta_v$. We first design an array of circular ring radiators which generates a radiation pattern with the beamwidth of Θ_h and the required sidelobe level using the methodology described in [18]. We use the outer and inner radii of these circular rings as the outer and inner major axes of elliptic rings of the array. We then determine the major and minor axes ratio δ for the given beamwidth $\Theta_h \times \Theta_v$. By using the angle mapping approach and imposing the sufficient condition $b_i = \delta a_i$ to the minor axes of elliptic rings for scale-invariance postulated by Theorem 1, we obtain the directivity function of the elliptic array given by Eq. (4.28). To evaluate the beamwidth, we set Eq. (4.28) to the value c corresponding to 3 dB down from its maximum value $D_a(0)$, which leads to an equation

$$D_a(u) = 2\pi\delta a_1^2 c_1 \frac{J_1(Tua_1/a_N)}{Tua_1/a_N} + \sum_{i=2}^{N} c_i \left\{ 2\pi\delta a_i^2 \frac{J_1(Tua_i/a_N)}{Tua_i/a_N} - 2\pi\delta a_{i-1}^2 \frac{J_1(Tua_{i-1}/a_N)}{Tua_{i-1}/a_N} \right\} = c. \quad (4.34)$$

It follows from Eq. (4.34) that

$$Tu = \text{const} \quad (4.35)$$

Substituting the expressions for T and u from Eqs. (4.30) and (4.29) in Eq. (4.35), we obtain a contour equation for all 3 dB down points in space angle (θ, ϕ)-domain, that is

$$Tu = ka_N \sin(\Theta/2)\sqrt{\cos^2\phi + \delta^2 \sin^2\phi} = \text{const.} \quad (4.36)$$

where Θ is the beamwidth and $\Theta/2$ is the 3 dB point in θ-domain. For a given Θ_h (on the plane $\phi = 0°$) and Θ_v (on the plane $\phi = 90°$), we obtain from Eq. (4.36)

$$ka_N \sin(\Theta_h/2) = \delta k a_N \sin(\Theta_v/2) \tag{4.37}$$

which gives us the required ratio of major and minor axes

$$\delta = \frac{\sin(\Theta_h/2)}{\sin(\Theta_v/2)} = \frac{b_i}{a_i} \quad \text{for } i = 1, 2, \ldots, N. \tag{4.38}$$

We consider a scale-invariant elliptic ring array satisfying Eq. (4.27). The design process is illustrated graphically in Fig. 4.7. Fig. 4.7(a) shows the previously designed radiation pattern of a circular ring array in the u-domain with a beamwidth of Θ_u and suitably suppressed sidelobes. This radiation pattern is the same as that of an elliptic ring array except for a different visible range. The maximum visible range for the elliptic ring array occurs on the plane $\phi = 0°$ and is equal to the visible range of the circular ring array. This maximum visible range is mapped onto a semicircle as shown in Fig. 4.7(b) and as discussed in Section 4.3 and illustrated in Fig. 4.3. The diameter of this semicircle determines the maximum major axis a_N of the elliptic ring array. The 3 dB down points A and B in the radiation pattern in Fig. 4.7(a) are mapped onto a sector of a semicircle corresponding to a certain ϕ obtained with the aid of Fig. 4.7(c). This mapping is shown in Fig. 4.7(b) by the dotted lines AC and BD for the case of $\phi = 0°$. The angles of sectors obtained in such a way indicate the beamwidth Θ for any given ϕ. A given 3 dB beamwidth Θ_v is represented by the angle DEC in Fig. 4.7(b). The rays which span this angle intersect the dotted lines AC and BD at the points D and C. The line segment ED or EC gives the diameter of the semicircle. This diameter determines the minor axis b_N. The axes ratio for all elliptic rings of the array is determined by

$$\delta = b_N/a_N \tag{4.39}$$

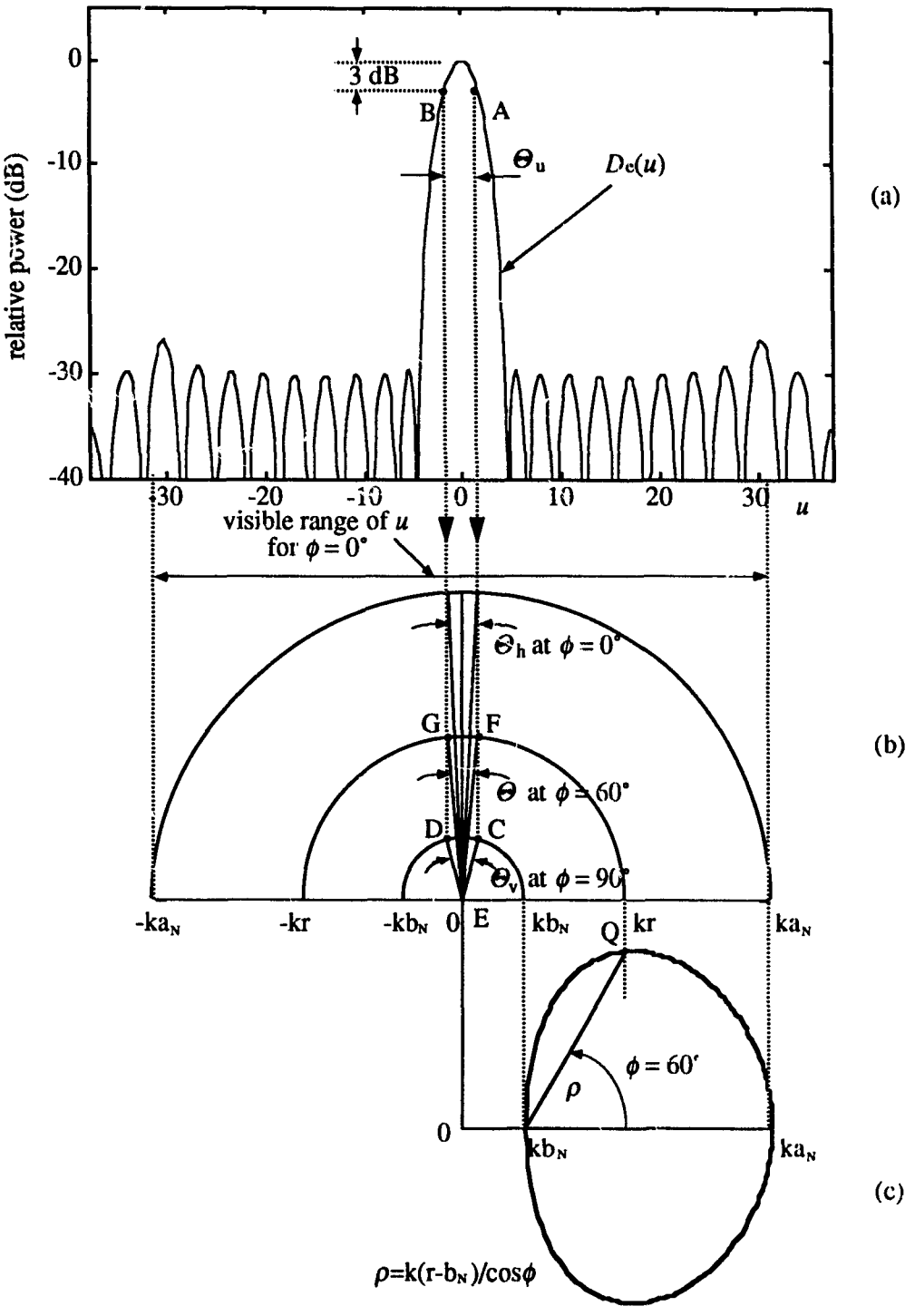

Figure 4.7: Beamwidths (3 dB) Θ of an array of elliptic ring radiators for different space angle ϕ obtained through transformations. (a) Radiation pattern in u-domain. (b) Transformation from θ, r to u. (c) Transformation from ϕ to r.

as postulated by Eq. (4.27). The 3 dB beamwidth Θ on any plane ϕ can be found by mapping the point Q (illustrated for $\phi = 60°$) shown in Fig. 4.7(c) onto the semicircle shown in Fig. 4.7(b). This semicircle intersects the dotted lines AC and BD at F and G. The angle FEG gives us the beamwidth corresponding to the given ϕ.

4.5.2 Equivalent Linear Array Approach

An equivalent linear array (ELA) method [18] was developed for the design of an array of circular ring radiators. The method benefits from existing design techniques developed for linear arrays. The developed methodology requires only simple matrix operations and does not involve nonlinear optimization. In this subsection we will extend the ELA method to the array of elliptic ring radiators using the equivalent radius concept described in Section 4.3. Such an elliptic ring array can generate a radiation pattern which approximates a desired radiation pattern D_d. The directivity function of an elliptic ring array D is given by Eq. (4.25). The error of approximation ϵ can be defined as

$$\epsilon^2 = \|D - D_d\|^2 \qquad =< D - D_d, D - D_d > . \tag{4.40}$$

Here we treat functions as vectors in Hilbert space and use the norm denoted by $\|\cdot\|$ to express the error function. The $< \cdot >$ denotes the inner product.

The objective of the design is to determine the array parameters as given in Eq. (4.25) which minimize the error ϵ. Nonlinear optimization algorithms can be used in array synthesis but are computationally intensive. This presents a practical difficulty for an array of a significant size. Furthermore, the size of the array can not be selected as a variable because of the nature of its effect on the objective function (i. e., approximation error ϵ^2 defined by Eq. (4.40)).

4.5.2.1 Equivalent Linear Array of an Elliptic Ring Radiator

A linear array with $2N$ point elements spaced uniformly by d has the directivity function given by [18]

$$D_l(u') = \sum_{j=1}^{N} w_j \cos((2j-1)u') \tag{4.41}$$

where $\{w_j\}$ are the weighting coefficients and u' is defined as

$$u' = \frac{\pi d}{\lambda} \sin\theta. \tag{4.42}$$

The directivity function of an elliptic ring radiator with equivalent outer and inner radii r_i and r_{i-1}, respectively, given by Eq. (4.22) can be rewritten in the u'-domain as

$$\begin{aligned} D_e(\phi,\theta) &= D_e(u') \\ &= \frac{\pi a_i b_i d}{r_i} \frac{J_1[(2r_i/d)u']}{u'} \\ &\quad - \frac{\pi a_i b_i d}{r_{i-1}} \frac{J_1[(2r_{i-1}/d)u']}{u'}. \end{aligned} \tag{4.43}$$

Assuming an infinite length linear array, it is possible, by proper selection of the weighting coefficients w_j, to obtain a directivity function equal to that of an elliptic ring radiator, that is

$$D_e(u') = \sum_{j=1}^{\infty} w_j \cos((2j-1)u'). \tag{4.44}$$

We call such an array the equivalent linear array to an elliptic ring radiator. As discussed in [18] the functions $\cos((2j-1)u')$ are orthogonal in the u'-domain; their inner products are defined as

$$< \cos((2i-1)u'), \cos((2j-1)u') > \;=\; \frac{4}{\pi} \int_0^{\frac{\pi}{2}} \cos((2i-1)u')$$

$$\cos((2j-1)u')du'$$

$$= \begin{cases} 1 & \text{for } i = j \\ 0 & \text{otherwise.} \end{cases} \tag{4.45}$$

Applying the inner product defined by Eq. (4.45) to Eq. (4.44) we obtain

$$\sum_{j=0}^{\infty} w_j < \cos((2j-1)u'), \cos((2i-1)u') > \; = \; < D_e(u'), \cos((2i-1)u') >$$

(4.46)

which leads to the explicit expression for w_j

$$w_j = \frac{4}{\pi} \int_0^{\frac{\pi}{2}} D_e(u') \cos((2j-1)u')du' \qquad j = 1, \ldots, \infty. \tag{4.47}$$

To express the radiation pattern of an elliptic ring radiator we need a set of equivalent linear arrays rather than one equivalent linear array as in the case of a circular ring radiator [18]. Each equivalent linear array produces a radiation pattern which represents the radiation pattern generated by the elliptic ring radiator on a certain plane ϕ. This is illustrated graphically in Fig. 4.8. The weighting coefficient w_j depends on ϕ and therefore depends on the equivalent outer and inner radii r_i and r_{i-1}. However, under the condition given by Theorem 2 this dependence can be eliminated.

Theorem 2: If the spacing d of the equivalent linear array is

$$d = T\lambda/2 \tag{4.48}$$

where T is given by Eq. (4.30), and if the major and minor axes of an elliptic ring radiator satisfy conditions $a_i = \delta b_i$ and $a_{i-1} = \delta b_{i-1}$, then the weighting coefficients w_j of the set of equivalent linear arrays for the elliptic ring radiator are independent of ϕ.

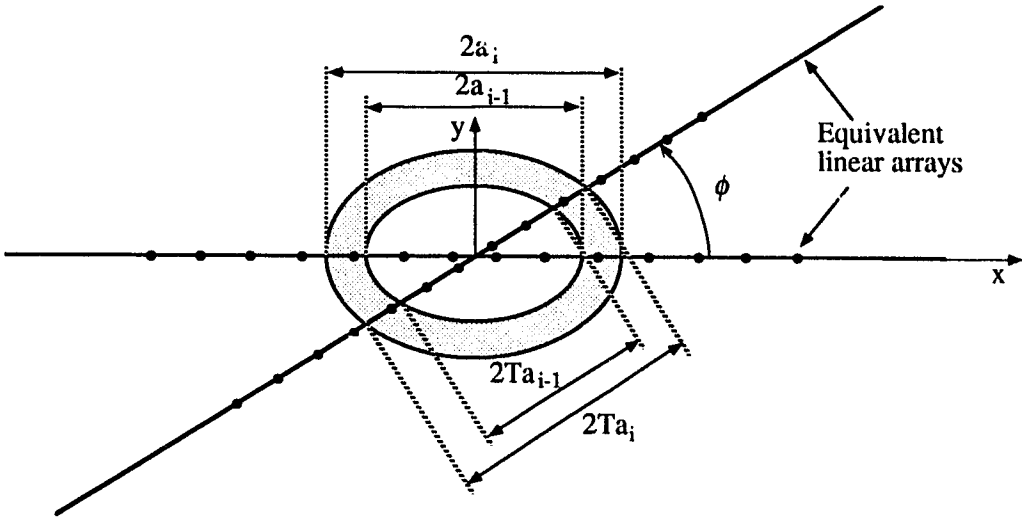

Figure 4.8: Front face of an elliptic ring radiator and its equivalent linear arrays.

Proof: Substituting Eqs. (4.23), (4.30) and (4.48) into Eq. (4.47) and calculating the weighting coefficients w_j, we have

$$\begin{aligned} w_j &= \frac{4}{\pi}\int_0^{\frac{\pi}{2}} \pi\delta a_i\lambda \frac{J_1[(4a_i/\lambda)u']}{2u'}\cos((2j-1)u')du' \\ &\quad -\frac{4}{\pi}\int_0^{\frac{\pi}{2}} \pi a_{i-1}\lambda \frac{J_1[(4a_{i-1}/\lambda)u']}{2u'}\cos((2j-1)u')du' \\ &= w_j|_{\phi=0^\circ} \qquad j=1,\ldots,\infty. \end{aligned} \tag{4.49}$$

Therefore, the coefficient w_j is independent of the space angle ϕ. Thus, Theorem 2 is true. □

The error of approximation given by Eq. (4.40) should be calculated only over the visible range of u' which is smaller than or equal (for $T = 1$) to the range $[0, \pi/2]$ of the inner product defined by Eq. (4.45). However, to simplify calculations we calculate the error over the entire range $[0, \pi/2]$. Because of the small amplitude of the directivity function in the invisible range we find that this step has negligible effect on the results.

4.5.2.2 Design of an Array of Elliptic Ring Radiators by the Equivalent Linear Array Method

The equivalent linear array method for the design of an array of elliptic ring radiators is a technique in which all elliptic ring radiators are represented by a series of sets of equivalent linear arrays, each for different ϕ. The directivity function of the array of elliptic ring radiators is then the sum of the directivity functions of all equivalent linear arrays. Each equivalent linear array of an elliptic ring radiator has in principle an infinite number of elements and associated weighting coefficients. In general, the magnitude of these coefficients decreases for elements far away from the center of the array. It is therefore possible to truncate the equivalent linear array to a finite number of elements by disregarding elements with small weighting coefficients. This truncating process is studied in [18]. As

an illustration of this process, Fig. 4.9(a)-(d) shows radiation patterns of the i-th elliptic ring radiator with $a_i = 4.5\lambda$, $a_{i-1} = 4.1\lambda$, $b_i = 0.9\lambda = 0.2a_i$, and $b_{i-1} = 0.82\lambda = 0.2a_{i-1}$, and its set of equivalent linear arrays truncated to 18 elements spaced by $d = T\lambda/2$ (corresponding to 9 terms in the directivity function). The radiation patterns of the equivalent linear arrays are shown by dotted lines. We observe only a small error (at higher order sidelobes) introduced by this truncation.

The following are the design steps for obtaining the weighting coefficients for the array of elliptic ring radiators using Theorem 2. The procedure presented here is only a summary. The design procedure is similar to that for arrays of circular ring radiators and is detailed in [18, 37, 39].

1. Design a linear array of point radiators with variable spacing $T\lambda/2$ which produces a desired radiation pattern (for example associated with a Dolph-Chebyshev array). As a result, the vector of weighting coefficients $\mathbf{w}_l$, and the size $2N$ (number of elements) of the array are obtained [3]. We call such an array a *prototype*.

2. Consider a series of N elliptic ring radiators, and find their equivalent linear arrays with spacing of $T\lambda/2$ and size of $2N$ by properly selecting their weighting coefficients. Note that in order to have the same spacing in all equivalent linear arrays for all elliptic rings we require the major and minor axes of elliptic rings to satisfy the sufficient condition for scale-invariance given by Eq. (4.27).

3. Arrange the weighting coefficients of the equivalent linear arrays to form a matrix of weighting coefficients as described in [18].

4. Find the weighting coefficients of the elliptic ring array by inverting the matrix formed in step 3 and multiplying it by the vector of weighting coefficients $\mathbf{w}_l$ of the prototype formed in step 1. Here Theorem 2 ensures

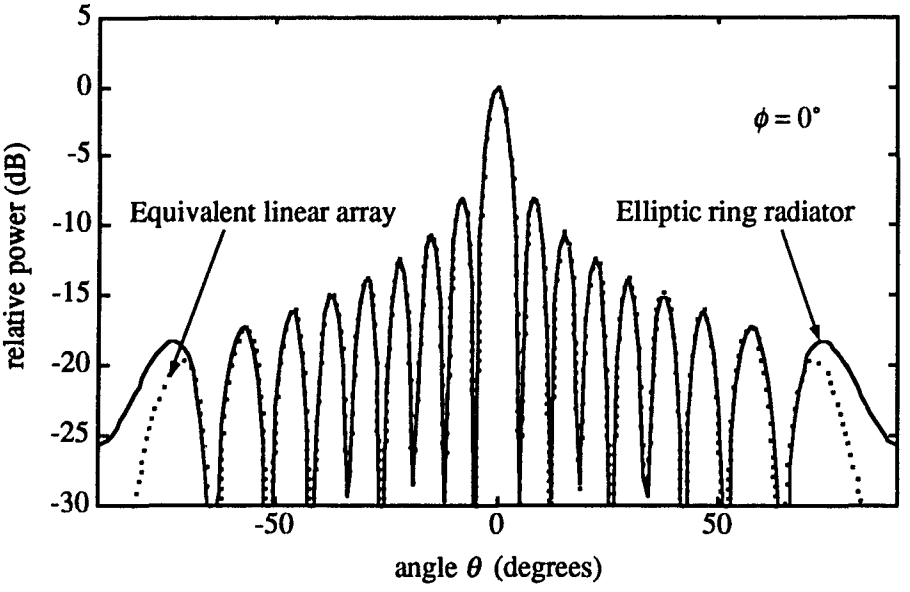

(a)

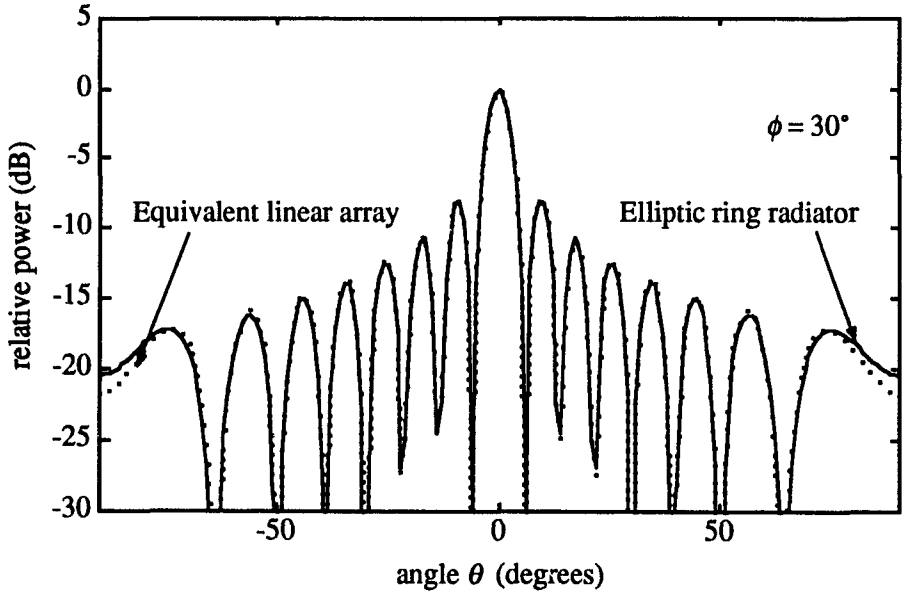

(b)

Figure 4.9: Radiation patterns of an elliptic ring radiator with $a_i = 4.5\lambda$, $a_{i-1} = 4.1\lambda$, $b_i = 0.2a_i$, $b_{i-1} = 0.2a_{i-1}$ and its equivalent linear arrays truncated to 18 elements (9 terms) for different ϕ. (a) $\phi = 0°$. (b) $\phi = 30°$. (c) $\phi = 60°$. (d) $\phi = 90°$.

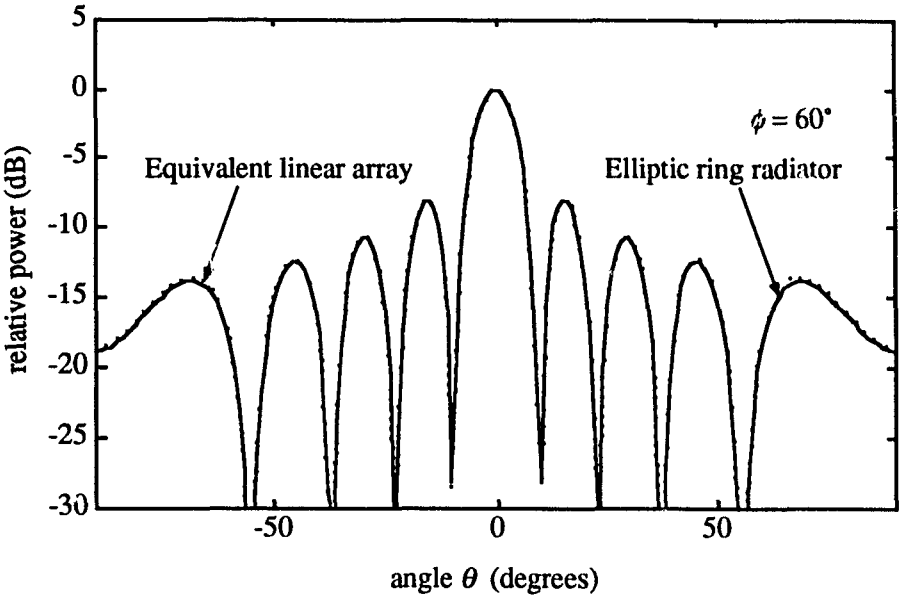

(c)

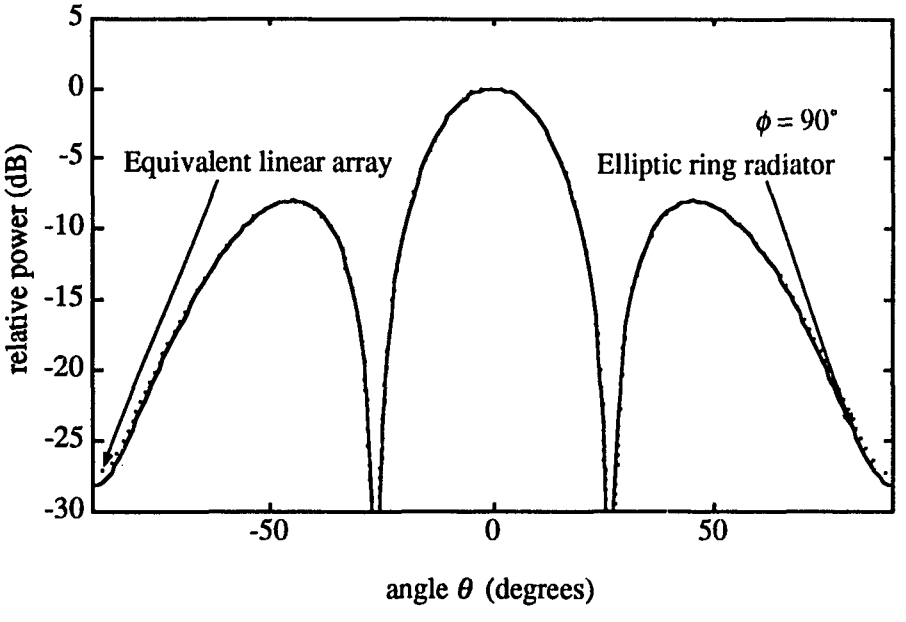

(d)

Figure 4.9: (Continued)

that the matrix of weighting coefficients is independent of ϕ. Therefore, we obtain a set of weighting coefficients of the array for all ϕ, since they are independent of ϕ.

We performed an array design by applying the above design technique to a Dolph-Chebyshev linear array as a prototype. We assumed a prototype of 20 elements spaced by $d = T\lambda/2$ with $\delta = 0.2$. Two cases are considered: 30 dB and 40 dB sidelobe suppression. The beamwidths of the prototype were 6.5° (on the plane $\phi = 0°$) ×32° (on the plane $\phi = 90°$) for sidelobe suppression of 30 dB and 7° (on the plane $\phi = 0°$) ×36° (on the plane $\phi = 90°$) for sidelobe suppression of 40 dB. The design of the elliptic ring array with closely matched radiation patterns was performed which resulted in an elliptic ring array of major axis 10λ consisting of 10 elliptic rings as shown in Fig. 4.10. The corresponding normalized weighting coefficients and ring sizes are tabulated in Table 4.1. The resulting radiation patterns generated by such array are shown in Fig. 4.11(a)-(d) and Fig. 4.12(a)-(d) for different angle ϕ and for 30 dB and 40 dB postulated sidelobe suppression respectively. The dotted lines indicate the radiation patterns of the Dolph-Chebyshev prototypes. We see that the resulting radiation patterns are almost identical to those of postulated Dolph-Chebyshev prototypes. Shown in Fig. 4.13(a) and (b) are the 3-D radiation patterns of the resultant elliptic ring array with postulated sidelobe suppression of 30 dB and 40 dB, respectively. We observe that this is a substantial improvement compared to the radiation pattern of a conventional linear array with rectangular elements.

We also applied the angle mapping approach to the design example presented above and obtained the similar results.

4.6 Summary

Using the novel configuration of an array of elliptic ring radiators it is possible to generate a fan-type beam with greatly suppressed sidelobes. Examples demon-

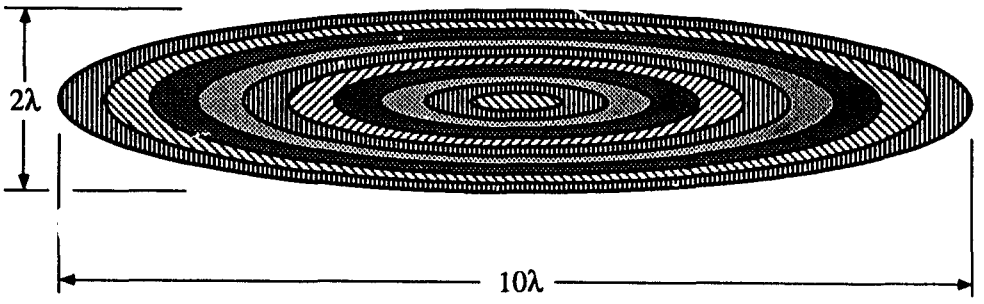

Figure 4.10: Geometry of an array of 10 elliptic ring radiators.

Table 4.1: Weighting coefficients and ring sizes of an array of elliptic ring radiators for different sidelobe suppression levels

Ring No.	Major Axis (λ)		Minor Axis (λ)		Weighting Coefficient	
i	outer	inner	outer	inner	30 dB	40 dB
1	0.5	0.0	0.1	0.0	0.9423	0.9894
2	1.0	0.6	0.2	0.12	1.0000	1.0000
3	1.5	1.1	0.3	0.22	0.8774	0.8957
4	2.0	1.6	0.4	0.32	0.8727	0.8134
5	2.5	2.1	0.5	0.42	0.7032	0.6691
6	3.0	2.6	0.6	0.52	0.6906	0.5617
7	3.5	3.1	0.7	0.62	0.4679	0.4048
8	4.0	3.6	0.8	0.72	0.5107	0.3224
9	4.5	4.1	0.9	0.82	0.0929	0.1528
10	5.0	4.6	1.0	0.92	0.6900	0.2221

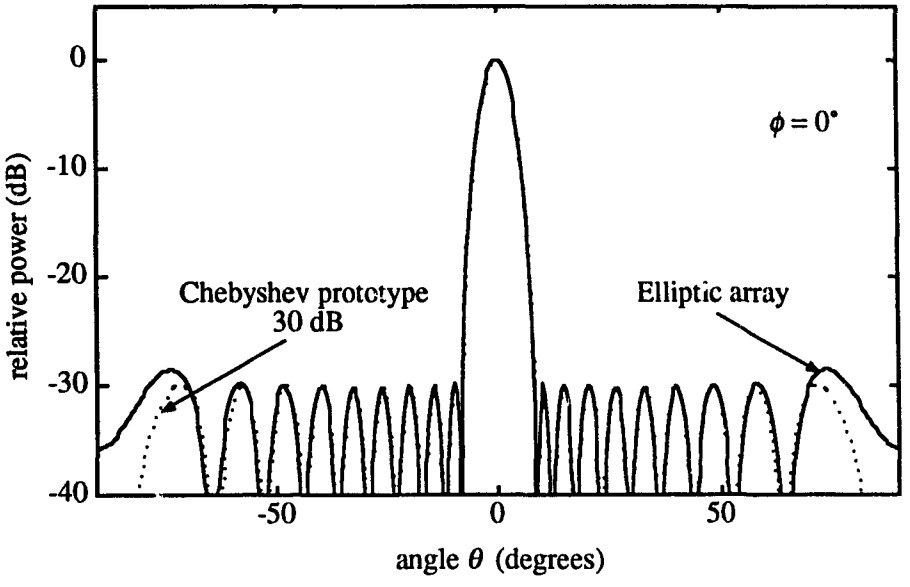

(a)

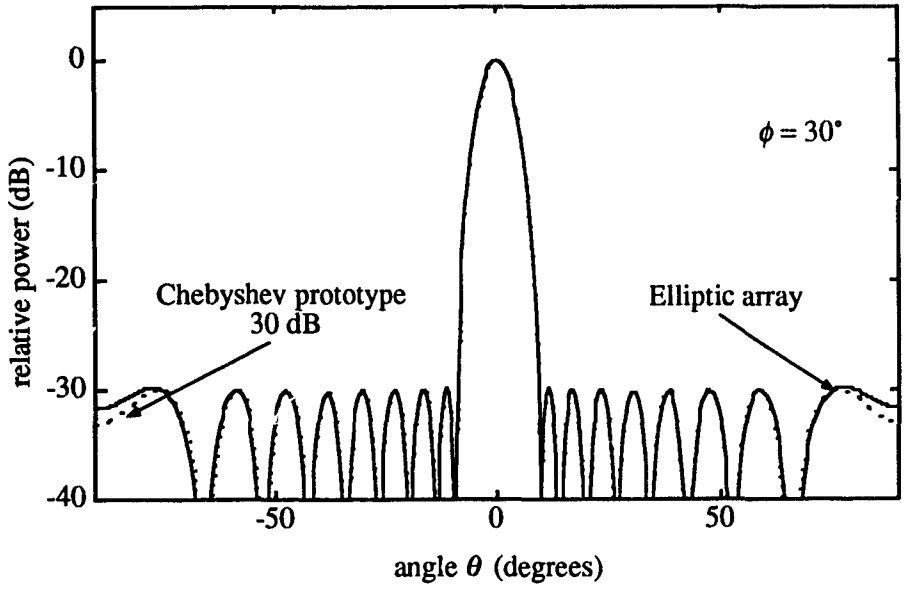

(b)

Figure 4.11: Radiation patterns of an array of elliptic ring radiators with postulated 30 dB sidelobe suppression for different ϕ. (a) $\phi = 0°$. (b) $\phi = 30°$. (c) $\phi = 60°$. (d) $\phi = 90°$.

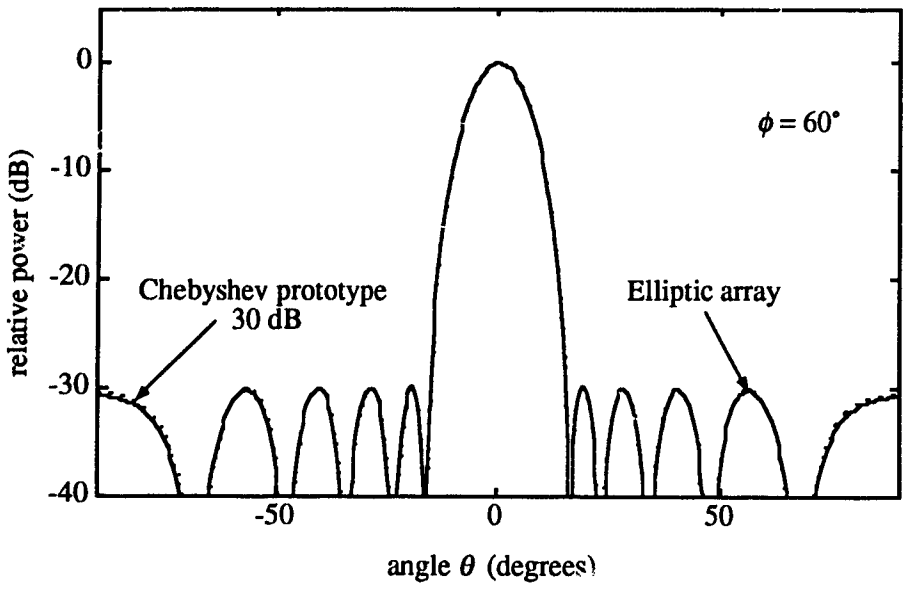

(c)

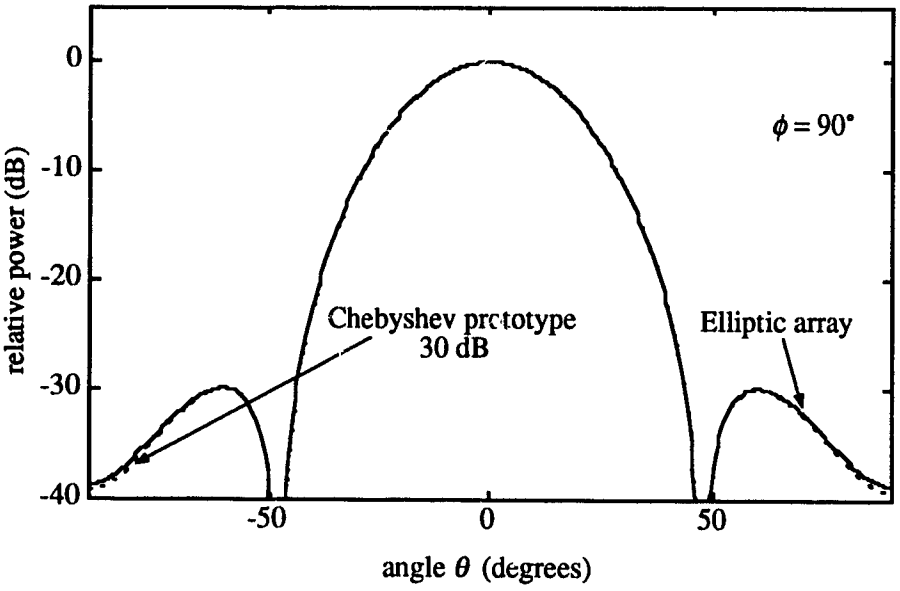

(d)

Figure 4.11: (Continued)

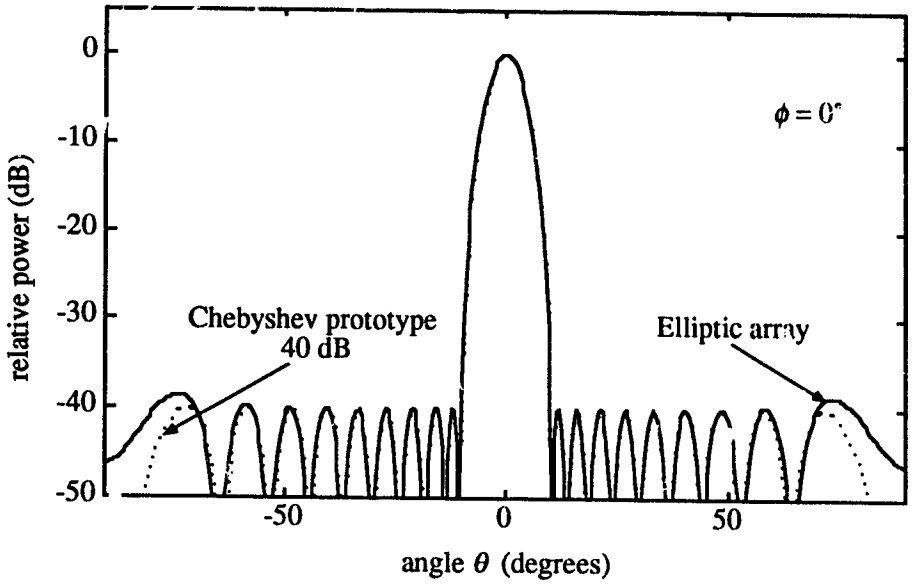

(a)

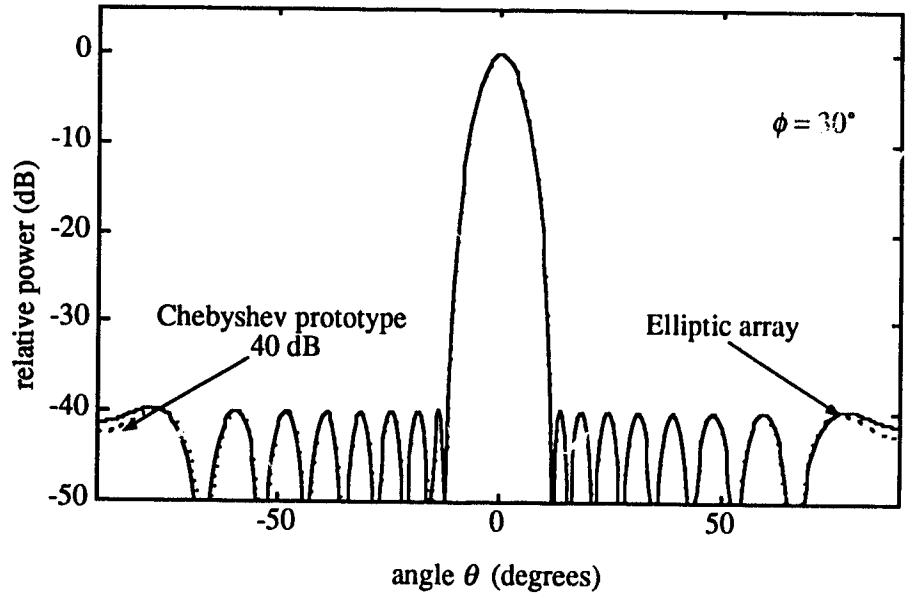

(b)

Figure 4.12: Radiation patterns of an array of elliptic ring radiators with postulated 40 dB sidelobe suppression for different ϕ. (a) $\phi = 0°$. (b) $\phi = 30°$. (c) $\phi = 60°$. (d) $\phi = 90°$.

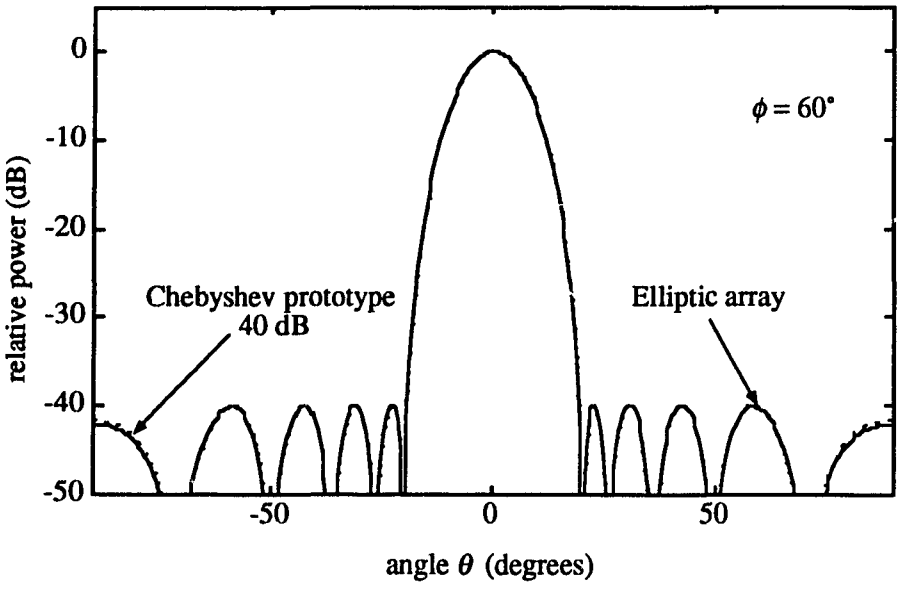

(c)

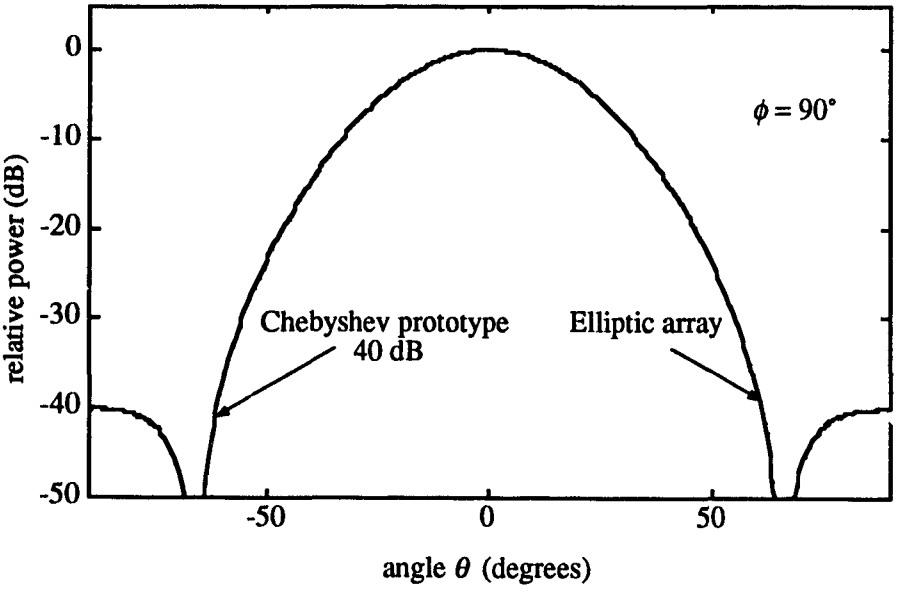

(d)

Figure 4.12: (Continued)

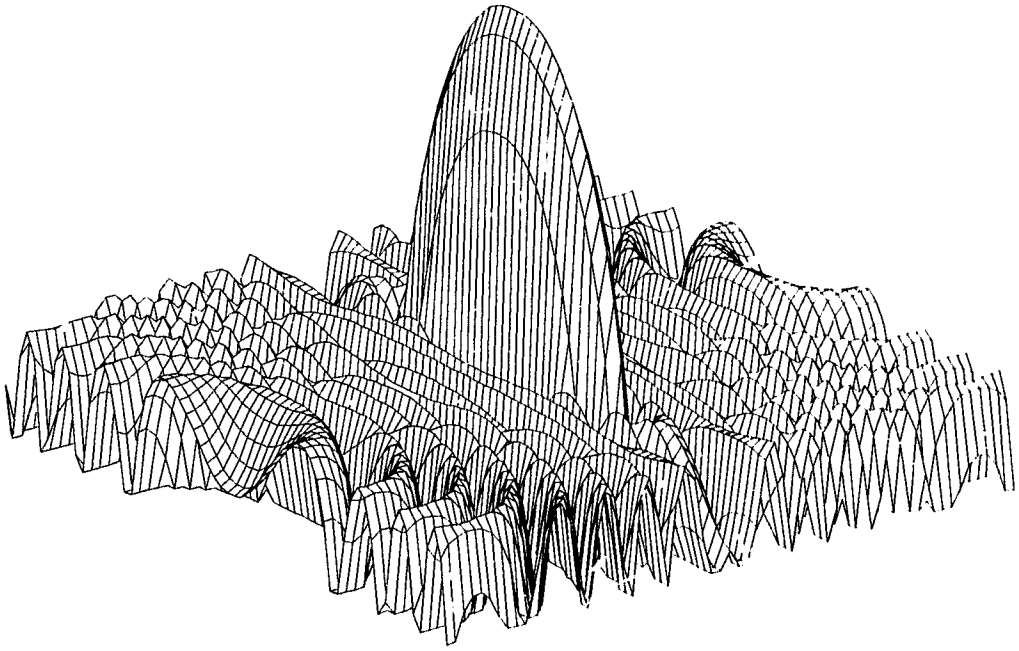

(a)

Figure 4.13: Three-dimensional radiation patterns of an array of elliptic ring radiators. (a) Postulated 30 dB sidelobe suppression. (b) Postulated 40 dB sidelobe suppression.

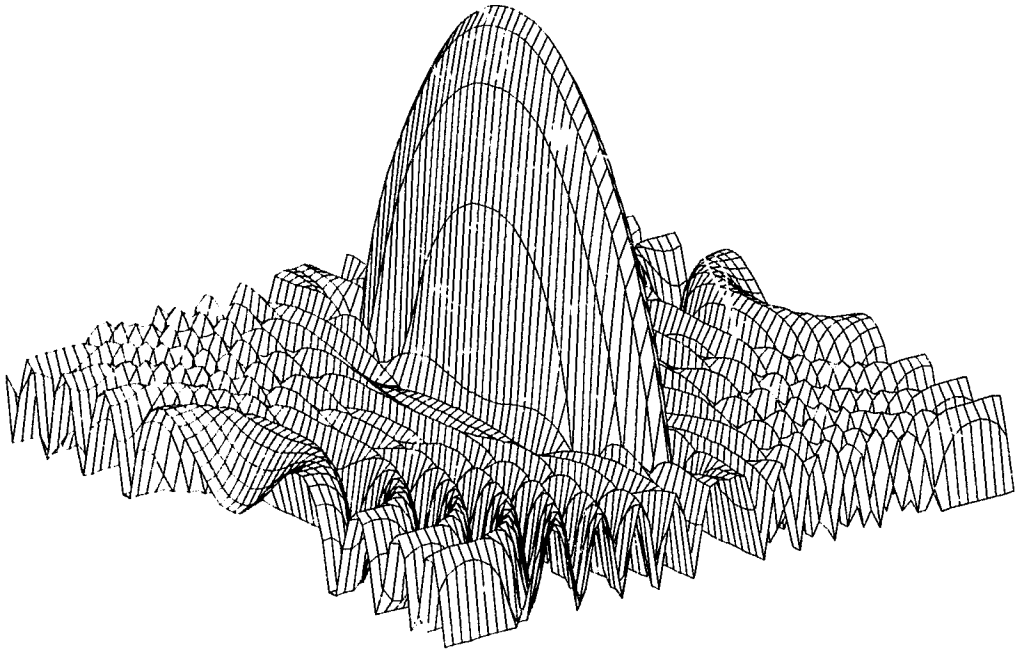

(b)

Figure 4.13: (Continued)

strate that sidelobe suppression of over 40 dB in all possible direction is achievable. This result shows the superior performance of elliptic ring arrays in comparison with rectangular element arrays used in sidescan sonar systems.

Chapter 5

Equivalent Linear Array Approach to Array Pattern Synthesis

In Chapter 2 we introduced the concept of an equivalent linear array for use in the design of novel circular ring arrays. We extended this concept to the design of novel elliptic ring arrays in Chapter 4. In this chapter we present a new and effective array pattern synthesis method based on the equivalent linear array concept.

5.1 Introduction

A large number of papers have been devoted to the important problem of array synthesis. Dolph's classic paper [21] derived the array weights for a uniformly spaced linear array of isotropic elements that yields the minimum beamwidth for a given sidelobe level. Villeneuve [22] described how Taylor's method [7] developed for continuous shading can be applied to discrete arrays. Elliot and Stern [25] presented additional pattern synthesis techniques for arrays. However, all of these techniques are applicable only to arrays consisting of uniformly spaced elements with nondirectional radiation patterns (isotropic elements).

In a recent paper [31] Olen and Compton, Jr. presented a numerical synthesis

technique that can be used for arrays consisting of a set of elements each with an arbitrary radiation pattern. However, this method is a numerical technique and it does not yield analytic solutions for the required weights. The aim of this chapter is to present a new analytic synthesis technique based on the linear equivalent array approach [18]. This approach does not involve any numerical optimization routine — only ordinary matrix operations are required. The proposed technique can be used to synthesize arrays of uniformly spaced elements each with an arbitrary radiation pattern.

5.2 Formulation

Let us consider a 2N-element linear array. Let $f_i'(\theta)$ be the directivity function of the ith element, such that $f_i'(\theta) = f_i'(-\theta)$, $f_i'(\theta) = f_i'(\pi - \theta)$, and $f_i'(\theta) \neq$ const. We call such an element a nonisotropic element. All elements are uniformly spaced by d from their centers as shown in Fig. 5.1. The directivity function of such an array is given by

$$D'(\theta) = \sum_{i=1}^{N} f_i'(\theta) w_i \cos\left[(2i-1)\frac{\pi d}{\lambda}\sin\theta\right] \tag{5.1}$$

where w_i is the weighting coefficient associated with the ith element. Array symmetry is assumed, that is $w_i = w_{-i}$ and $f_i'(\theta) = f_{-i}'(\theta)$. We intend to find a set of weighting coefficients w_i such that the resulting radiation pattern $D(\theta)$ approximates a desired radiation pattern.

In the following developments it is convenient to map the angle θ into the u domain defined as

$$u = \frac{\pi d}{\lambda}\sin\theta. \tag{5.2}$$

With this mapping Eq. (5.1) can be written as

$$D(u) = \sum_{i=1}^{N} f_i(u) w_i \cos[(2i-1)u]; \qquad -\frac{\pi d}{\lambda} \leq u \leq \frac{\pi d}{\lambda}. \tag{5.3}$$

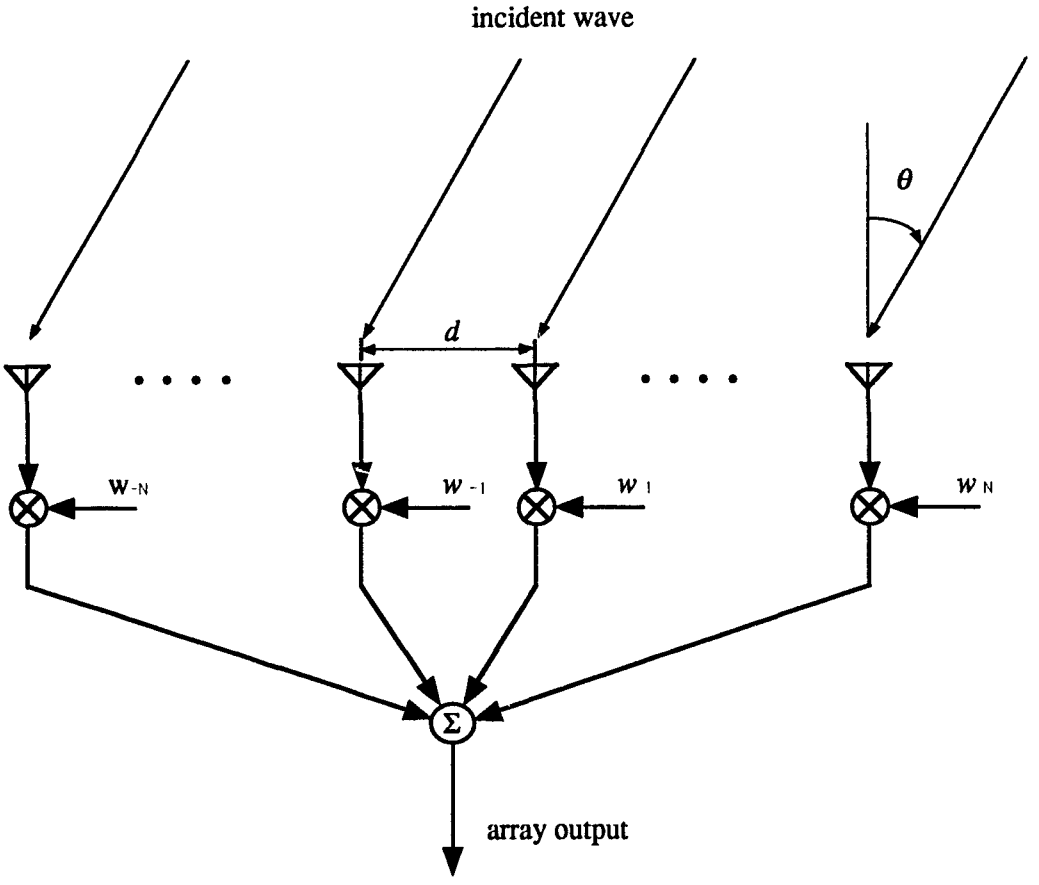

Figure 5.1: Arrangement of a linear array of $2N$ elements.

Any arbitrary directivity function $f_i(u)$ with $f_i(\pi/2) = 0$ in Eq. (5.3) can be generated by an infinite length linear array consisting of an even number of point (isotropic) elements with properly selected weighting coefficients $a_{i,j}$, that is

$$f_i(u) = \sum_{j=1}^{\infty} a_{i,j} \cos[(2j-1)u]. \tag{5.4}$$

We call such an array the equivalent linear array to the ith element.

It can be shown that the functions $\cos[(2i-1)u]$; $i = 1, \ldots, \infty$ form an orthogonal set spanning the Hilbert space $\mathcal{H}$ with inner product, defined as

$$\begin{aligned} < \cos[(2i-1)u], \cos[(2j-1)u] > &= \frac{4}{\pi} \int_0^{\frac{\pi}{2}} \cos[(2i-1)u] \cos[(2j-1)u] du \\ &= \begin{cases} 1, & \text{for } i = j \\ 0, & \text{otherwise.} \end{cases} \end{aligned} \tag{5.5}$$

The inner product as given by Eq. (5.5) constrains the u-domain to range $[0, \pi/2]$. This implies that the constant d in Eq. (5.2) must be equal to $\lambda/2$. Later on we will discuss the case of $d \neq \lambda/2$. Note that the cosine family in Eq. (5.4) includes odd harmonics only. Therefore, we impose a condition that $f_i(\pi/2) = 0$. In general, for $f_i(\pi/2) = c \neq 0$, we might consider a cosine family which includes even harmonics only. Such a family yields smaller approximation error.

Applying the inner product defined by Eq. (5.5) to Eq. (5.4) we obtain:

$$\sum_{j=0}^{\infty} a_{i,j} < \cos[(2j-1)u], \cos[(2k-1)u] > \;=\; < f_i(u), \cos[(2k-1)u] > \tag{5.6}$$

which leads to the explicit expression for weights $a_{i,j}$:

$$a_{i,j} = \frac{4}{\pi} \int_0^{\frac{\pi}{2}} f_i(u) \cos[(2j-1)u] du \qquad j = 1, \ldots, \infty. \tag{5.7}$$

We now represent all nonisotropic elements by a series of equivalent linear arrays with isotropic elements. The directional response of the array of nonisotropic elements is then the sum of the directivity functions of all equivalent linear arrays, which is

$$D(u) = \sum_{i=1}^{N} \sum_{j=1}^{\infty} a_{i,j} \cos[(2j-1)u] w_i \cos[(2i-1)u]. \tag{5.8}$$

The equivalent linear array of a nonisotropic element has in principle an infinite number of elements and associated weighting coefficients. However, it can be shown that the amplitudes of these coefficients decrease for elements far away from the center of the array. It is therefore possible to truncate the equivalent linear array to a finite number of elements M and have a negligible truncation error by disregarding elements with small weighting coefficients. We can then express the directivity function using a finite number of terms, that is

$$\hat{D}(u) = \sum_{i=1}^{N} \sum_{j=1}^{M} a_{i,j} \cos[(2j-1)u] w_i \cos[(2i-1)u]. \tag{5.9}$$

Eq. (5.9) can be written as

$$\hat{D}(u) = \sum_{i=1}^{N} \sum_{j=1}^{M} \frac{1}{2} a_{i,j} w_i \{\cos[2(i+j-1)u] + \cos[2(i-j)u]\} \tag{5.10}$$

or in matrix form for $M > N$ as

$$\hat{D}(u) = \frac{1}{2} \mathbf{c}^T (\mathbf{A} + \mathbf{B} + \mathbf{D}) \mathbf{w} \tag{5.11}$$

where the superscript T denotes the transpose and

$$\mathbf{c} = [\ 1 \quad \cos 2u \quad \cos 4u \quad \ldots \quad \cos(2(M+N-1)u)\ ]^T; \tag{5.12}$$

$$\mathbf{w} = [\ w_1 \quad w_2 \quad w_3 \quad \ldots \quad w_N\ ]^T; \tag{5.13}$$

$$\mathbf{A} = \begin{bmatrix} 0 & \cdots & & & & \\ a_{1,1} & & & & & \\ a_{1,2} & a_{2,1} & & & & \\ a_{1,3} & a_{2,2} & a_{3,1} & & & \\ \vdots & & & \ddots & & \\ & & & & a_{N-1,1} & 0 \\ & & & & & a_{N,1} \\ a_{1,M} & a_{2,M-1} & \cdots & & & \vdots \\ 0 & a_{2,M} & \cdots & & & \\ & & a_{3,M} & \cdots & & \\ \vdots & & & \ddots & & \\ & & & & a_{N-1,M} & a_{N,M-1} \\ & & & & 0 & a_{N,M} \end{bmatrix}; \tag{5.14}$$

$$\mathbf{B} = \begin{bmatrix} a_{1,1} & a_{2,2} & \cdots & & & a_{N,N} \\ a_{1,2} & a_{2,3} & \cdots & & & a_{N,N+1} \\ \vdots & & & & & \vdots \\ & & & & & a_{N,M} \\ & & & & a_{N-1,M} & 0 \\ \vdots & & & & & \vdots \\ a_{1,M-2} & a_{2,M-1} & a_{3,M} & & & \\ a_{1,M-1} & a_{2,M} & & & & \\ a_{1,M} & & & & & \\ 0 & & & & & \\ \vdots & & & & & \end{bmatrix}; \tag{5.15}$$

$$\mathbf{D} = \begin{bmatrix} 0 & \cdots & & & & \\ 0 & a_{2,1} & a_{3,2} & \cdots & & a_{N,N-1} \\ \vdots & & a_{3,1} & \cdots & & a_{N,N-2} \\ & & & \ddots & & \vdots \\ & & & & a_{N-1,1} & a_{N,2} \\ & & & & & a_{N,1} \\ & & & & & 0 \\ & & & & & \vdots \end{bmatrix}. \tag{5.16}$$

The purpose of the design is to find a vector of weighting coefficients $\mathbf{w}$ which minimizes the mean square error between a desired radiation pattern $D_p(u)$ and

the synthesised pattern $\hat{D}(u)$ as given by Eq. (5.11). There are many synthesis methods available but they differ only in the choice of the error criterion and the algorithm used for its minimization [30]. Here we choose the mean square error criterion which leads to a closed form solution.

We begin with a linear array of $2K+1$ isotropic elements called a prototype. We design a prototype using methods developed for linear arrays of isotropic elements. For instance, using the Dolph-Chebyshev approach we can achieve a desired sidelobe suppression by proper selection of weighting coefficients p_i, $i = -K, \ldots, 0, \ldots, K$ such that $p_i = p_{-i}$. The directivity function of the prototype is given by

$$\hat{D}_p(u) = \mathbf{c}^T \mathbf{p} \tag{5.17}$$

where the $(M+N) \times 1$ augmented vector is

$$\mathbf{p} = [\ p_0 \quad 2p_1 \quad 2p_2 \quad \ldots \quad 2p_K \quad 0 \quad \ldots \quad 0\ ]^T. \tag{5.18}$$

We next approximate the directivity function $\hat{D}_p(u)$ by $D(u)$ through a proper choice of vector $\mathbf{w}$.

The mean square approximation error e is

$$\begin{aligned} e^2 &= \|D - D_p\|^2 \\ &= < D - D_p, D - D_p > . \end{aligned} \tag{5.19}$$

Here we treat functions as vectors in Hilbert space and use the norm denoted by $\|\cdot\|$ to express the error function.

We postulate a sufficiently large number M of elements in Eq. (5.9) such that the error associated with the truncation is negligible compared to the approximation error given by Eq. (5.19). If we ignore this truncation error we can write $\hat{D}(u) = D(u)$. In such a situation, we can express the approximation error in

matrix form as

$$\begin{aligned} e^2 &= < \mathbf{c}^T\mathbf{G}\mathbf{w} - \mathbf{c}^T\mathbf{p}, \mathbf{c}^T\mathbf{G}\mathbf{w} - \mathbf{c}^T\mathbf{p} > \\ &= (\mathbf{G}\mathbf{w})^T < \mathbf{c}\mathbf{c}^T > \mathbf{G}\mathbf{w} - \mathbf{p}^T < \mathbf{c}\mathbf{c}^T > \mathbf{G}\mathbf{w} \\ &\quad -(\mathbf{G}\mathbf{w})^T < \mathbf{c}\mathbf{c}^T > \mathbf{p} + \mathbf{p}^T < \mathbf{c}\mathbf{c}^T > \mathbf{p} \\ &= (\mathbf{G}\mathbf{w} - \mathbf{p})^T(\mathbf{G}\mathbf{w} - \mathbf{p}) \end{aligned} \tag{5.20}$$

where

$$\mathbf{G} = \mathbf{A} + \mathbf{B} + \mathbf{D}. \tag{5.21}$$

Note that scale factors are dropped in Eq. (5.20).

The vector of weighting coefficients which minimizes the approximation error e is obtained as

$$\mathbf{w} = (\mathbf{G}^T\mathbf{G})^{-1}\mathbf{G}^T\mathbf{p}, \tag{5.22}$$

and the minimum error is

$$e^2 = (\mathbf{G}(\mathbf{G}^T\mathbf{G})^{-1}\mathbf{G}^T\mathbf{p} - \mathbf{p})^T(\mathbf{G}(\mathbf{G}^T\mathbf{G})^{-1}\mathbf{G}^T\mathbf{p} - \mathbf{p}). \tag{5.23}$$

A similar matrix equation can be obtained for an array with an odd number of elements.

The elements of the matrices **A**, **B** and **D** are the weighting coefficients of the equivalent linear arrays of the nonisotropic elements. The dominant weighting coefficients are $a_{1,1}, a_{2,1}, \ldots, a_{N,1}$ (first term in the expansion of $f_i(u)$ in Eq. (5.4). Since $\mathbf{G} = \mathbf{A} + \mathbf{B} + \mathbf{D}$ we find that the matrix **G** can be expressed as

$$\mathbf{G} = \begin{bmatrix} a_{1,1} & \cdots & & & & \\ a_{1,1} + \delta_1 & a_{2,1} + \delta_2 & & & & \\ \vdots & a_{2,1} + \delta_3 & & & & \\ & & \ddots & & \vdots & \\ & & & a_{N-1,1} + \delta_{2N-3} & a_{N,1} + \delta_{2N-2} & \\ & & & & a_{N,1} + \delta_{2N-1} & \\ & & & & \vdots & \end{bmatrix}; \tag{5.24}$$

where δ_i are the small numbers compared with the dominant weighting coefficients $a_{i,1}$ and the rest elements of the matrix $\mathbf{G}$ are either zeros or small numbers. It is clear that the matrix $\mathbf{G}$ has full rank. Thus the matrix $\mathbf{G}^T\mathbf{G}$ is invertible and Eq. (5.22) has an unique solution.

Shown in Fig. 5.2 is an example to illustrate the equivalent linear array concept graphically. We consider a linear array of 4 nonisotropic elements spaced equally by d and weighted by a set of weighting coefficients $\{w_i\}$, $i = -2, -1, 1, 2$ (as shown in Fig. 5.2(a)). As discussed earlier, each nonisotropic element can be represented by its equivalent linear array of isotropic elements. We call such an array an elementary equivalent array. These representations are illustrated in Fig. 5.2(b) for the elementary equivalent arrays truncated to 4 isotropic elements (small dots in Fig. 5.2 indicate isotropic elements). The associated weighting coefficients of the elementary equivalent arrays are $\{a_i\}$, $\{b_i\}$, $\{c_i\}$ and $\{d_i\}$, $i = -2, -1, 1, 2$, respectively. Finally, as shown in Fig. 5.2(c), we use superposition to obtain an equivalent array with 7 equally spaced isotropic elements which approximates the original 4-nonisotropic-element array. We call this array the global equivalent array. The weighting coefficients of the global equivalent array are $\{e_i\}$, $i = -3, \ldots, 3$. Thus, the original synthesis problem of an array of nonisotropic elements becomes one of an array with isotropic elements. Therefore, we can utilize all existing synthesis techniques developed for such arrays.

It should be emphasized that the above approach does not impose any restriction on the radiation pattern of each nonisotropic element. The only requirement is the equal spacing between elements. This condition is needed to ensure that we obtain a global equivalent array of equally spaced isotropic elements after each nonisotropic element is represented by its elementary equivalent linear array. Note that the spacing between elements in the elementary equivalent array can be d/n, where n is a positive integer chosen so as to minimize the approximation error. Such a spacing makes it possible to avoid the grating lobes in the elementary

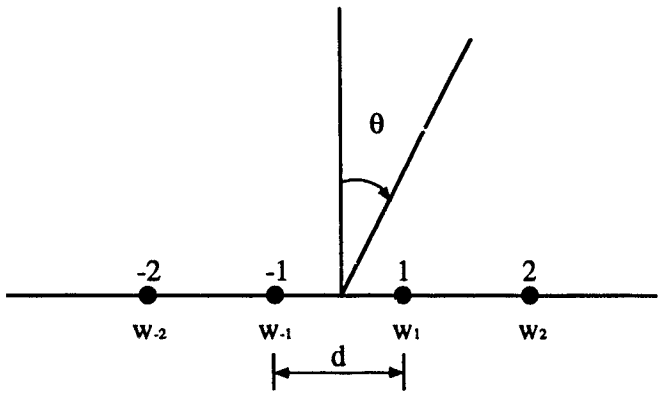

(a)

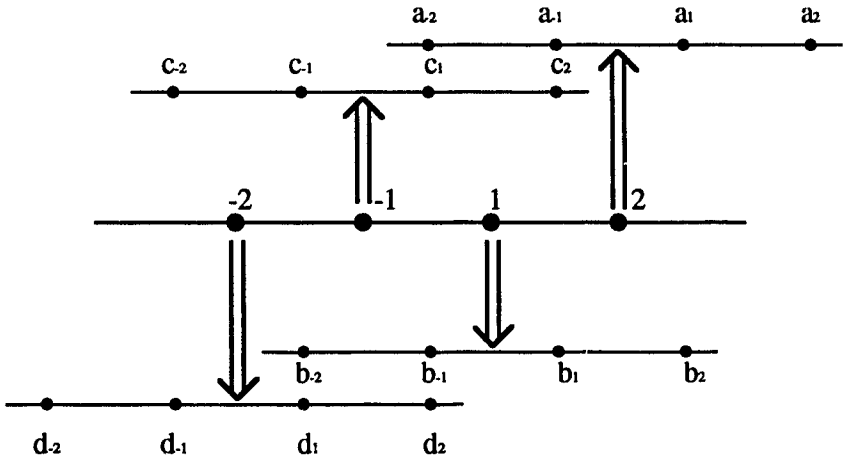

(b)

Figure 5.2: Equivalent linear array concept for a 4-element array. (a) A linear array of 4 nonisotropic elements weighted by w_i, $i = -2, -1, 1, 2$. (b) Each element is represented by its equivalent linear array truncated to 4 elements. (c) The equivalent array of 7 isotropic elements for the 4-nonisotropic-element array is obtained by superposition.

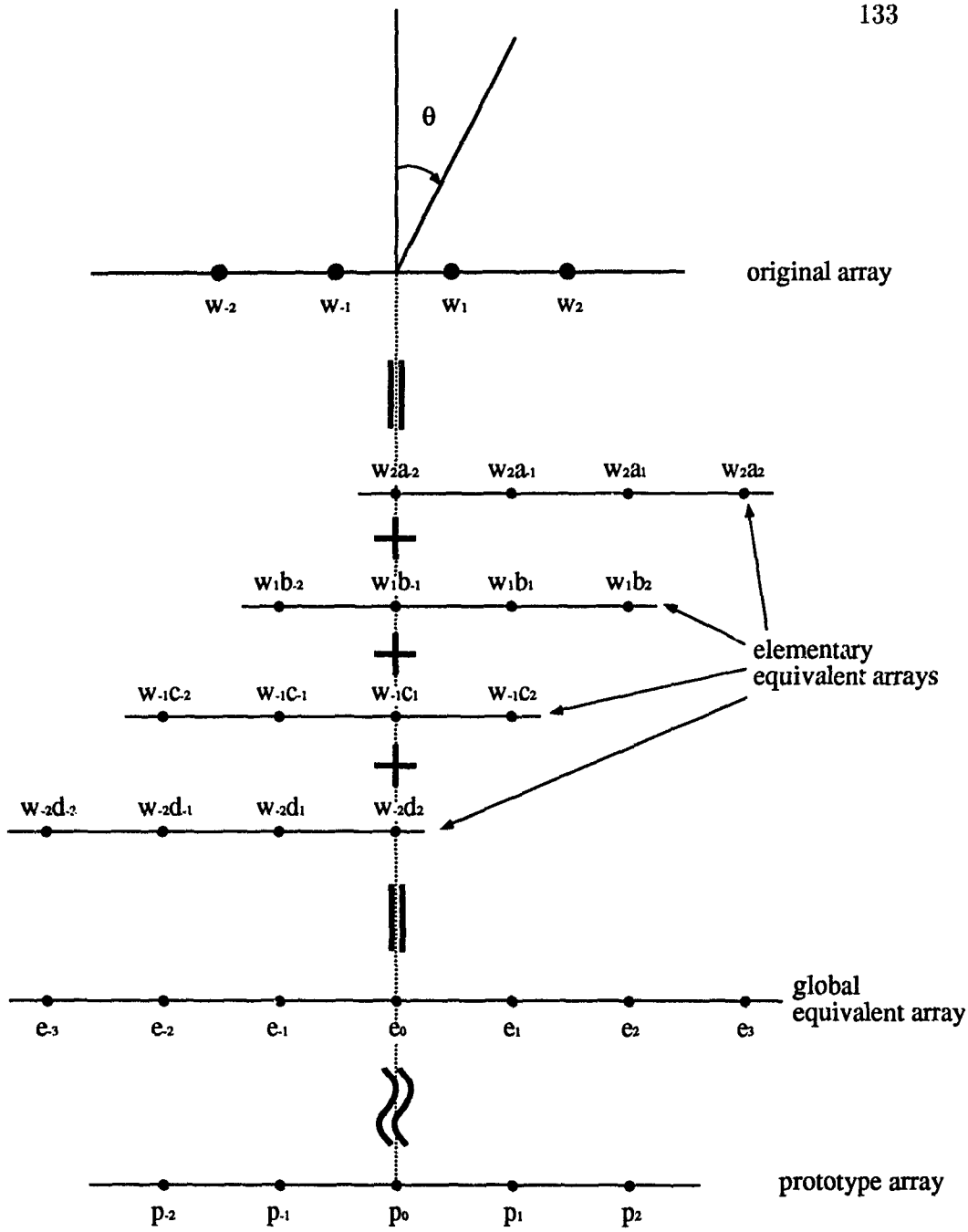

(c)

Figure 5.2: (Continued)

equivalent array for the case of $d \geq \lambda$.

Consider our illustrative example again. Suppose that the weighting coefficients d_{-2} and a_2 shown in Fig. 5.2(b) in the truncated elementary equivalent arrays are small compared to the other weighting coefficients $\{d_{-1}, d_1, d_2\}$ and $\{a_{-2}, a_{-1}, a_1\}$, respectively. We call the elements associated with weighting coefficients $\{d_{-1}, d_1, d_2\}$ and $\{a_{-2}, a_{-1}, a_1\}$ the dominant elements. This leads to the small associated weighting coefficients e_{-3} and e_3 of the global equivalent array in Fig. 5.2(c). Since the negative 3rd and positive 3rd elements of the global equivalent array make only minor contributions to the radiation pattern, we can postulate that the suitable prototype array for synthesizing the global equivalent array has only 5 isotropic elements. Through a proper choice of the weighting coefficients $\{w_i\}$, we can then minimize the approximation error of the radiation patterns between the 5-element prototype array and the 7-element global equivalent array shown in Fig. 5.2(c). In general, because there are a certain number of dominant elements in a global equivalent array, we can always find a suitable prototype array by varying its size such that its radiation pattern can be approximated by the global equivalent array with minimum approximation error.

In practical calculation, in order to be sure that the approximation error associated with an elementary equivalent array is negligible, we set a large number of elements. We then postulate a minimum size of the prototype. In this particular example we postulate that the elements associated with weighting coefficients $\{d_1, d_2\}$, $\{c_{-1}, c_1, c_2\}$, $\{b_{-2}, b_{-1}, b_1\}$ and $\{a_{-2}, a_{-1}\}$ are dominant. This leads to the minimum size of 3 of the prototype array. After calculating the approximation error for such an initial prototype, we increase the size of the prototype to 5 which corresponds to the situation that only two elements in each elementary equivalent array are dominant. Since this is not always the case we repeat the calculation of approximation error with the prototype size increased to $7, 9, \ldots$, until a global minimum of the approximation error is reached. Once the prototype size is determined we proceed with finding the weighting coefficients $\{w_i\}$ which

minimize the approximation error of the radiation patterns between the global equivalent array and the prototype array.

With some minor modifications, the approach described above for the case of $d = \lambda/2$, can also be used for the case $d \neq \lambda/2$. The fact that $d \neq \lambda/2$ implies that the functions in Eq. (5.5) are no longer orthogonal. The approach presented is still applicable; however, a matrix inversion is required.

To illustrate this point we replace the directivity function of the ith element by that of a truncated equivalent linear array of $2M$ elements. The optimum weighting coefficients in the sense of minimum mean square error are then given by

$$\mathbf{a}_i = \mathbf{H}^{-1}\mathbf{f}_i \tag{5.25}$$

where

$$\mathbf{a}_i = [\ a_{i,1} \quad a_{i,2} \quad \ldots \quad a_{i,M}\ ]^T; \tag{5.26}$$

$$\mathbf{f}_i = [\ < f_i(u), \cos u > \quad \ldots \quad < f_i(u), \cos((2M-1)u) >\ ]^T; \tag{5.27}$$

and the elements of matrix $\mathbf{H}$ are

$$\begin{aligned} h_{j,k} &= < \cos[(2j-1)u].\cos[(2k-1)u] > \\ &= \frac{2\lambda}{\pi d}\int_0^{\frac{\pi d}{\lambda}} \cos[(2j-1)u]\cos[(2k-1)u]du. \end{aligned} \tag{5.28}$$

Note that the inner product defined by Eq. (5.5) now has a range $[0, \pi d/\lambda]$ in the u-domain. The error function is then

$$\begin{aligned} \epsilon^2 &= (\mathbf{Gw})^T < \mathbf{cc}^T > \mathbf{Gw} - \mathbf{p}^T < \mathbf{cc}^T > \mathbf{Gw} \\ &\quad -(\mathbf{Gw})^T < \mathbf{cc}^T > \mathbf{p} + \mathbf{p}^T < \mathbf{cc}^T > \mathbf{p} \end{aligned} \tag{5.29}$$

The optimum solution for the weighting coefficients vector which minimizes the error ϵ is obtained as

$$\mathbf{w} = (\mathbf{G}^T < \mathbf{cc}^T > \mathbf{G})^{-1}\mathbf{G}^T < \mathbf{cc}^T > \mathbf{p} \tag{5.30}$$

It is interesting to note an analogy between the equivalent linear array approach and the Woodward-Lawson method [27, 28]. The latter method, proposed for radio aerials, is applicable strictly to continuous transducers. It can be applied to point arrays provided that the elements are uniformly spaced and are sufficiently numerous. The method is based on the weighted superposition of a number of $(\sin u)/u$ patterns deflected by different amounts to one or the other side of the $u = 0$ axis, and with peak amplitudes suitably chosen. In the equivalent linear array approach we use superposition to decompose a radiation pattern of an array of nonisotropic elements to a sum of the radiation patterns of linear arrays of isotropic elements. Each of the linear arrays has a characteristic set of weighting coefficients with an adjustable multiplier which is a weighting coefficient associated with the nonisotropic element of the original array. We use these multipliers in similar function to the peak amplitudes in the Woodward-Lawson method to generate a desired radiation pattern.

5.3 Algorithm

The following are the design steps required to obtain the weighting coefficient vector for the array of uniformly spaced, nonisotropic elements generating a radiation pattern which approximates a desired one.

1. Find equivalent linear arrays with spacing d of all nonisotropic elements using Eq. (5.7) for the case of $d = \lambda/2$ and Eqs. (5.25) (5.28) for the case $d \neq \lambda/2$. Such an array has in principle an infinite number of elements (and associated weighting coefficients).

2. Truncate the above arrays to a finite size $2M$ by removing elements with coefficients less than a certain small percentage of the largest one. The resulting radiation pattern should be such that the truncation error is negligible.

3. Form matrices **A**, **B**, **D**, and then **G** using Eqs. (5.14)-(5.16) and (5.21).

4. Design a prototype linear array of $2N-1$ isotropic elements which produces a desirable radiation pattern (for example associated with a Dolph-Chebyshev array). Therefore, the weighting coefficients p_i, spacing d and size N of the array are given [3].

5. Form $(M+N)\times 1$ augmented vector **p** using Eq. (5.18) and calculate the minimum mean square error e^2 using Eq. (5.23).

6. Increase the size of the prototype by two elements and repeat Steps 4–6 until a global minimum of e has been found.

7. Apply Eq. (5.22) to obtain the weighting coefficient vector **w** of the array which yields a global minimum of e.

Although the equivalent linear array approach allows formulation of the array synthesis problem as an optimization problem, the algorithm presented here does not involve any numerical optimization, and requires only ordinary matrix operations.

Nonlinear optimization algorithms can be used in array synthesis but are computationally intensive. This presents a practical difficulty for an array of a significant size. Furthermore, the size of the array cannot be selected as a variable because of the nature of its effect on the objective function (i. e., approximation error e^2 defined by Eq. (5.19)). The method proposed here allows for better control of the resultant directivity function, and also allows the desired directivity function to be defined in a more flexible form. Increasing the number of elements in an array during the optimum search is simply implemented by adding columns in the matrices **A**, **B** and **D**, whereas selecting a different prototype array requires only a change in the augmented vector **p**. Therefore, we can easily extend the proposed algorithm to include the variability of the desired directivity function.

Despite a requirement of matrix inversion in Eq. (5.22), the equivalent linear array approach is considerably less computationally intensive than the nonlinear optimization technique. As a comparison, consider a Davidon-Fletcher-Powell (DFP) algorithm [4] used both for the nonlinear optimization as well as a matrix inversion associated with the equivalent linear array approach. The DFP algorithm leads to the matrix inversion in at most N iterations, where N is the number of weighting coefficients $\{w_i\}$, whereas more than N iterations are needed for nonlinear optimization. Indeed, we can eliminate the matrix inversion in Eq. (5.22) completely by solving a set of simultaneous linear equations $\mathbf{G}^T\mathbf{G}\mathbf{w} = \mathbf{G}^T\mathbf{p}$ for the weighting coefficients $\{w_i\}$ [40]. It is known that this approach is computationally more efficient than matrix inversion.

With some minor modifications, the algorithm described in this section for an array of a fixed number of elements can also be used for an array with a variable size. To include this variability we only need to add columns formed by the associated weighting coefficients of the equivalent linear arrays to matrices $\mathbf{A}$, $\mathbf{B}$ and $\mathbf{D}$ whenever additional nonisotropic elements are added in the array. In order to determine the suitable size of a resultant array, we start the iterative computational algorithm at a minimum size array and add elements in each iteration as discussed in the previous section. The approximation error decreases with the increase of the size of the array. We terminate the iteration when this decrease becomes insignificant. This indicates that the resulting weighting coefficients associated with these new added elements are close to zero.

5.4 Applications

The previously described algorithm can be applied to a broad class of arrays. The examples given here are intended as illustrations of its effectiveness. One example deals with an array with equal nonisotropic element patterns while the other example involves elements with nonequal radiation patterns.

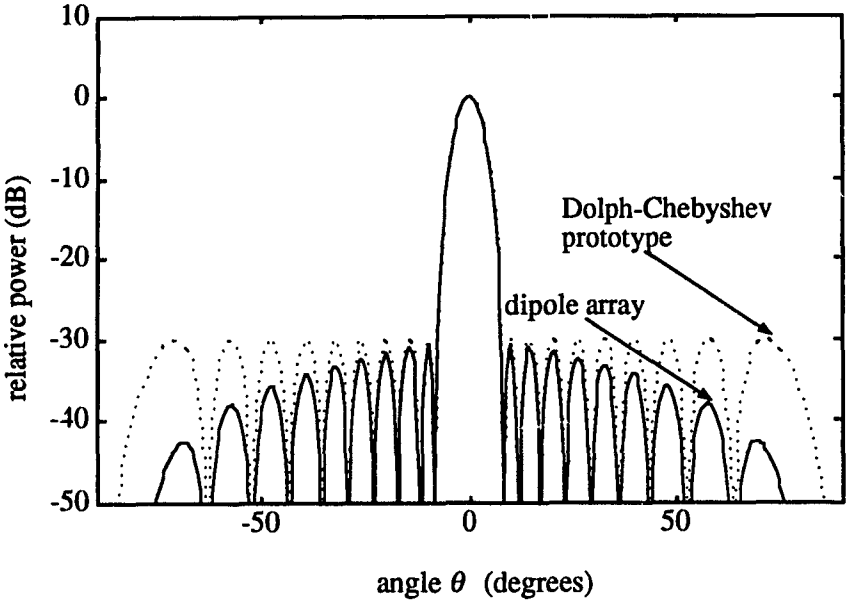

Figure 5.3: Radiation patterns of a dipole linear array with weighting coefficients obtained by the Dolph-Chebyshev method.

Consider a 20-element linear array with elements spaced every half-wavelength and with the element directivity function $f_i(\theta) = \cos(\theta)$. Such a directivity function is produced by a dipole [2]. We postulate a radiation pattern with equal sidelobes suppressed by 30 dB with respect to the main lobe, such as associated with Dolph-Chebyshev arrays [21]. We intend to find a set of weighting coefficients which will yield the best approximation of the postulated radiation pattern.

Applying the classical Dolph-Chebyshev method for isotropic-element arrays we can obtain the desired level of sidelobe suppression. However, because of the directivity function $\cos(\theta)$ of each element, sidelobes are not equal as shown in

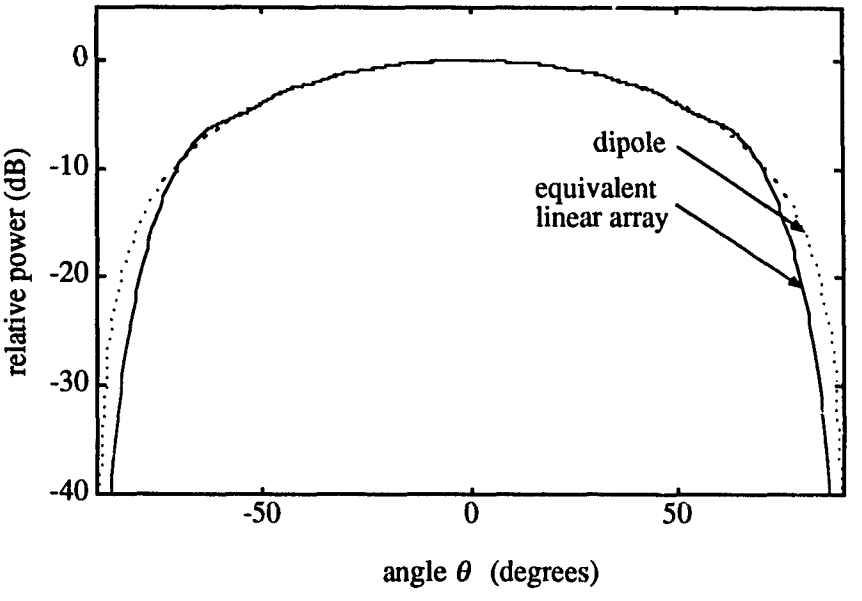

Figure 5.4: Radiation patterns of a dipole and its equivalent linear array.

Fig. 5.3. As we will observe later, the radiation pattern with equal sidelobes has a main lobe with smaller beamwidth. We now use the proposed approach to accomplish this. The radiation patterns associated with each element and its equivalent linear array with a finite length of $2M = 20$ are shown in Fig. 5.4. The weighting coefficients of the array obtained by repeating Steps 4-6 for different sizes of prototypes are tabulated in Table 5.1, and the corresponding radiation patterns are plotted in Figs. 5.5-5.7. We see that the global minimum of the approximation error e occurs when the length of the prototype is equal to 21 as shown in Fig. 5.6(b). The sidelobes of the resulting radiation pattern closely meet the original design objective. Furthermore, the best approximation is for a prototype of 21 elements (Fig. 5.6(b)) rather than 20 elements as in Fig. 5.3. This implies a narrower main lobe associated with the Dolph-Chebyshev array of 21 elements while the actual array has only 20 dipole elements.

In next example we illustrate the ability of the proposed method to synthesize a radiation pattern using elements each with a different radiation pattern. We consider here an array of identical circular loop elements discussed in [32], but we generalize such an array by allowing variable radii of the loops as illustrated in Fig. 5.8. The directivity function of a single loop assuming a uniform current on the entire loop is given by [32]

$$f(\theta) = J_1(ka\cos\theta) \tag{5.31}$$

where $J_1(\cdot)$ is the first-order Bessel function of the first kind, k is the wavenumber of the radiated signal, and a is the radius of the circular loop. The scale factor in the above equation has been dropped.

We intend to synthesize an array with a desired radiation pattern for equal excitation of each loop such that only one driving power amplifier is required. This can be accomplished by choosing a suitable radius for each loop.

We now apply the equivalent linear array approach to this array. First, we design a prototype Dolph-Chebyshev linear array of 11 isotropic elements with

Table 5.1: Weighting coefficients of a dipole array for different prototype sizes

Element	Weighting Coefficient for Different Prototype					
No.	15	17	19	21	23	25
1	1.0087	0.9819	1.0151	0.9742	0.9989	0.9825
2	0.9257	0.9732	0.9453	0.9993	0.9743	0.9986
3	0.8641	0.8526	0.9284	0.8823	0.9368	0.9172
4	0.6764	0.8001	0.7760	0.8947	0.8673	0.9265
5	0.5949	0.5966	0.7513	0.6916	0.7965	0.7786
6	0.3417	0.5591	0.5258	0.7289	0.7004	0.8006
7	0.3568	0.2933	0.5398	0.4454	0.6070	0.5917
8	0.1368	0.3737	0.2464	0.5531	0.5090	0.6497
9	-0.0535	0.1380	0.4003	0.1727	0.3963	0.3753
10	0.0321	-0.0435	0.1284	0.4745	0.3503	0.5225

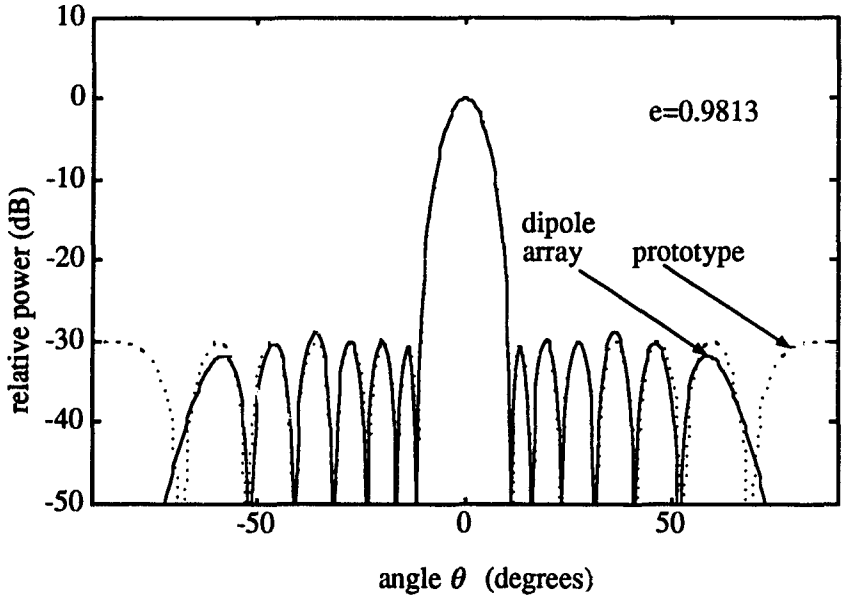

(a)

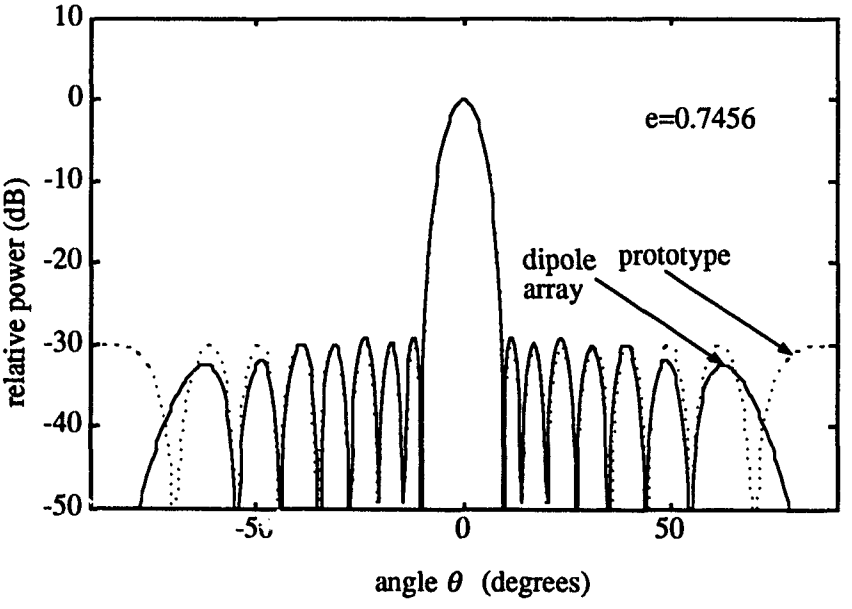

(b)

Figure 5.5: Radiation patterns of a 20-dipole array. (a) 15 elements in the prototype. (b) 17 elements in the prototype.

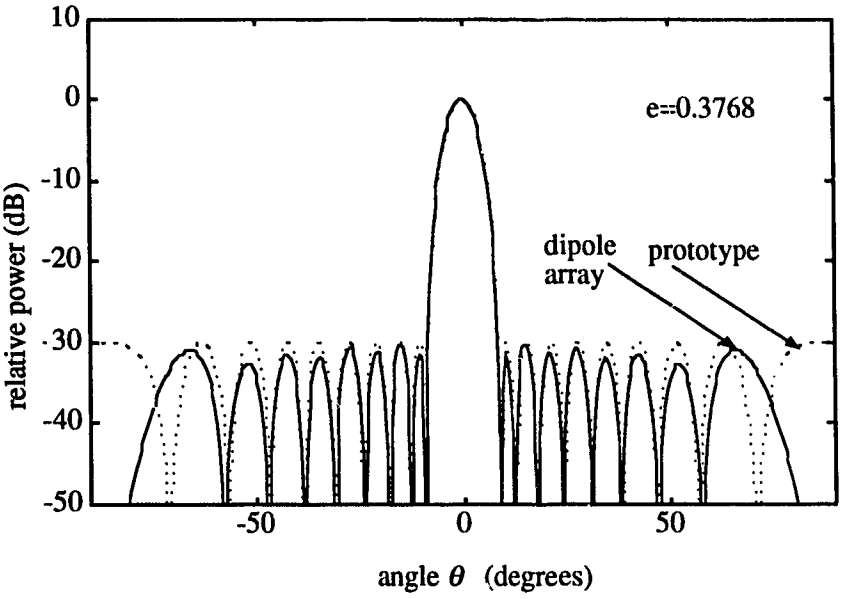

(a)

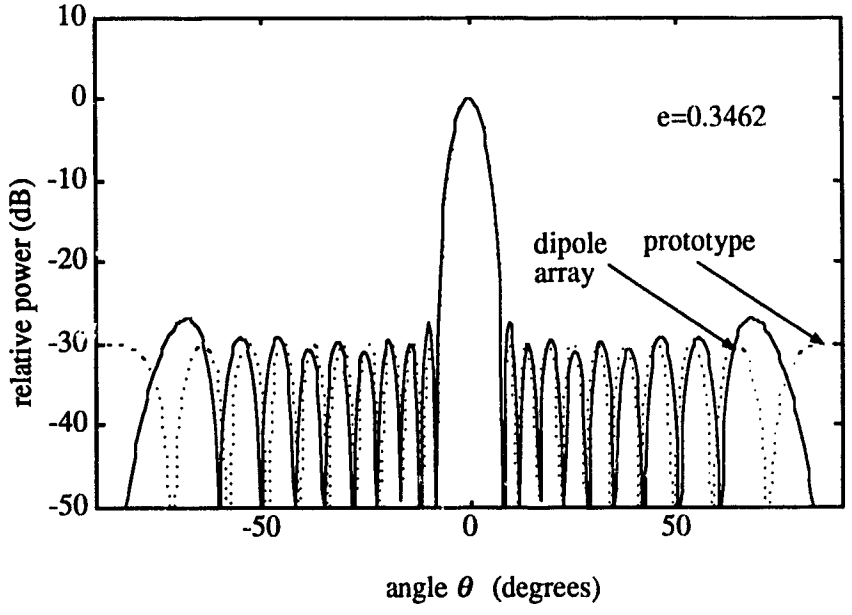

(b)

Figure 5.6: Radiation patterns of a 20-dipole array. (a) 19 elements in the prototype. (b) 21 elements in the prototype.

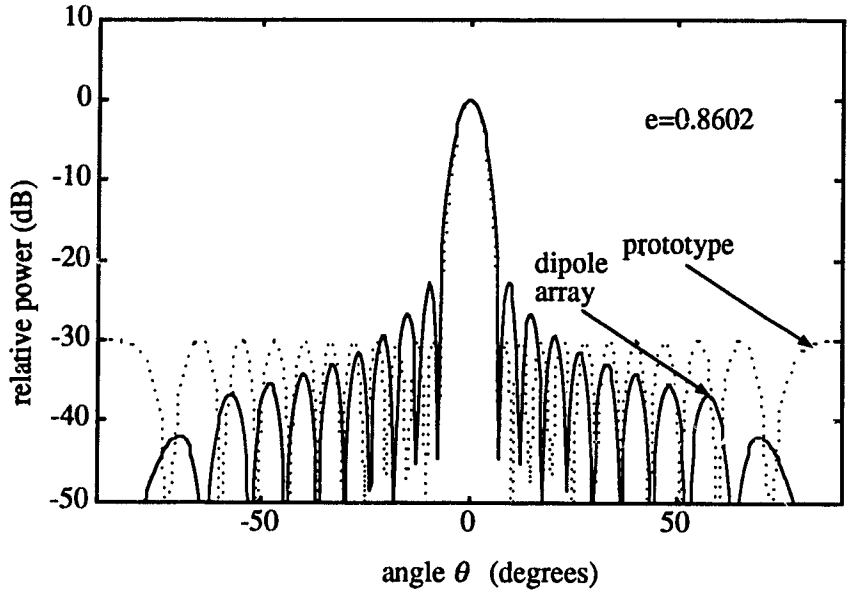

(a)

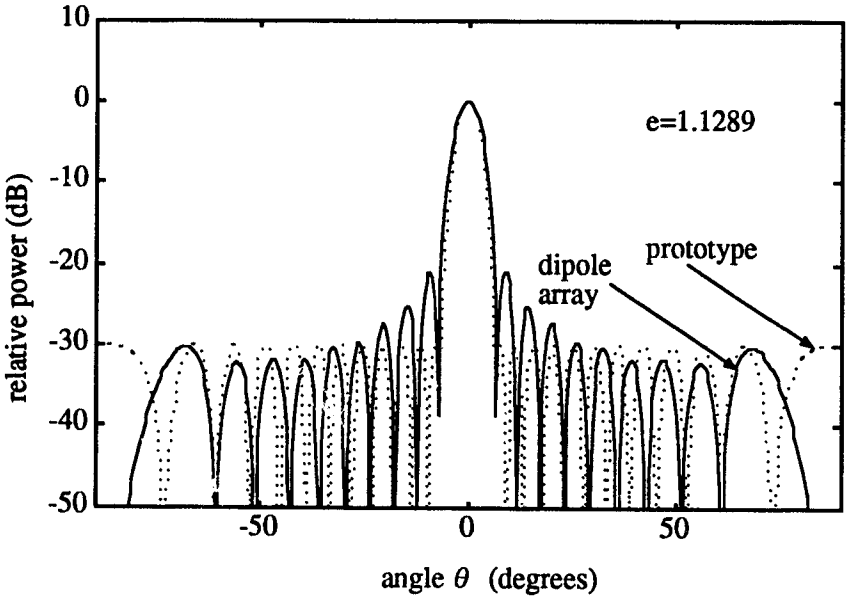

(b)

Figure 5.7: Radiation patterns of a 20-dipole array. (a) 23 elements in the prototype. (b) 25 elements in the prototype.

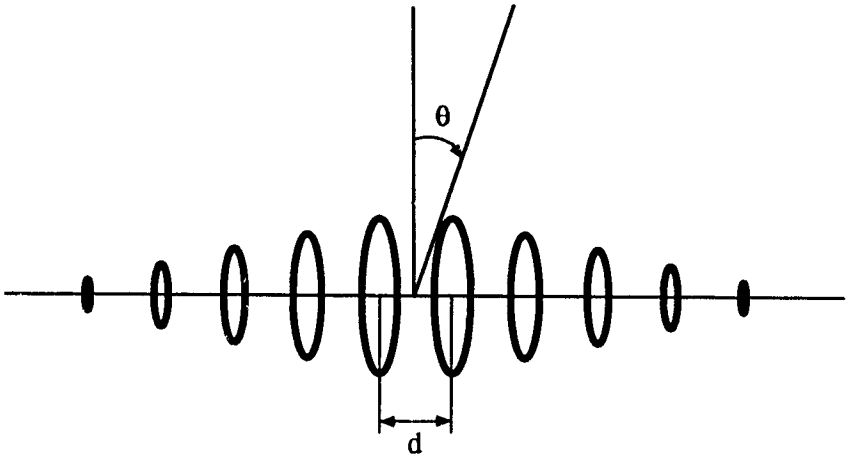

Figure 5.8: Linear array of 10 equally spaced circular loops each with a different radius.

an equal spacing $d = \lambda/2$ between elements. The prototype generates a radiation pattern with a desired beamwidth of 13° and a desired equal sidelobe suppression of 30 dB down with respect to the main lobe maximum as shown by the dotted line in Fig. 5.9. Next, we arrange the circular loops with different radii symmetrically to form a linear array as shown in Fig. 5.8. The maximum radius of the two center loops is $a = 0.5\lambda$; this radius decreases in steps of 0.125λ proceeding further from the center. Choice of such a step value is rather arbitrary at this point, but it can be modified later in an iterative process as needed to meet the design requirements. Subsequently, the circular loops are represented by their equivalent linear arrays truncated to 20 elements. To form the matrix $\mathbf{G}$, we initially start with a small array of 6 circular loops and then increase the number of the elements. This is accomplished by adding columns into the matrix $\mathbf{G}$. After obtaining a global approximation error, the resultant 10-loop array is found with the radiation pattern shown in Fig. 5.9. As we can see, there is a 3 dB difference in the sidelobe suppression between the resulting radiation pattern and the desired one. To improve the results, we simply postulate a prototype array of 33 dB sidelobe suppression. This causes only negligible effect on the beamwidth. Fig. 5.10(a) shows the radiation pattern of the resultant array which meets the original postulated 30 dB sidelobe suppression level. To show the consistency of the algorithm, we postulate a prototype array of 44 dB sidelobe suppression. This leads to the resultant radiation pattern with 40 dB sidelobe suppression shown in Fig. 5.10(b). The radius and the current for each circular loop are tabulated in Table 5.2.

Note that the currents for the loops are not exactly the same as desired, and that decreasing the radius of the loop results in less current required. We use these observations to readjust some radii and then repeat the whole process. The results tabulated in Table 5.3 indicate that the distribution of currents in each loop is more even. Additional adjustments can further improve the current distribution. The radiation patterns of the resultant array are shown in Fig. 5.11.

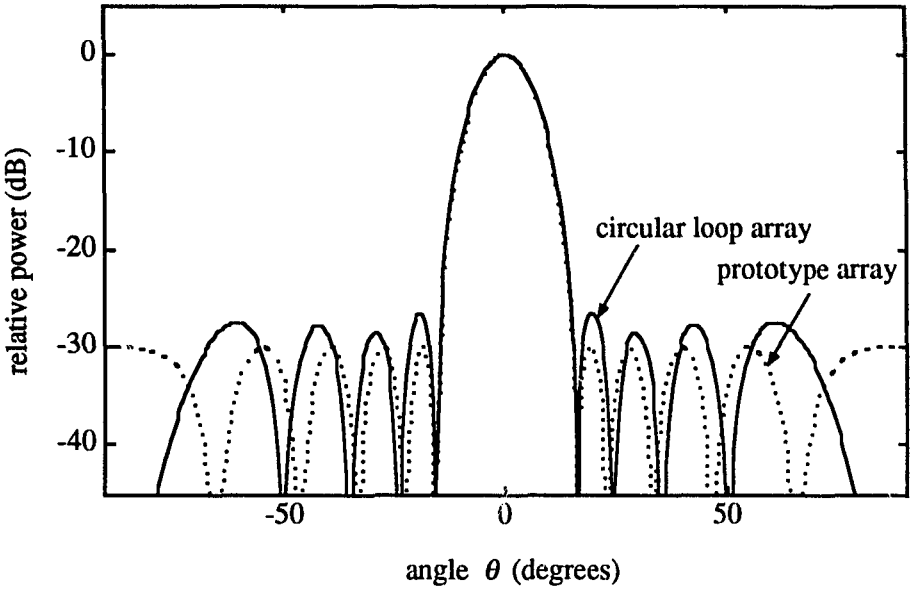

Figure 5.9: Radiation pattern of a 10-circular-loop array postulated sidelobe suppression of 30 dB.

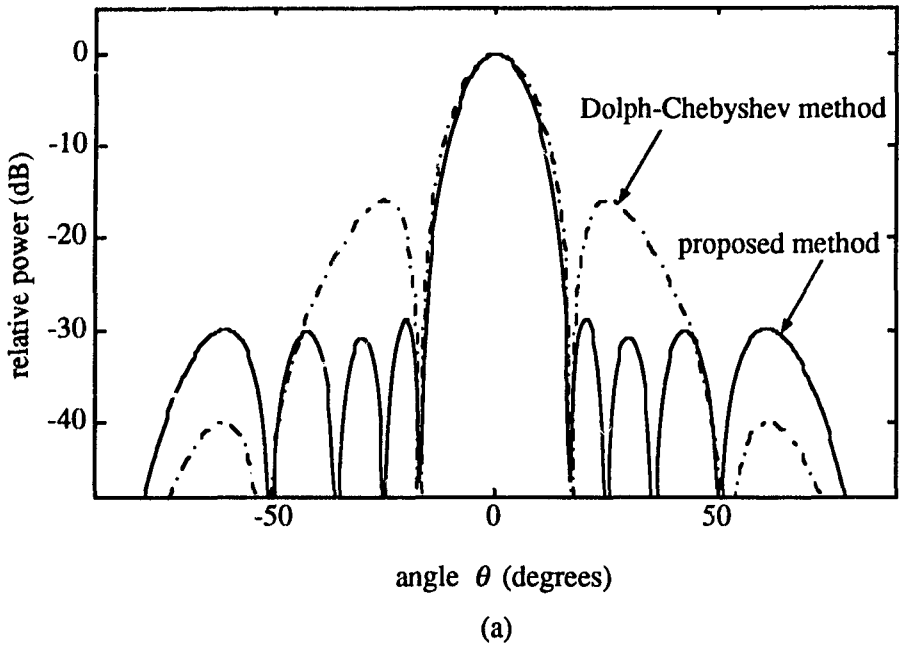

(a)

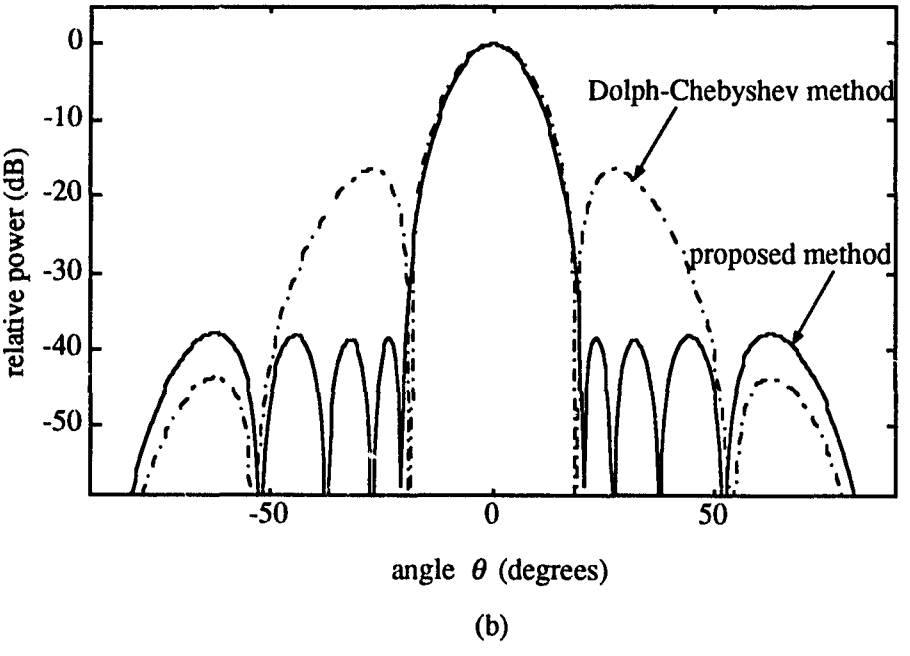

(b)

Figure 5.10: Radiation patterns of a 10-circular-loop array for different design methods. (a) Postulated sidelobe suppression of 33 dB. (b) Postulated sidelobe suppression of 44 dB.

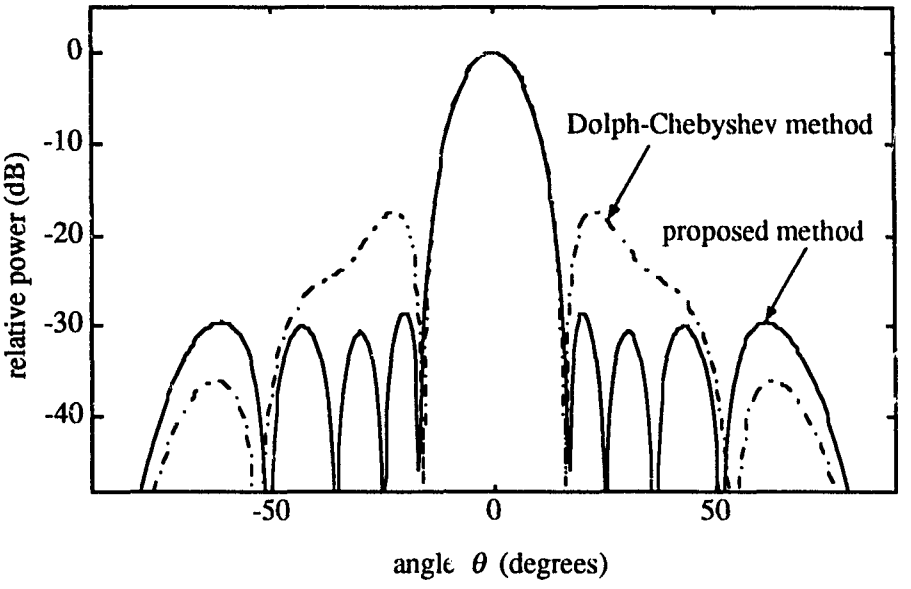

(a)

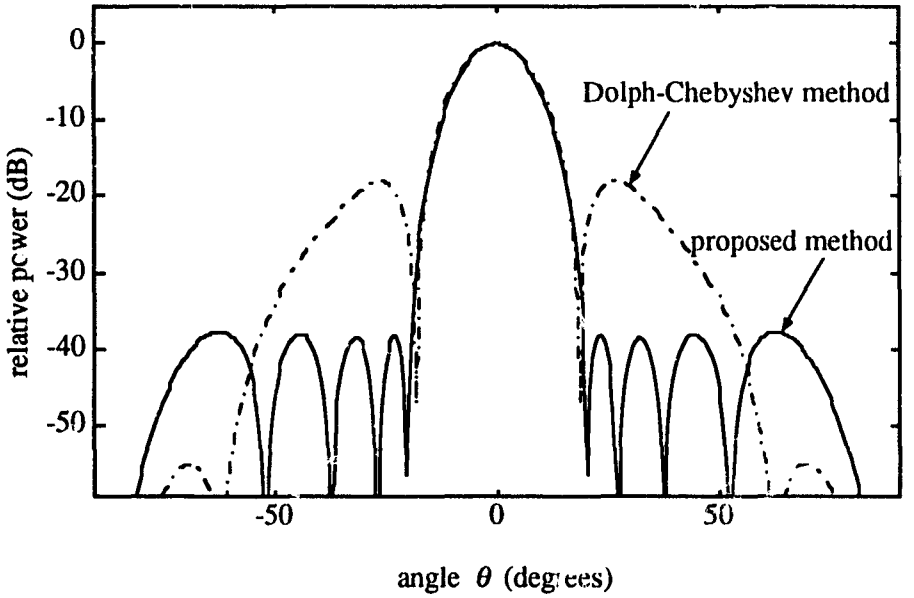

(b)

Figure 5.11: Radiation patterns of a 10-circular-loop array with adjusted radii for different design methods. (a) Postulated sidelobe suppression of 33 dB. (b) Postulated sidelobe suppression of 44 dB.

Table 5.2: Currents and radii of a circular loop array for different sidelobe suppression levels

Loop Element No.	Current and Radius for Different Sidelobe Suppression			
	radius	30 dB	radius	40 dB
1	0.50λ	0.9044	0.50λ	0.9001
2	0.375λ	0.8071	0.375λ	0.7837
3	0.25λ	0.8172	0.25λ	0.7057
4	0.125λ	1.5734	0.125λ	1.2684
5	0.0625λ	4.2583	0.0625λ	2.1837

Table 5.3: Currents and radii of an adjusted circular loop array for different sidelobe suppression levels

Loop Element No	Current and Radius for Different Sidelobe Suppression			
	radius	30 dB	radius	40 dB
1	0.50λ	0.8846	0.50λ	0.8815
2	0.35λ	0.8559	0.35λ	0.8260
3	0.25λ	0.7913	0.225λ	0.8003
4	0.175λ	0.8695	0.15λ	0.9009
5	0.15λ	0.7986	0.10λ	0.8798

If we choose to ignore the nonisotropic characteristics of the circular loops and use the Dolph-Chebyshev method for isotropic element arrays, we obtain arrays with the unsatisfactory radiation patterns shown in dash-dot lines in Figs. 5.10 and 5.11.

5.5 Summary

In this chapter we presented a new and effective method for array pattern synthesis. The synthesis problem is first formulated as a general optimization problem according to the given requirements. The proposed solution involves matrix operations based on the linear equivalent array approach, which leads to an easy and effective computation. This closed-form approach does not involve any numerical optimization routine and can be extended to planar arrays.

Illustrations were presented to highlight the various aspects of the method. The proposed algorithm can be used to design arrays of uniformly spaced elements with nonisotropic and unequal radiation patterns.

Chapter 6

Iterative Method for Array Pattern Synthesis

In Chapter 3 we discussed an example of a compact transmitting/receiving array, in which we required an arbitrary sidelobe envelope in the receiving pattern to compensate for its transmitting pattern. In this chapter we present a new and powerful iterative method for array pattern synthesis based on the concept of constraint directions.

6.1 Introduction

A large number of papers are devoted to the important problem of array synthesis. Dolph in his classic paper [21] derived the array weights for a uniformly spaced linear array of isotropic elements that yields the minimum beamwidth for a given sidelobe level. Villeneuve [22] described how Taylor's method [7] developed for arrays with continuous shading can be applied to discrete arrays. Elliot and Stern [25] presented additional pattern synthesis techniques for arrays. However, all of these techniques are applicable only to arrays consisting of uniformly spaced elements with nondirectional radiation patterns (isotropic elements).

In a recent paper [31] Olen and Compton, Jr. presented a numerical technique that can be used for arrays consisting of elements each with an arbitrary radiation

pattern. In this chapter we propose a novel iterative method for array synthesis which can be used to synthesize radiation patterns of linear arrays with arbitrary sidelobe envelopes, with nonisotropic elements, and with nonuniform spacing between elements. Various design examples are presented and compared with other methods. The proposed iterative method converges rapidly and yields superior results over the other methods.

6.2 Formulation

We assume that the geometry of an array is given and will investigate its radiation pattern as a function of weighting coefficients only. We intend to find a set of weighting coefficients to obtain a radiation pattern which best approximates a desired pattern in some sense. In other words, we are looking for a radiation pattern (directivity function) which minimizes the error suitably defined between the desired pattern and the synthesized pattern.

There are many available synthesis methods, which differ in their choice of the error criterion [30]. The mean square error of the approximation is frequently used and is defined as

$$\begin{aligned} e_{rms}^2 &= \|D(\theta,\phi) - D_d(\theta,\phi)\|^2 \\ &= < D(\theta,\phi) - D_d(\theta,\phi), D(\theta,\phi) - D_d(\theta,\phi) > \end{aligned} \tag{6.1}$$

where $D_d(\theta,\phi)$ is a desired radiation pattern, $D(\theta,\phi)$ is a synthesized radiation pattern of the array, and the angles θ, ϕ are as indicated in Fig. 6.1 for the case of a linear array. Here we treat functions as vectors in Hilbert space and use the norm denoted by $\|\cdot\|$ to express the error function. The $<\cdot>$ denotes the inner product.

A common definition of the inner product is the integral over the visible range of θ, ϕ, and the error measure e_{rms}^2 as given by Eq. (6.1) counts errors at all angle directions. However, arrays which are designed to minimize e_{rms}^2 obtained

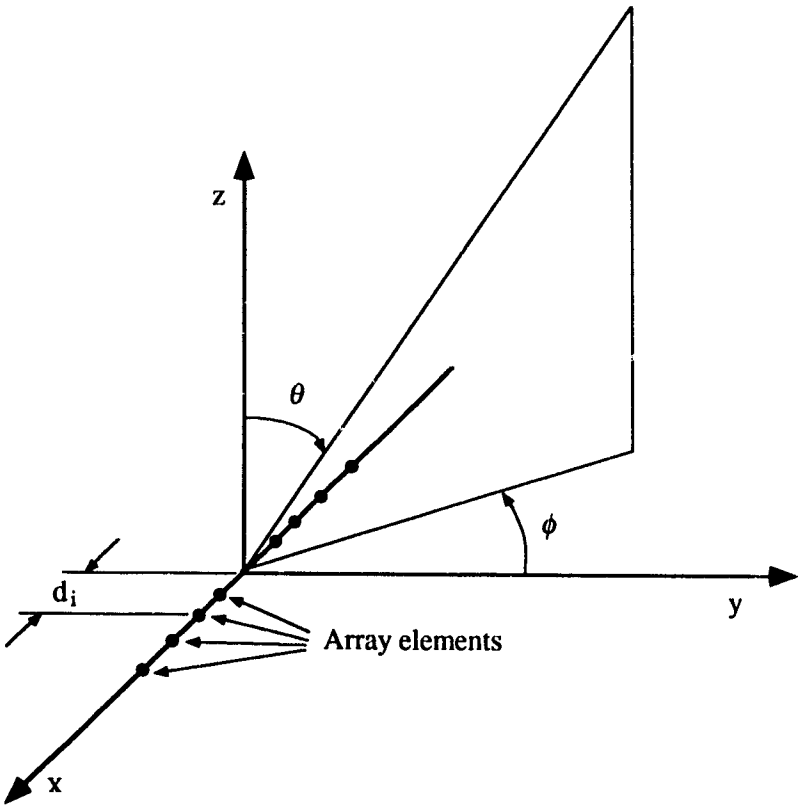

Figure 6.1: Geometry of a linear array.

in such a way may not always be satisfactory; they may suffer from large ripples in the sidelobe regions. Furthermore, the integration over all θ and ϕ requires extensive computations. These difficulties can be partially alleviated by defining an approximation error e^2 only at certain suitably chosen angle directions, that is

$$e^2 = \sum_m v_m[D(\theta_m, \phi_m) - D_d(\theta_m, \phi_m)]^2. \tag{6.2}$$

The set of these angle directions $\{(\theta_m, \phi_m)\}$, called the *constraint directions*, corresponds to a finite number of discrete locations in the angle (θ, ϕ)-domain, and the positive numbers v_m denote weighting values on errors associated with these directions. In regions of the angle domain where small error is demanded we increase the number of the constraint directions and/or increase their weights. As a practical matter, the number of the constraint directions should be greater than or equal to the number of degrees of freedom associated with a radiation pattern, that is, the number of available distinct weighting coefficients. Therefore, the problem is a well-determined or over-determined optimization problem [4].

Consider a linear array of $2N$ nonisotropic elements spaced nonuniformly as shown in Fig. 6.1. Let $f_i'(\theta)$ be a symmetric directivity function of the ith element, such that $f_i'(\theta) = f_i'(-\theta)$ and $f_i'(\theta) = f_i'(\pi - \theta)$. The directivity function of the whole array is given by

$$D'(\theta) = \sum_{i=1}^{N} w_i f_i'(\theta) \cos(2\pi d_i \sin\theta) \tag{6.3}$$

where d_i is the distance between the ith element and the array center expressed in multiples of wavelength, and w_i is the weighting coefficient associated with the ith element. Array symmetry is assumed, that is $d_i = d_{-i}$, $w_i = w_{-i}$ and $f_i'(\theta) = f_{-i}'(\theta)$.

We intend to find a set of weighting coefficients $\{w_i\}$ such that the synthesized radiation pattern $D'(\theta)$ best approximates a desired radiation pattern in the sense of minimum error defined by Eq. (6.2).

In the following development it is convenient to map the angle θ into the u-domain defined as

$$u = \sin\theta. \tag{6.4}$$

Using this mapping Eq. (6.3) can be written as

$$D(u) = \sum_{i=1}^{N} w_i f_i(u) \cos(2\pi d_i u). \tag{6.5}$$

The directivity function $D(u)$ can be viewed as a sum of sinusoidal "signals" in the u-domain, each modulated by a "slowly" varying envelope $f_i(u)$. The envelope of such a signal is determined by the positions u_m and the amplitudes $D(u_m)$ of its peaks (sidelobes). We propose to use the locations of these peaks as the constraint directions for error calculation and subsequent optimization. This is consistent with the fact that in many applications the radiation pattern with a specified sidelobe envelope is required.

The approximation error ϵ^2 given by Eq. (6.2) for $v_m = 1$ and $D(u)$ given by Eq. (6.5) is therefore

$$\begin{aligned} \epsilon^2 &= \sum_m (D(u_m) - D_d(m))^2 \qquad (6.6) \\ &= \sum_m (\sum_{i=1}^{N} w_i g_i(u_m) - D_d(m))^2 \end{aligned}$$

where u_m is the constraint angle direction in the u-domain, $D_d(m)$ is the amplitude of the desired radiation pattern at the direction u_m, and

$$g_i(u) = f_i(u) \cos(2\pi d_i u). \tag{6.7}$$

In general the constraint direction u_m depends on the weighting coefficient w_i. Therefore, finding the set of N weighting coefficients $\{w_i\}$ that minimizes ϵ^2 involves the solution of N simultaneous nonlinear equations in N unknowns.

6.3 Algorithm

In the previous section, we suggested to use the locations of peaks in the radiation pattern given by Eq. (6.5) as the constraint directions. However, finding the weighting coefficients w_i that minimize the approximation error e^2 is not an easy task, because the constraint direction u_m depends on the weighting coefficients w_i. In this section we present a new and simple iterative method to accomplish this task.

With the constraint directions given by $u_m(\mathbf{w})$, the approximation error e^2 becomes

$$e^2 = \sum_m (\sum_{i=1}^{N} w_i g_i[u_m(\mathbf{w})] - D_d(m))^2 \tag{6.8}$$

where we use the vector $\mathbf{w} = [w_1\ w_2\ \cdots\ w_n]^T$ to indicate the dependence of u_m on the set of weighting coefficients $\{w_i\}$.

Since in general we cannot get an explicit expression for $u_m(\mathbf{w})$, finding the set of optimum weighting coefficients which minimize e^2 is very computationally intensive. As an alternative, we propose here an iterative method for obtaining the set of optimum weighting coefficients. First, we select an initial set of weighting coefficients $\{w_i\}$ and use it to determine the constraint directions $u_m(\mathbf{w})$ (location of the peaks of the main lobe and sidelobes). Using these fixed constraint directions we then search for the set of optimum w_i which minimizes the error e^2 given by Eq. (6.8). The set of weighting coefficients obtained in this step is used to fix the constraint directions for the next step. This process is repeated until a satisfactory result is obtained. Since u_m is fixed during the search for the optimum w_i, the approximation error e^2 has a quadratic form and the optimum $\mathbf{w}^{(k)}$ at the kth iteration is the solution of N simultaneous linear equations in N

unknowns given by

$$\sum_{i=1}^{N} w_i^{(k)} g_{in} = D_n \qquad n = 1, 2, \ldots, N \tag{6.9}$$

with

$$g_{in} = \sum_m g_i[u_m(\mathbf{w^{(k-1)}})] g_n[u_m(\mathbf{w^{(k-1)}})] \tag{6.10}$$

and

$$D_n = \sum_m g_n[u_m(\mathbf{w^{(k-1)}})] D_d(m). \tag{6.11}$$

The above leads to the following steps in the computational algorithm:

1. Choose an initial set of weighting coefficients for the first step, $k = 0$.

2. Set $w_i = w_i^{(k)}$ in the directivity function $D(u)$ given by Eq. (6.5), and find the constraint direction $u_m^{(k)}$.

3. Minimize ϵ^2 by solving N simultaneous linear equations in N unknowns given by Eqs. (6.9), (6.10) and (6.11). The solution is $\mathbf{w^{(k+1)}}$.

4. If the final convergence criterion

$$\|\mathbf{w^{(k+1)}} - \mathbf{w^{(k)}}\| < \delta \tag{6.12}$$

   is satisfied, then stop the iteration.

5. Otherwise, return to step 2 using $\mathbf{w^{(k+1)}}$ obtained in step 3.

Any suitable algorithm for finding extreme points of $D(u)$ can be used in step 2; for instance, Newton's method [40]. A typical value of δ in the convergence criterion for terminating the iteration is about 10^{-3}. It is convenient to use a

uniform weighting array as a starting array, that is, $\mathbf{w^{(0)}} = c[1 \ \cdots \ 1]^T$, where c is a constant.

The advantage of this algorithm is that the element patterns $f_i(u)$ and the spacing d_i are included directly in the algorithm. Therefore, we can apply this algorithm to the array synthesis problems in which the elements are nonuniformly spaced, and the element radiation patterns are directional and unequal.

Although the algorithm discussed here is for the case of linear arrays, it can be extended to planar and three-dimensional arrays.

6.4 Applications

In the previous section the iterative method for array pattern synthesis was proposed and a computational algorithm was presented. In this section we apply this method to several cases of practical importance and demonstrate its usefulness.

6.4.1 Dolph-Chebyshev Patterns

An important array, with many practical applications, is the Dolph-Chebyshev linear array of isotropic, equally spaced elements. The pattern synthesis method was originally introduced by Dolph [21] and investigated afterward by others [41, 42, 43, 44, 35]. Such a radiation pattern has equal sidelobe levels and has the minimum beamwidth for a given sidelobe suppression.

We now demonstrate the effectness of the iterative method for such an array by iteratively deriving the weighting coefficients rather than using derived formulas. We assume that the number of elements, the spacing between elements, and the sidelobe suppression level (ratio of major-to-minor lobe intensity) are known. The objective of the design is to find the weighting coefficients which minimize the error given by Eq. (6.8).

We assume an array of 20 ($N = 10$) elements with half wavelength spacing between elements and with equal sidelobe suppression of 30 dB. The directivity

function of the array for this case is given by

$$D(u) = \sum_{i=1}^{10} w_i \cos(0.5\pi(2i-1)u). \tag{6.13}$$

We require that the main lobe points at the direction $\theta = 0°$ or $u = u_1 = 0$ direction ($m = 1$) and arbitrarily set mean lobe peak amplitude to unity. Therefore, Eq. (6.13) becomes

$$D(0) = \sum_{i=1}^{10} w_i = 1. \tag{6.14}$$

The amplitudes of the desired pattern at other constraint directions are equal to $\pm 10^{-30/20}$ and are determined by the desired sidelobe suppression.

We use uniform weighting coefficients for the first step of the iteration described in Section 6.3, that is, $\mathbf{w^{(0)}} = [1 \cdots 1]^T/10$. The evolution of the patterns during iterations is shown in Fig. 6.2(a)-(d). The weighting coefficients at each iteration are tabulated in Table 6.1. The resulting radiation pattern obtained after three iterations is shown in Fig. 6.2(d). The resulting weighting coefficients associated with this radiation pattern are the same as those obtained by other synthesis methods.

6.4.2 Modified Dolph-Chebyshev Patterns

Optimum designs of radiation patterns often call for the minimum beamwidth for a given sidelobe suppression level, that can be generated by a linear array of specified spacing and number of elements. However, not all directions in space may be equally important insofar as sidelobe suppression is concerned. Since there is a trade-off between beamwidth and sidelobe suppression, the requirement of all sidelobes to be suppressed equally, as in Dolph-Chebyshev patterns, may not be optimum in some applications. This leads to the consideration of designs which permit higher sidelobes in unimportant sectors, while maintaining low sidelobes in

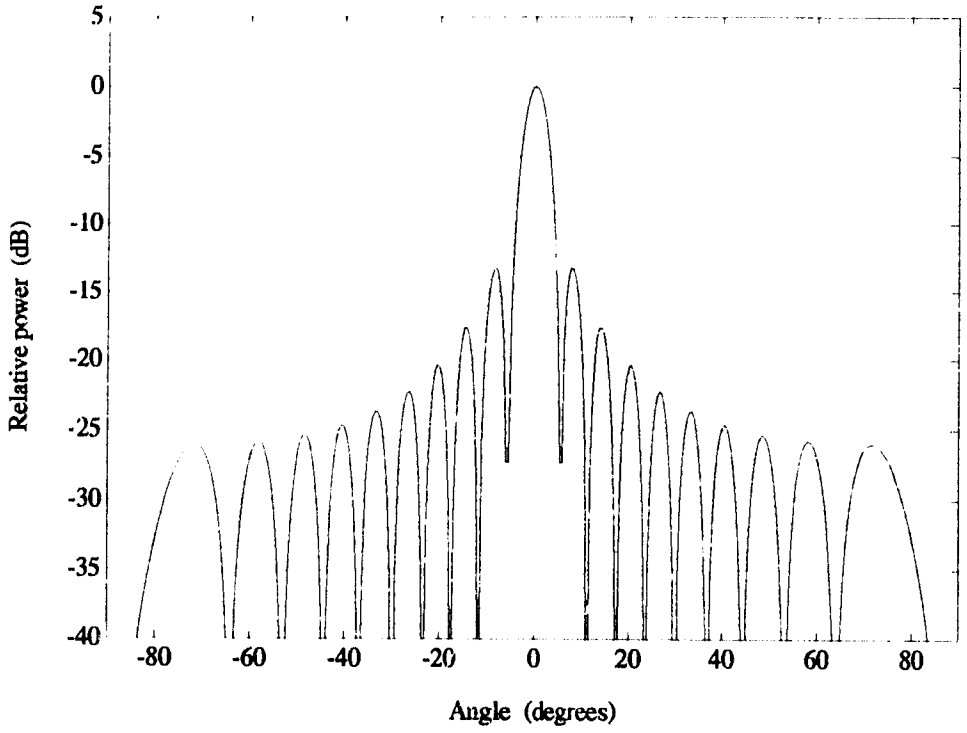

(a)

Figure 6.2: The evolution of a Dolph-Chebyshev pattern with a postulated 30 dB sidelobe suppression. (a) Starting pattern: uniform weighting array. (b) Resulting pattern after the first iteration. (c) Resulting pattern after the second iteration. (d) Resulting pattern after the third iteration.

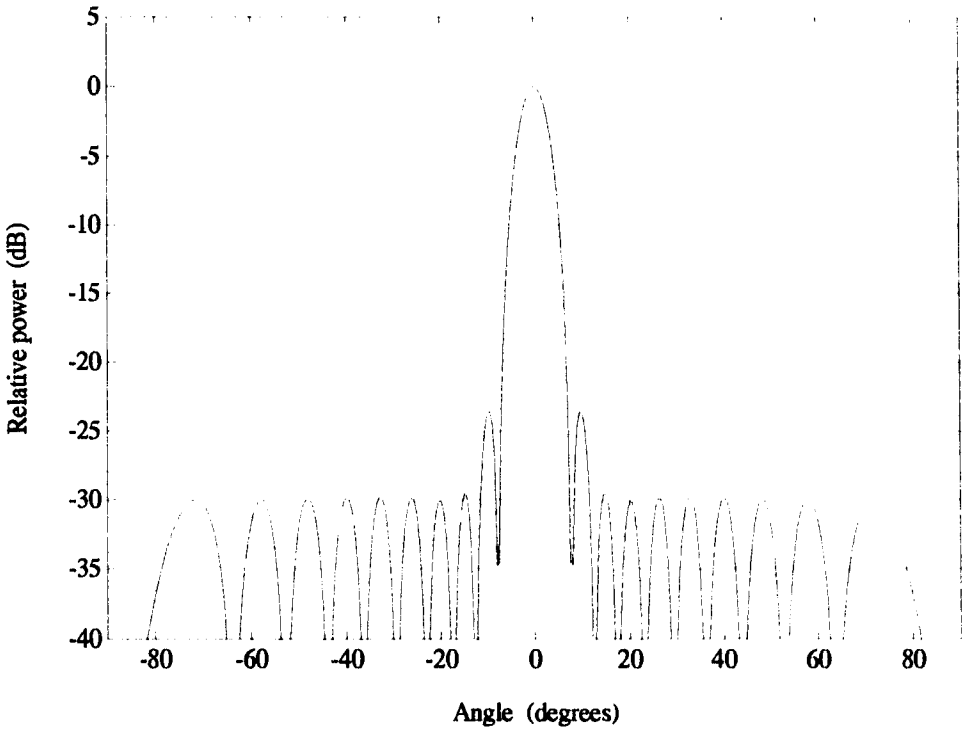

(b)

Figure 6.2: (Continued)

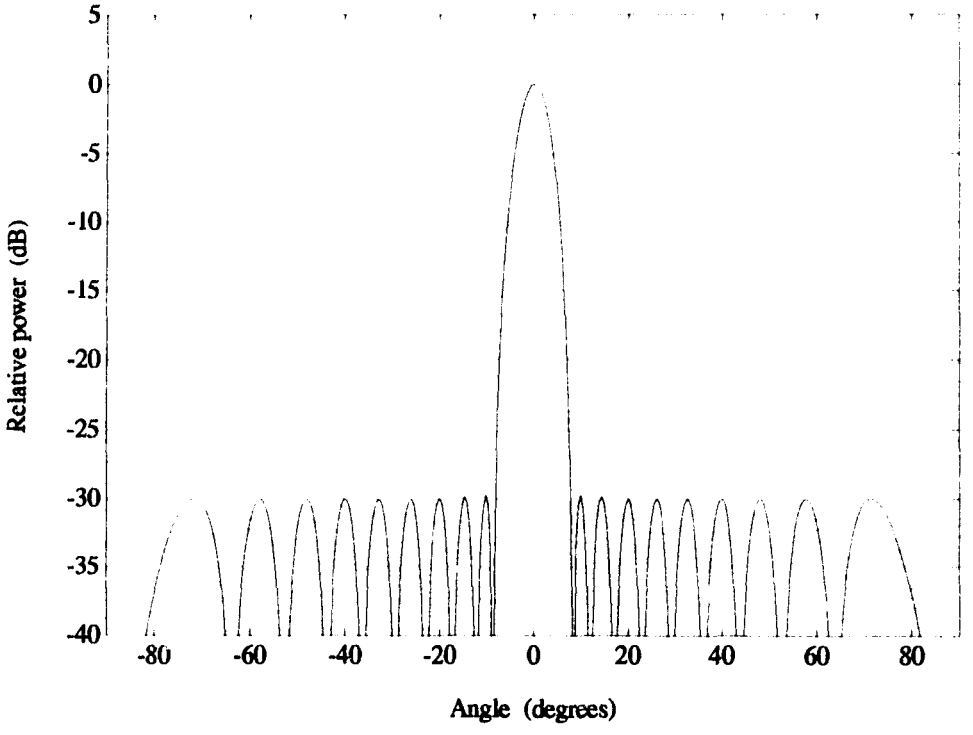

(c)

Figure 6.2: (Continued)

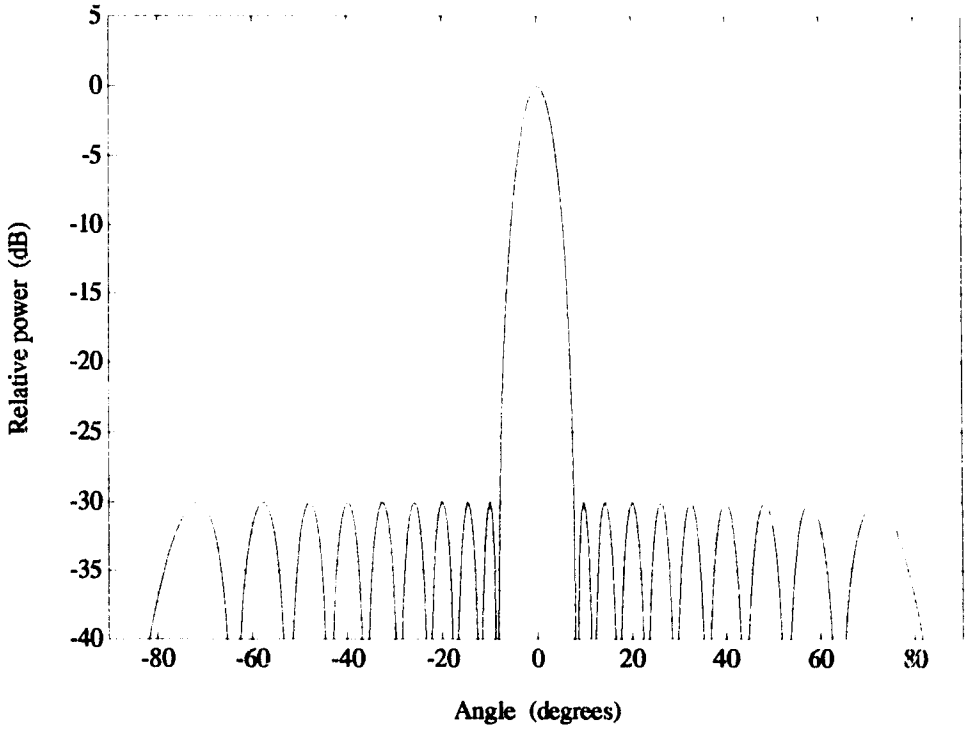

(d)

Figure 6.2: (Continued)

Table 6.1: Weighting coefficients for radiation patterns of Fig. 6.2

Element No.	Weighting Coefficient			
i	$w_i^{(0)}$	$w_i^{(1)}$	$w_i^{(2)}$	$w_i^{(3)}$
1	0.1000	0.1411	0.1518	0.1522
2	0.1000	0.1383	0.1473	0.1476
3	0.1000	0.1327	0.1386	0.1388
4	0.1000	0.1243	0.1263	0.1264
5	0.1000	0.1133	0.1113	0.1113
6	0.1000	0.0996	0.0945	0.0944
7	0.1000	0.0837	0.0770	0.0768
8	0.1000	0.0660	0.0598	0.0595
9	0.1000	0.0490	0.0438	0.0435
10	0.1000	0.0521	0.0497	0.0495

critical sectors. Elliott used a perturbation procedure to modify a Taylor pattern so that all the sidelobes have individually arbitrary heights [45]. We use the proposed iterative method to modify a Dolph-Chebyshev pattern.

As an illustration, we consider a symmetric array of 20 elements with uniform spacing of half wavelength. This spacing and the number of elements lead to 18 sidelobes in the radiation pattern. We assume that the three innermost pairs of sidelobes are to be suppressed by 45 dB, and the level of the next six pairs must be 30 dB down from the main lobe maximum. It is reasonable to use the weighting coefficients of a Dolph-Chebyshev pattern with 30 dB sidelobe suppression as an initial set of weighting coefficients in the algorithm. The evolution of the patterns during the iterations is shown in Fig. 6.3(a)-(d). We see that after the third iteration, all sidelobes satisfy the specification. The weighting coefficients at each iteration are tabulated in Table 6.2.

6.4.3 Radiation Pattern with Arbitrary Sidelobe Envelope

In some applications there is a need to produce a radiation pattern with an arbitrary sidelobe envelope. One such application is the compensation of *two-way* radiation patterns in transmitting/receiving array design [39, 18].

We consider a receiving/transmitting array where the weighting coefficients of the transmitting elements are fixed, while the receiving array consists of the same (or more) transmitting elements properly weighted to generate a desired transmitting/receiving two-way radiation pattern. In some applications the transmitting array has uniform weights in order to reduce the complexity of power distribution. A typical application of such an array is found in sonar systems.

We now apply our iterative method to synthesize such arrays. We assume that the transmitting array has 20 elements spaced by half wavelength and a prescribed

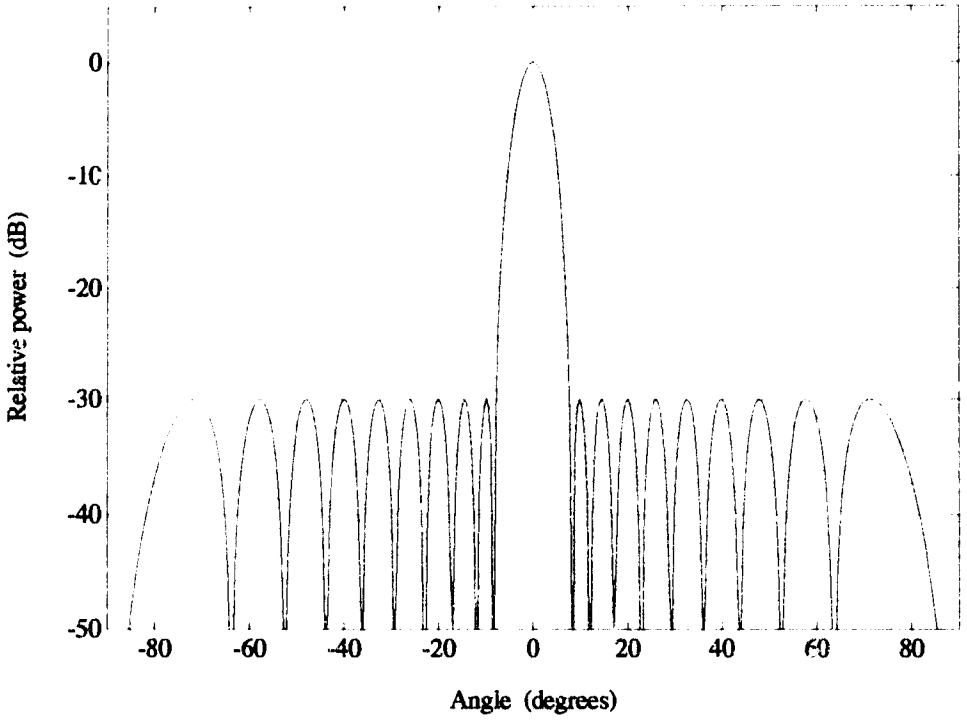

(a)

Figure 6.3: The evolution of a modified Dolph-Chebyshev pattern with the three innermost pairs of sidelobes at -45 dB and the next six pairs at -30 dB. (a) Starting pattern: Dolph-Chebyshev array with a 30 dB sidelobe suppression. (b) Resulting pattern after the first iteration. (c) Resulting pattern after the second iteration. (d) Resulting pattern after the third iteration.

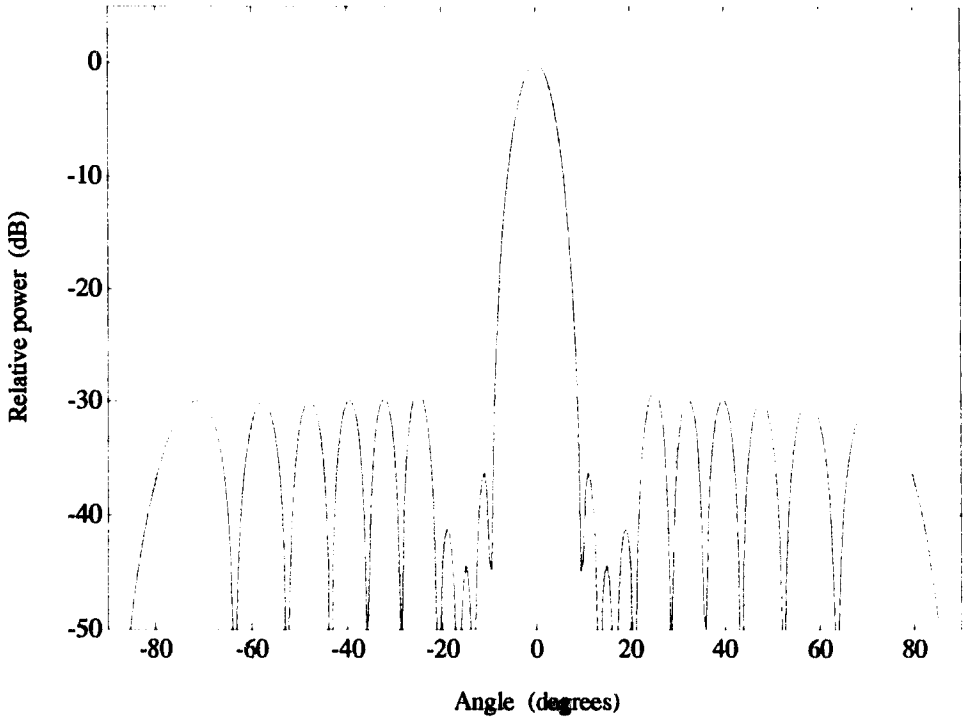

(b)

Figure 6.3: (Continued)

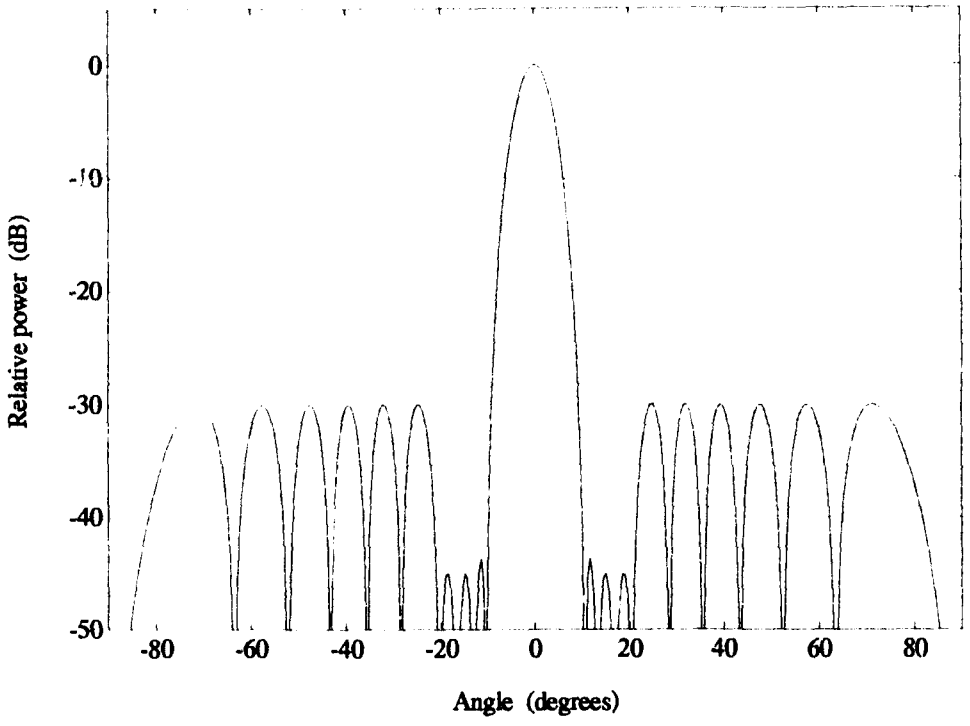

(c)

Figure 6.3: (Continued)

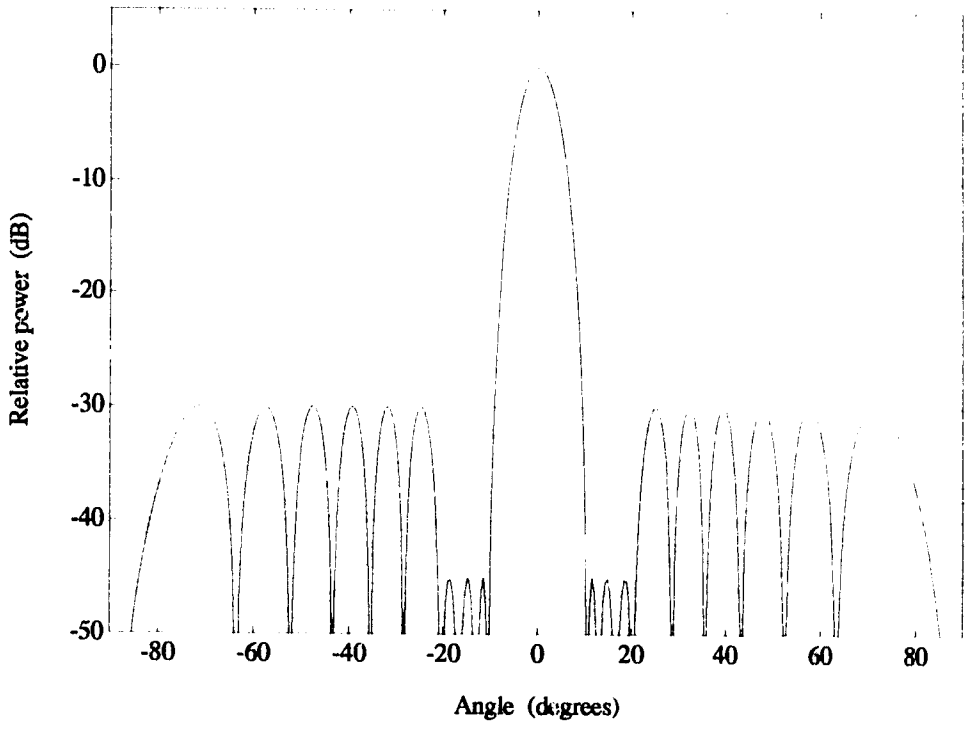

(d)

Figure 6.3: (Continued)

Table 6.2: Weighting coefficients for radiation patterns of Fig. 6.3

Element No.	Weighting Coefficient			
i	$w_i^{(0)}$	$w_i^{(1)}$	$w_i^{(2)}$	$w_i^{(3)}$
1	0.1522	0.1668	0.1723	0.1728
2	0.1476	0.1582	0.1631	0.1635
3	0.1388	0.1450	0.1482	0.1485
4	0.1264	0.1309	0.1316	0.1316
5	0.1113	0.1158	0.1143	0.1142
6	0.0944	0.0965	0.0944	0.0941
7	0.0768	0.0720	0.0701	0.0698
8	0.0595	0.0464	0.0440	0.0438
9	0.0435	0.0270	0.0231	0.0228
10	0.0495	0.0415	0.0391	0.0389

vector of transmitting weighting coefficients given by

$$\mathbf{w}_t = \begin{bmatrix} 0.1588 \\ 0.1561 \\ 0.1514 \\ 0.1426 \\ 0.1322 \\ 0.1145 \\ 0.0947 \\ 0.0499 \\ -0.0014 \\ 0.0013 \end{bmatrix}. \tag{6.15}$$

These specific weighting coefficients are obtained from an array described in [37]. The transmitting pattern corresponding to the weighting coefficients given by Eq. (6.15) is shown in Fig. 6.4(a) by dotted line. We intend to find the receiving weighting coefficients of the same array in the receiving mode such that the transmitting/receiving two-way radiation pattern meets a prescribed sidelobe envelope.

The two-way directivity function $D(u)$ is given by

$$D(u) = D_t(u)D_r(u) \tag{6.16}$$

where $D_t(u)$ and $D_r(u)$ are the transmitting and receiving directivity functions, respectively. Since the transmitting directivity function $D_t(u)$ is known, the sidelobe envelope is also known. We postulate a desired envelope of $D(u)$ and use it to derive a desired sidelobe envelope of $D_r(u)$. In this example the postulated envelope of $D(u)$ is a constant corresponding to equal sidelobe suppression of 60 dB down from the main lobe. The corresponding desired envelope of $D_r(u)$ is given by the peak amplitudes of sidelobes, and represented by the numbers (0 42 39 36 30 28 27 26.5 24.5 22). The first number represents the main lobe maximum, while the rest represent sidelobe peaks expressed in dB down from the main lobe maximum of the radiation pattern. After four iterations we obtain the receiving pattern shown in Fig. 6.4(a) by solid line. The corresponding vector of

weighting coefficients for the receiving array is given by

$$\mathbf{w}_r = \begin{bmatrix} 0.1633 \\ 0.1569 \\ 0.1445 \\ 0.1311 \\ 0.1093 \\ 0.0980 \\ 0.0679 \\ 0.0585 \\ 0.0147 \\ 0.0558 \end{bmatrix}. \tag{6.17}$$

The transmitting/receiving two-way radiation pattern is shown in Fig. 6.4(b). We see that the objective of the design is closely met.

6.4.4 Nonuniformly Spaced Arrays

Nonuniformly spaced linear arrays have been considered in the past. A synthesis technique for such arrays, proposed by Unz [46, 47], utilizes the expansion of a desired radiation pattern $D(u)$ in a series of Bessel functions. Another technique, proposed by Harrington [48], uses the assumption that the inter-element spacings deviate slightly from the uniform case to synthesize the desired radiation pattern. That is, $d_i = id + \epsilon_i$ with $\epsilon_i \ll d$. Such a consideration plays an important role in dealing with actual arrays of finite spacing tolerances. We next apply our iterative method to such a case.

Consider a symmetric linear array of 20 elements with nonuniform spacing between elements. The arbitrarily assumed distances between elements and the center reference point are [1.1; 3.0; 4.9; 7 0; 9.1; 11.0; 12.9; 15; 17.1; 19], expressed in multiples of a quarter-wavelength. The desired radiation pattern has an equal sidelobe level of 30 dB down from the main lobe maximum. We start the iteration process from a uniformly weighted array; after three iterations we obtain the radiation pattern shown in Fig. 6.5. For comparison, we also apply the Dolph method to this case by neglecting the deviations of spacings, in other words, by

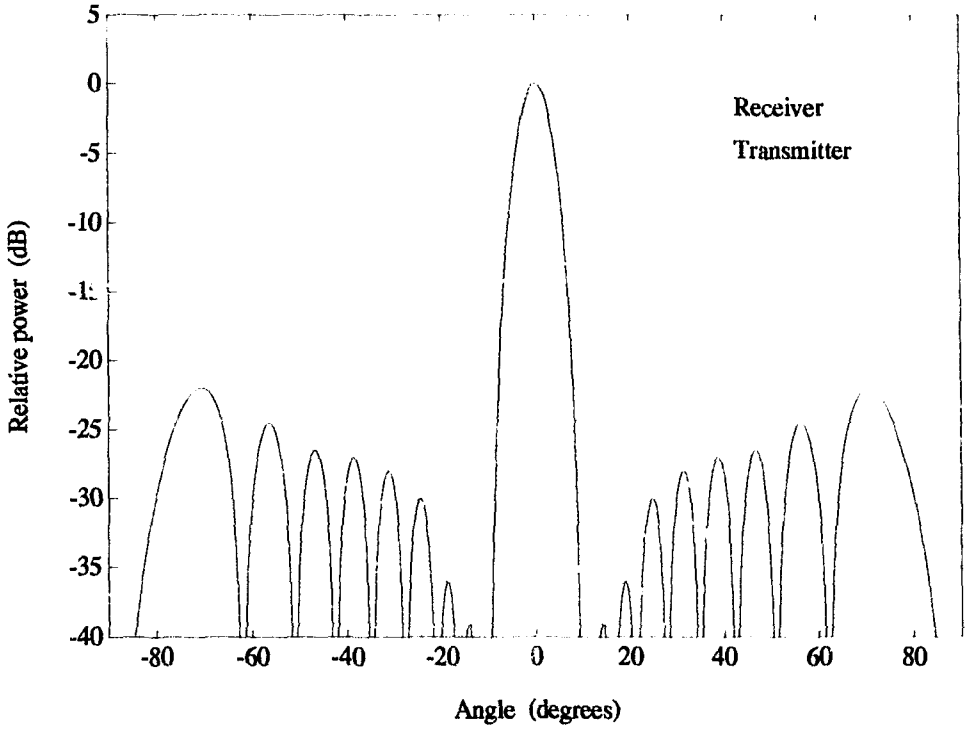

(a)

Figure 6.4: Radiation patterns of a transmitting/receiving array of 20 elements with prescribed transmitting weighting coefficients. The receiving weighting coefficients are obtained by the proposed iterative algorithm. (a) Transmitting and receiving patterns. (b) Transmitting/receiving 2-way radiation pattern of (a).

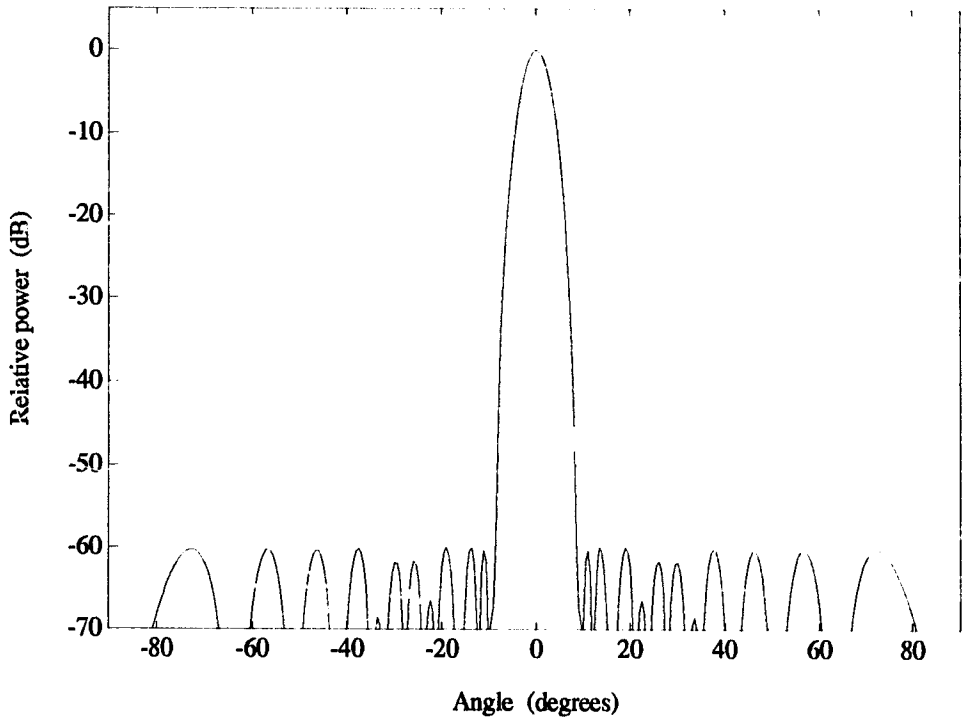

(b)

Figure 6.4: (Continued)

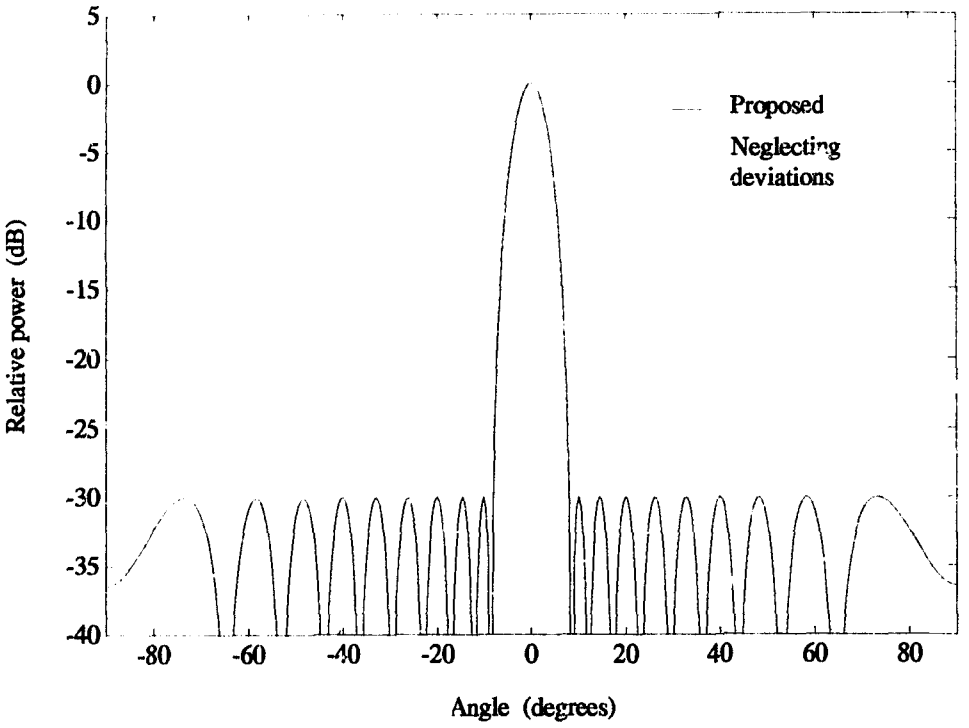

Figure 6.5: Radiation patterns of a 23-element linear array with nonuniform spacing postulated 30 dB sidelobe suppression for different synthesis methods.

assuming an equal spacing between elements. The radiation pattern obtained in such a way is shown in Fig. 6.5 by dotted line. Note the marked deterioration of the pattern due to this incorrect assumption.

6.4.5 Linear Arrays with Nonisotropic Elements

Although a large number of papers are devoted to the problem of array synthesis, most of developed synthesis techniques, however, are applicable only to arrays consisting of uniformly spaced elements with nondirectional radiation patterns (isotropic point elements). Olen and Compton, Jr. presented a numerical synthesis technique based on adaptive array theory that can be used for arrays consisting of a set of elements each with an arbitrary radiation pattern [31]. We

next demonstrate that our iterative metho' with rapid convergence can be used for arrays with nonisotropic element patterns.

Consider a 20-element linear array with elements spaced every half-wavelength and the element directivity function $f_i(\theta) = \cos(\theta)$. Such a directivity function is produced by a dipole [2]. We postulate a radiation pattern with equal sidelobes suppression of 30 dB down from the main lobe maximum. We intend to find a set of weighting coefficients which will yield the best approximation of the postulated radiation pattern.

We use the weighting coefficients obtained from a Dolph-Chebyshev array of 20 isotropic elements with 30 dB sidelobe suppression as the initial $\mathbf{w}^{(0)}$. The resulting radiation pattern obtained after only three iterations is shown in Fig. 6.6 by solid line. The sidelobes of the resulting radiation pattern closely meet the original design objective. Compared with the method by Olen and Compton, Jr., the proposed method requires less iterations and does not require any iteration parameter, such as K in [31]. Applying the classical Dolph's method for an isotropic element array one can obtain the desired level of sidelobe suppression. However, because of the $\cos(\theta)$ factor in the directivity function of each element, the sidelobes are not equal. This pattern is shown in Fig. 6.6 by dotted line and results in a 3.2% broader beamwidth compared with the equal sidelobe case. Although the gain in this case is small, the general principle is still valid.

6.5 Summary

In this chapter we presented a new and effective iterative method for array pattern synthesis which rapidly converges to an optimum solution. Various design examples are presented to highlight the usefulness of the method. The proposed algorithm can be used to design arrays of nonuniformly spaced elements with nonisotropic and unequal radiation patterns.

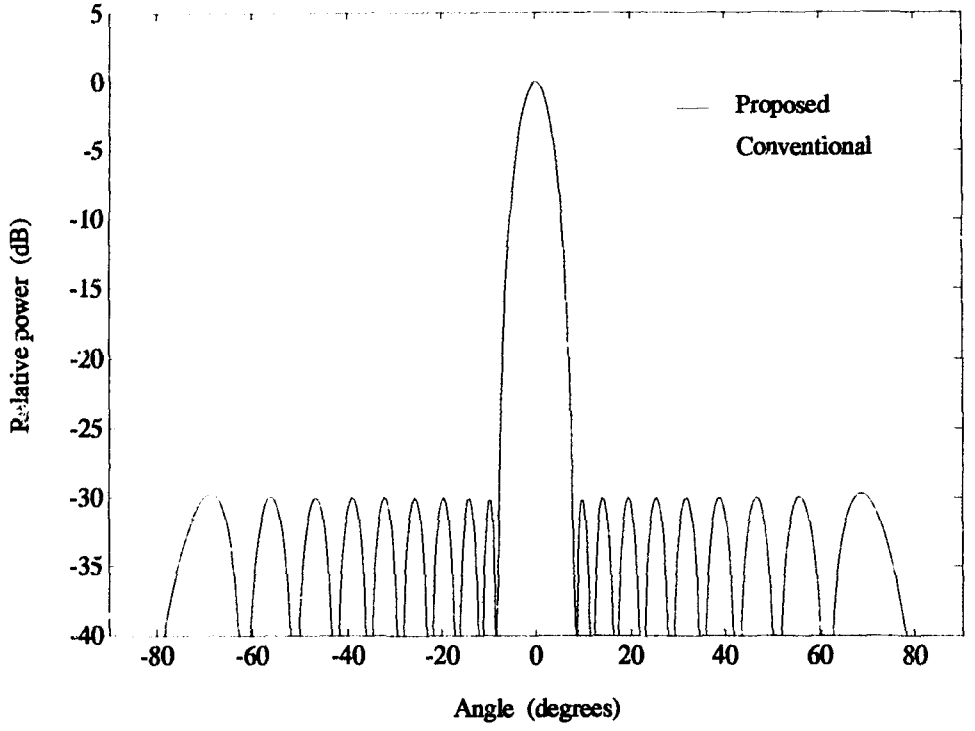

Figure 6.6: Radiation patterns of a linear array of 20 dipole elements postulated 30 dB sidelobe suppression for different synthesis methods.

Chapter 7

Summary and Future Research Considerations

7.1 Introduction

The goal of this thesis was to develop novel acoustic arrays and new array pattern synthesis methods in order to obtain desired radiation patterns and to improve sonar system performance. In this chapter the significant findings described in this thesis are summarized and suggestions for future research are presented.

7.2 Contributions

In Chapter 2 a novel array of circular ring radiators was proposed to generate a symmetric search-light type narrow beam with greatly reduced sidelobes. A new concept called the equivalent linear array was developed. The design method based on this concept benefits from existing design techniques developed for linear arrays. The developed methodology requires only simple matrix operations and does not involve nonlinear optimization.

The equivalent linear array concept was further developed in Chapter 5, leading to a new and effective method for array radiation pattern synthesis. The proposed synthesis method can be used to design arrays of uniformly spaced elements with nonisotropic and unequal radiation patterns.

In Chapter 4 a novel array of elliptic ring radiators was proposed to generate a fan-type beam with controllable sidelobe level. A new concept of scale-invariance was developed, and subsequently two possible approaches to the design were presented. One approach utilizes a mapping which transforms a radiation pattern generated by a circular ring array into that of an elliptic ring array. This approach takes advantage of methodologies developed for the design of circular ring arrays. The other approach uses the concept of the equivalent linear array. This approach benefits from the existing design techniques developed for linear arrays.

Convenient procedures for the design of novel arrays were introduced and several practical aspects associated with implementation of such arrays were investigated in Chapter 3. These novel acoustic arrays require fewer elements than conventional arrays to yield the same results. Chapter 3 also described a new compact receiving/transmitting array, in which the transmitting element was a piston, while the receiving array consisted of the same transmitting piston surrounded by several concentric rings made of piezoelectric film or several concentric hollow cylinders operating in longitudinal mode.

With the need for compact receiving/transmitting array design, an iterative method was developed for array pattern synthesis in Chapter 6. The concept of constraint directions was introduced, and the iterative algorithm for obtaining an optimum solution was presented which did not involve any nonlinear optimization but required only simple matrix operations. The proposed method was applied to the problems of synthesizing radiation patterns of linear arrays with arbitrary sidelobe envelope, with nonisotropic elements, and with nonuniform spacing between elements.

7.3 Suggestions for Future Research

The following paragraphs summarize three application areas where future research in the use of the proposed methodologies could provide improved design and

performance.

A compact receiving/transmitting assembly array configuration for sidescan sonar would be of interest to manufactures of sonar systems. In such a configuration, the transmitting element could be a simple rectangular or elliptic piston, while the receiving array could consist of the same transmitting piston surrounded by several concentric elliptic rings made of piezoelectric film.

Some interesting properties of novel ring arrays should be further explored. For instance, it can be shown that it is possible to generate a horn-type beam by properly phasing each ring radiator. Such a beam may be of use in fish stock assessment. Partitioning of each ring into segments is another possibility. It is expected that such a segmented ring array would generate a steerable search light type beam and have fewer elements than a 2-D planar array.

Investigation of other suitable configurations of acoustic arrays, such as a spiral-type array utilizing piezoelectric film and wire would also be of interest. The results of such an investigation could have direct application in underwater communication systems, specialized sonar systems, and in acoustic imaging systems. The associated array pattern synthesis methods developed for acoustic application could also easily be adapted to antenna arrays.

Appendix A

Derivation of the Optimum Weighting Coefficients

The error of approximation ϵ can be defined as

$$\begin{aligned} \epsilon^2 &= \|D - D_p\|^2 \\ &= < D - D_p, D - D_p > \end{aligned} \tag{A.1}$$

where D is the directivity function of the ring array and D_p is the desired directivity function produced by a prototype linear array. Here we treat functions as vectors in Hilbert space and use the norm denoted by $\|\cdot\|$ to express the error function. The $< \cdot >$ denotes the inner product.

Consider a 2N-element linear array of uniformly spaced, isotropic elements as a prototype. The directivity function of such an array is given by

$$D_p(\theta) = \sum_{i=1}^{N} w_{pi} \cos\left[(2i-1)\frac{\pi d}{\lambda}\sin\theta\right] \tag{A.2}$$

where p_i is the weighting coefficient of ith element, d is the spacing between elements and λ is the wavelength.

In the following developments it is convenient to map pointing angle θ into the u domain defined as

$$u = \frac{\pi d}{\lambda}\sin\theta. \tag{A.3}$$

Equation (A.2) can then be written as

$$D_p(u) = \sum_{i=1}^{N} w_{pi} \cos[(2i-1)u] \tag{A.4}$$

or in matrix form as

$$D_p(u) = \mathbf{c}^T \mathbf{w}_p \tag{A.5}$$

where the superscript T denotes the transpose and

$$\mathbf{c} = [\ \cos u \quad \cos 3u \quad \cos 5u \quad \ldots \quad \cos(2N-1)u\ ]^T. \tag{A.6}$$

It can be shown that for $d = \lambda/2$ the functions $\cos[(2i-1)u];\ i = 1, \ldots, \infty$ form an orthogonal set spanning the Hilbert space $\mathcal{H}$, namely their inner products, defined as

$$\begin{aligned} & < \cos[(2i-1)u], \cos[(2j-1)u] > \\ = \ & \frac{4}{\pi} \int_0^{\frac{\pi}{2}} \cos[(2i-1)u] \cos[(2j-1)u] du \\ = \ & \begin{cases} 1, & \text{for } i = j \\ 0, & \text{otherwise.} \end{cases} \end{aligned} \tag{A.7}$$

If we neglect the error introduced by truncation of the equivalent linear array, we can express the directivity function of the ring array as

$$D(u) = \mathbf{c}^T(\mathbf{W}\mathbf{w}_r). \tag{A.8}$$

Applying Eqs. (A.5) and (A.8) to Eq. (A.1) and calculating the inner product defined by Eq. (A.7), we obtain the error function e in matrix form as

$$e = (\mathbf{W}\mathbf{w}_r - \mathbf{w}_p)^T(\mathbf{W}\mathbf{w}_r - \mathbf{w}_p). \tag{A.9}$$

The vector of weighting coefficient $\mathbf{w}_r$ which minimize the above error is given by

$$\mathbf{w}_r = (\mathbf{W}^T\mathbf{W})^{-1}\mathbf{W}^T\mathbf{w}_p \tag{A.10}$$

and the corresponding minimum mean square error is then

$$e^2 = (\mathbf{W}(\mathbf{W}^T\mathbf{W})^{-1}\mathbf{W}^T\mathbf{w}_p - \mathbf{w}_p)^T(\mathbf{W}(\mathbf{W}^T\mathbf{W})^{-1}\mathbf{W}^T\mathbf{w}_p - \mathbf{w}_p). \tag{A.11}$$

Bibliography

[1] R. J. Urick, *Principles of Underwater Sound*, New York: McGraw-Hill, Edition 3, 1983.

[2] C. S. Clay and H. Medwin, *Acoustical Oceanography: Principles and Applications*, New York: John Wiley & Sons, 1977.

[3] R. E. Elliot, *The Theory of Antenna Arrays*, Vol. 2 of Microwave Scanning Antennas, ed. R. C. Hansen, New York: Academic Press, 1966.

[4] D. G. Luenberger, *Linear and Nonlinear Programming*, New York: Addison-Wesley, 1984.

[5] W. Sachse and N. N. Hsu, "Ultrasonic transducer for materials testing and their characterization," in *Phys. Acoust.*, vol. XIV, W. P. Mason and R. N. Thurston, eds. New York: Academic Press, 1979, pp. 277-406.

[6] T. Sullivan and J. Powers, "Piezoelectrical polymer flexural disk hydrophone," *J. Acoust. Soc. Am.* vol 63, May 1978, pp. 1396-1401.

[7] T. T. Taylor, "Design of line source antennas for narrow beamwidth and low sidelobes," *IRE Trans. Antennas Propagat.*, vol. AP-3, pp. 16-28, 1955.

[8] S. I. Aanonsen, T. Barkve, J. N. Tjotta, and S. Tjotta, "Distortion and harmonic generation in the near field of a finite amplitude sound beam", *J. Acoust. Soc. Am.*, vol. 75, pp. 749-768, 1984.

[9] K. V. Haselberg and J. Krautkramer, "Ein ultraschall-strahler fur die werk stoffprufung mit verbessertem nahfeld," *Acustica*, vol. 9, pp. 359-364, 1959.

[10] F. D. Martin and M. A. Breazeale, "A simple way to eliminate diffraction lobes emitted by ultrasonic transducers," *J. Acoust. Soc. Am.*, vol. 49, pp. 1668-1669, 1971.

[11] G. Du and M. A. Breazeale, "Ultrasonic field of a Gaussian transducer," *J. Acoust. Soc. Am.*, vol. 78, pp. 2083-2086, 1985.

[12] P. S. Zerwekh and R. O. Claus, "Ultrasonic transducer with Gaussian radial velocity distribution," *Proc. 1981 IEEE Ultrason. Symp.*, vol. 2, B. R. McAvoy, ed., New York: IEEE, 1981, pp. 974-976.

[13] R. O. Claus and P. S. Zerwekh, "Ultrasonic transducer with a two dimensional Gaussian field profile," *IEEE Trans. Sonics Ultrason.*, vol. 30, pp. 36-39, 1983.

[14] National Defense Research Committee, Division 6, *Design and Construction of Crystal Transducers*, Summary Tech. Rpt. vol. 12, Washington, D. C., 1946.

[15] National Defense Research Committee, Division 6, *The Design and Construction of Magnetostriction Transducers*, Summary Tech. Rpt. vol. 12, Washington, D. C., 1946.

[16] G. E. Martin and J. S. Hickman, "Directional properties of continuous plane radiators with bizonal amplitude shading," *J. Acoust. Soc. Am.*, vol. 27, pp. 1120-1127, 1955.

[17] C. J. Drost, "Near and far field of strip-sharped acoustic radiator," *J. Acoust. Soc. Am.*, vol. 65, pp. 565-572, 1979.

[18] A. Zielinski and L. Wu, "A novel array of ring radiators," *IEEE J. Oceanic Eng.*, vol. 16, no. 1, pp. 136-141, Jan. 1991.

[19] D. McGehee and J. S. Jaffe, "A design approach for optimizing segmented transducers," *Proc. OCEANS '91*, Honolulu, vol. 3, pp. 1550-1555, 1991.

[20] S. A. Schelkunoff, "A mathematical theory of linear array," *Bell Syst. Tech. J.*, vol. 22, p. 80, 1943.

[21] C. L. Dolph, "A current distribution for broadside arrays which optimizes the relationship between beamwidth and sidelobe level," *Pro. IRE*, vol. 34, pp. 335-348, 1946.

[22] A. T. Villeneuve, "Taylor patterns for discrete arrays," *IEEE Trans. Antennas and Propagat.*, vol. AP-32, pp. 1089-1093, Oct. 1984.

[23] R. F. Hyneman, "A technique for the synthesis of line-source antenna pattern having specified sidelobe behavior," *IEEE Trans. Antennas and Propagat.*, vol. AP-16, pp. 430-435, July 1968.

[24] R. F. Hyneman and R. M. Johson, "A technique for the synthesis of shaped beam radiation patterns with approximately equal percentage ripple," *IEEE Trans. Antennas and Propagat.*, vol. AP-15, pp. 736-743, Nov. 1967.

[25] R. S. Elliott and G. J. Stern, "A new technique for shaped beam synthesis of equispaced arrays," *IEEE Trans. Antennas and Propagat.*, vol. AP-32, pp. 1129-1133, Oct. 1984.

[26] H. J. Orchard, R. S. Elliott and G. J. Stern, "Optimizing the synthesis of shaped beam antenna patterns," *Proc. Inst. Elec. Eng.*, vol. 132, pt. 4, pp. 63-68, Feb. 1985.

[27] P. M. Woodward, "A method of calculating the field over a plane aperture required to produce a given polar diagram," *J. Inst. Elect. Engrs.*, vol 95, pt IIIA, pp. 1554-1558, 1946.

[28] P. M. Woodward and J. D. Lawson, "The theoretical precision with which an arbitrary radiation pattern may be obtained from a source of finite size," *J. Inst. Elect. Engrs.*, vol. 95, pt III, no. 37, pp. 363-370, Sep. 1948.

[29] W. D. White, "A flexible synthesis procedure for line source antennas," *IEEE Trans. Antennas and Propagat.*, vol. AP-24, p. 857, Nov. 1976.

[30] A. C. Schell and A. Ishimaru, *Antenna Pattern Synthesis*, section 14.10 of Antenna Theory, ed. R. E. Collin and F. J. Zucker, New York: MaGraw-Hill, 1969.

[31] C. A. Olen and R. T. Compton, Jr., "A numerical pattern synthesis algorithm for arrays," *IEEE Trans. Antennas and Propagat.*, vol. AP-38, pp. 1666-1676, 1990.

[32] C. A. Balanis, *Antenna Theory Analysis and Design* New York: Harper & Row, 1982.

[33] V. M. Ristic, *Principle of Acoustic Devices* New York: John Wiley & Sons, 1983.

[34] E. A. L'vova and A. S. Khimunin, "Structure of the Acoustic Field of Ring Radiators of Finite Width", *Soviet Journal of Nondestructive Testing (English translation of Defektoskopiya)*, Vol 6, No 12, Dec 1980, pp. 924-931.

[35] A. Zielinski, "Matrix Formulation for Dolph-Chebyshev Beamforming", *Proc. of the IEEE*, Vol 74, No 12, 1986, pp. 1799-1800.

[36] P. J. Kielczynski, W. Pajewski and M. Szalewski, "Ring Piezoelectric Transducers Radiating Ultrasonic Energy into the Air", *IEEE Trans. Ultrason. Ferroelect. Freq. Contr.*, vol. UFFC-34, no. 1, pp. 38-43, Jan. 1990.

[37] L. Wu and A. Zielinski, "Design Considerations for Acoustic Ring Arrays", *IEEE Pacific Rim Conf. on Communications, Computers and Signal Processing*, Victoria, May 1991, pp. 132-137.

[38] O. B. Wilson, *Introduction to Theory and Design of Sonar Transducers*, Los Altos: Peninsula, 1988.

[39] L. Wu and A. Zielinski, "Compact acoustic transmitting/receiving ring arrays", *Proc. OCEAN '91, MTS-IEEE Conf.*, Honolulu, 1991, pp. 1539-1544.

[40] C. F. Gerald and P. O. Wheatley, *Applied Numerical Analysis*, New York: Addison-Wesley, 1984.

[41] H. J. Riblet, "A current distribution for broadside arrays which optimizes the relationship between beamwidth and side-lobe level," *Proceedings of the IRE*, pp. 489-492, May 1947.

[42] D. Barbiera, "A method for calculating the current distribution of Tschebyscheff arrays," *Proceedings of the IRE*, pp. 78-82, January 1952.

[43] R. J. Stegen, "Excitation coefficients and beamwidths of Tschebyscheff arrays," *Proceedings of the IRE*, pp. 1671-1674, November 1953.

[44] C. J. Drane, Jr., "Useful approximations for the directivity and beamwidth of large scanning Dolph-Chebyshev arrays," *Proceedings of the IEEE*, pp. 1779-1787, November 1968.

[45] R. S. Elliot, "Design of line-source antenna for sum patterns with sidelobes of individually arbitrary heights," *IEEE Trans. Antennas and Propagat.*, vol. AP-24, pp. 76-83, 1976.

[46] H. Unz, "Linear arrays with arbitrarily distributed elements," *IRE Trans. Antennas Propagation*, vol. 8, pp. 222-223, 1960.

[47] H. Unz, "Non-uniform arrays with spacing larger than one wavelength," *IRE Trans. Antennas Propagation*, vol. 10, pp. 647-648, 1962.

[48] R. F. Harrington, "Sidelobe reduction by Non-uniform element spacing," *IRE Trans. Antennas Propagation*, vol. 9, pp. 187-192, 1961.